NASA Contractor Report 159158

ARGON/UF_6 PLASMA EXHAUST GAS RECONSTITUTION EXPERIMENTS USING PREHEATED FLUORINE AND ON-LINE DIAGNOSTICS

Ward C. Roman

UNITED TECHNOLOGIES RESEARCH CENTER
East Hartford, Connecticut 06108

NASA Contract NAS1-14329
October 1979

National Aeronautics and
Space Administration

Langley Research Center
Hampton, Virginia 23665

TABLE OF CONTENTS

SUMMARY

An experimental and analytical investigation was conducted using the United Technologies Research Center (UTRC) 1.2 MW rf induction heater, a dc plasma torch and uranium tetrafluoride (UF_4) feeder system, and both batch and flowing (room temperature and preheated) fluorine/uranium hexafluoride (UF_6) reconstitution systems to aid in developing some of the technology necessary for designing a self-critical fissioning uranium plasma core reactor (PCR). This technology is also applicable to gaseous UF_6 nuclear pumped laser systems.

A specific objective of this portion of the research program was the development of a regeneration system for the rf-heated uranium plasma experiments which would aid in establishing the reliability of a hot, pressurized UF_6 handling and regeneration system that would be applicable to future closed-cycle UF_6 PCR experiments.

Pure, high temperature UF_6 was injected into an argon fluid-mechanically-confined, steady-state, rf heated plasma contained within a water-cooled, fused-silica cylindrical test chamber (5.7-cm-ID x 10-cm-long). Fluid-mechanical confinement was achieved with vortex flow driven by a set of injectors located on the periphery of one endwall. On-axis UF_6 injection was used on one endwall; the plasma effluent was extracted on the opposing endwall using a combination of on-axis thru-flow exhaust and axial bypass exhaust. Prior results (Ref. 1) using this configuration included development of (1) x-ray absorption, and (2) simultaneous plasma emission/dye laser absorption measurement techniques for determining the confined uranium number density.

The plasma exhaust products, both gas and solid, were analyzed using complementary techniques. Solids analysis was performed with infrared, photo-acoustic, scanning electron micropobe, ion scattering, and secondary ion mass spectrometry techniques. UO_2F_2 and UF_4 were the dominant solids identified. Exhaust gas analysis was performed on-line using a specially built ruggedized time-of-flight (T.O.F.) mass spectrometer system. Nickel sampling probes and a data acquisition system permitted quantitative analysis of the UF_6 and associated impurities at various locations in the exhaust system. This non-commercial spectrometer was specifically designed to operate in a high rf

background and to withstand the corrosive environment of UF_6 and related halide compounds. By employing a cryopumped ion source, contamination of the spectrometer was minimized; hence, measurements of UF_6 down to 0.003 percent (30 ppm) were achieved. Based on prior results (Ref. 2) using a batch-type UF_4/UF_6 regeneration apparatus, and exploratory tests using a high-pressure fluorine sonic injection system, a flowing high-pressure, high-temperature pure fluorine/UF_6 reconstitution system was developed for on-line conversion of the uranium compounds present in the plasma exhaust back to pure UF_6. Fluorine preheat temperatures up to approximately 1000 K (reaction times of tens of milliseconds) resulted in on-line UF_6 regeneration efficiencies up to about 90 percent. In comparison, the prior batch-type experiments resulted in UF_6 conversion efficiencies up to 100 percent but required reaction times of typically minutes and reaction temperatures of about 700 K.

The overall test results have demonstrated the feasibility of employing a flowing, high-temperature, pure fluorine/UF_6 regeneration system to efficiently convert a large fraction of the effluent plasma exhaust back to pure UF_6. The custom built T.O.F. mass spectrometer sampling system permitted on-line measurements of the UF_6 concentration at different locations in the exhaust system. Negligible amounts (<100 ppm) of UF_6 were detected in the axial bypass exhaust duct and the exhaust ducts downstream of the cryogenic trap system used to collect the UF_6, thus verifying the overall system efficiency over a range of operating conditions. Use of a porous Monel duct as part of the exhaust duct system, including provision for injection of pure fluorine, provided a viable technique to eliminate uranium compound residue on the inside surface of the exhaust ducts. Typical uranium compound mass deposition per unit area of duct was 2 $\mu g/cm^2$. This porous duct technique is directly applicable to future uranium compound transfer exhaust systems. Throughout these experiments, additional basic data on the corrosion aspects of hot, pressurized UF_6/fluorine were also accumulated.

RESULTS AND CONCLUSIONS

Argon dc arc plasma torch tests using pure UF_4 and fluorine injection yielded the following results.

1. For the test configuration and range of test conditions used in these experiments, no conversion of the uranium compound exhaust products to UF_6 occurred at reaction chamber exit centerline temperatures less than about 650 K.

2. Increasing the reference centerline temperature to 880 K resulted in a conversion efficiency (i.e., fraction of the total injected UF_4 that was converted to pure UF_6) of approximately 55 percent.

3. Increasing the reference centerline temperature to about 1000 K (corresponding to the start of the region of fluorine attack on material properties) increased the conversion efficiency to about 80 percent. In this series of tests the corresponding chamber pressure was 1.5 atm, and the room temperature fluorine flow rate was 0.2 g/s. Throughout these tests the importance of minimizing all sources of contaminants was demonstrated.

4. A specially designed fluorine preheater system, together with a fluorine sonic injector assembly, permitted injecting pure fluorine into the flowing argon/UF_4 mixture at temperatures up to approximately 1000 K. At these conditions, approximately 40 percent of the fluorine was in the atomic state. At reaction chamber exit centerline temperatures of about 1000 K, conversion efficiencies of 85 percent were achieved. The maximum conversion achievable was 94.8 percent; this occurred at a centerline temperature of 1180 K, an argon flow rate of 2.31 g/s, a preheated fluorine ($\approx$ 1000 K) flow rate of 0.2 g/s, and a UF_4 flow rate of 0.15 g/s. This temperature was the approximate upper limit based on safety considerations (severe degradation of material properties due to fluorine attack). Achieving approximately 95 percent conversion back to pure UF_6 using a single reactant in a flowing system at test conditions comparable to those anticipated in rf plasma closed-cycle type tests was considered a significant accomplishment.

RF plasma tests with pure UF_6 injection using the UTRC 1.2 MW induction heater system, a specially designed fluorine supply, preheater, flow control, test chamber, exhaust trap, and fluorine leak detection system, and the on-line T.O.F. mass spectrometer gas sampling system yielded the following results.

1. Employing a nonpreheated fluorine sonic injector system resulted in UF_6 conversion efficiencies, η_c, of about 72 percent at reaction chamber centerline temperatures of $\approx$ 1000 K. Adding additional fluorine through a

porous Monel duct assembly downstream of the sonic fluorine injector/reaction chamber resulted in an additional enhancement to the conversion ($\approx$ 77 percent at 1000 K).

2. Incorporating a fluorine preheater assembly resulted in a η_c enhancement over the temperature range from about 970 K to the maximum tested of 1202 K. At the 1202 K test condition, 88 percent of the total UF_6 initially injected into the rf plasma test chamber was reconstituted back to pure UF_6.

3. A long run time test was conducted operating with both the sonic fluorine injector (preheated fluorine) and the porous Monel duct assembly. After five minutes of operation a complete post-test disassembly, inspection, and chemical analysis of all test components was conducted. The results indicated that for the total mass of UF_6 uniformly injected into the rf plasma test chamber of 11.1 gms, approximately 0.4 g was deposited out on the different components (3.6 percent of the total). The residue deposition per unit area ranged from a minimum of 2 $\mu g/cm^2$ (porous duct assembly) to a maximum of 760 $\mu g/cm^2$ (UF_6 injector assembly). Within the confines of the rf test chamber, 0.0195 g was deposited out. This represents about 0.18 percent of the total mass of UF_6 injected. Future techniques employing porous material for the endwalls of the test chamber could further reduce this level to near zero.

4. Test results obtained using the on-line T.O.F. mass spectrometer/gas analysis system indicated negligible amounts of UF_6 were detected ($<$100 ppm = 0.01 percent) in the axial bypass exhaust duct system. Results obtained using the sampling probe system downstream of the cryogenic cold trap system indicated essentially no UF_6 ($<$50 ppm = 0.005 percent) escaped the cold trap system and subsequently was not entrained in the downstream exhaust gas system. Sampling probe measurements taken at different radial locations of the exhaust duct downstream of the UF_6 regeneration reaction chamber indicated a positive radial concentration gradient of UF_6 was present; stronger concentrations of UF_6 were measured in the annular region surrounding the duct centerline. This could be attributed to a combination of temperature gradient and the mass species/kinetics present at that particular temperature. This data points out the complex temperature kinetics and uranium chemistry occurring in the exhaust system.

5. Separate tests using alternate post-test conversion trap schemes and analysis techniques verified that the UF_6 regenerated was relatively moisture free and agreed to within 2 percent with the theoretical uranium weight percentage.

6. A system design and passivation scheme was established which permitted safe operation with high-pressure, high-temperature fluorine for long test times with minimum corrosion to components of the system. Nickel was used throughout and a rigid chemical cleaning/prepassivation/passivation procedure was followed.

7. Based on separate calorimetric and wall temperature measurements completed throughout this test series, an initial heat transfer analysis was conducted for the key components of the system. This information can be used in future fluorine/UF_6 systems requiring scale-up of the components as applicable to closed-loop uranium plasma reactor and nuclear pumped laser systems.

INTRODUCTION

Uranium nuclear reactors which employ gaseous fissile fuel can be operated at high temperatures. This leads conceptually to power conversion systems for space and terrestrial applications with performance characteristics and thermodynamic cycle efficiencies significantly improved over conventional solid fuel element nuclear reactors. In addition to aerospace propulsion applications, several new space power and/or terrestrial options are being considered, some of which use the direct coupling of energy in the form of electromagnetic radiation. These include laser pumping, photochemical or thermochemical processes, MHD, and advanced closed-cycle gas turbine driven electrical generator systems (Refs. 4, 5, and 6).

The continuous reprocessing of gaseous nuclear fuel also leads to a low steady-state fission product inventory in the reactor and limits the buildup of long half-life transuranium elements. This, together with the low critical mass, could result in increased safety and higher nuclear fuel resource utilization. References 4, 5, and 6 summarize various reactor concepts, designs, principles of operation, applications, and associated performance estimates.

Several principal technologies are required to establish the feasibility of fissioning uranium plasma core reactors: (1) the fluid mechanical confinement of the hot fissioning uranium plasma with sufficient containment to both sustain nuclear criticality and minimize deposition of uranium or uranium compounds on the confinement chamber peripheral walls; (2) a reliable argon/UF_6 handling, injection, reconstitution, and recirculation system applicable to closed-fuel-cycle gas-core nuclear reactor systems.

Figure 1 is a sketch of one unit cell configuration of a plasma core reactor (PCR). The reactor would consist of one or more such cells imbedded in beryllium oxide and/or heavy water moderator and surrounded by a pressure vessel. In the central plasma fuel zone, gaseous uranium (injected in the form of UF_6) is confined by argon buffer gas injected tangentially at the periphery of the cell. Section AA at the bottom of Fig. 1 shows the UF_6 inlet and the on-axis and axial bypass exhaust ducts. The mixture of nuclear fuel and argon buffer gas is withdrawn from one or both endwalls at the axial centerline. In applications in which it is desired to couple thermal radiation from the fissioning uranium plasma to a separate working fluid, the thermal radiation is transmitted through the argon buffer gas layer and, subsequently, through internally-cooled transparent walls to a working fluid channel such as shown in Fig. 1. For other applications, the working fluid channel would be removed and lasing gas mixtures would be mixed with either the uranium fuel or the buffer gas (Ref. 7).

A long-range program plan to establish the feasibility of fissioning gaseous UF_6 and uranium plasma reactors has been formulated by the National Aeronautics and Space Administration (NASA). Reference 8 summarizes the plan which comprises a series of experiments with reflector-moderator cavity reactors. Los Alamos Scientific Laboratory (LASL) is currently performing these experiments in cooperation with UTRC. Integrated into this plan is the demonstration of an argon/UF_6 injection, separation, and recirculation system to efficiently separate UF_6 from argon in a form adaptable to subsequent recycling in the uranium plasma experiment. A review of the past work is contained in Ref. 9.

Performance of static UF_6 critical experiments has been accomplished (Ref. 10). Flowing UF_6 reactor experiments are in progress. Key objectives of these experiments are (1) to facilitate research on gaseous cavity reactor physics, (2) demonstration of optical radiation from fissioning UF_6, (3) demonstration of physical applications of nonequilibrium optical radiation such as nuclear pumped lasers, and (4) demonstration of methods for heat extraction for low proliferation risk power generation and propulsion applications.

Plasma core reactor technology studies at UTRC consist of several experiments and theoretical investigations directed toward evaluating the feasibility of the PCR concept. Reference 11 summarizes some of the past fluid mechanics (nonplasma) experiments. Reference 12 includes test results on confinement of argon rf plasmas. In general, these exploratory test results confirmed that simulated fuels could be confined fluid-mechanically with steep concentration gradients at the edge-of-the-fuel location. Reference 12 summarizes the results of initial laboratory-scale experiments in which pure UF_6 was injected into an argon-confined, steady-state, rf-heated plasma to investigate some of the characteristics of PCRs. Reference 2 summarizes experimental results on developing a primary exhaust system capable of transporting the UF_6 effluent exhaust gas to a downstream trap system with minimum uranium compound wall deposition. The different exhaust systems employed included provision for varying the temperature of the individual endwalls and primary exhaust duct sections, in addition to the use of an exploratory porous exhaust duct assembly (sintered Monel material) incorporating a diluent-bleed radial flow injection of argon. These techniques were effective in aiding to reduce the wall coatings due to uranium compound deposition. The development of complementary diagnostic measurements included both off- and on-line IR spectrometric absorption and T.O.F. mass spectrometer techniques. In selected tests, post-test residue analysis was conducted on the material deposited on the various key components of the test chamber and exhaust system. The overall results demonstrated that operating the test components at a high temperature and using appropriate traps and getters on the inlet gas systems (eliminate sources of contamination) together with auxiliary diluent gas injection significantly reduced the uranium compound coatings on the wall (to

levels of about 0.04-0.4 mg/cm^2, greater than an order of magnitude reduction compared to earlier test results) and thereby make a large fraction of the total UF_6 injected into the test chamber available for recovery/regeneration back to pure UF_6.

Reference 3 summarizes results of tests employing a batch-type fluorine/UF_6 regeneration system. The results of batch-type UF_6 regeneration experiments utilizing UF_4 and other uranium compounds operating at sample temperatures between 300-773 K, indicated total (100 percent efficient) conversion of a 250 mg sample of laboratory pure UF_4 powder to pure gaseous UF_6 was obtained after a five minute exposure to a 1 atm pressure pure fluorine environment. Similar results were obtained using solid test sample residue obtained from the rf plasma exhaust. Also included in these experiments was the development of a system for the safe handling, flow metering, and collection of fluorine and the development of a dedicated on-line exhaust gas constituent monitoring diagnostic system. Included was a complete data acquisition, signal analyzer, and data processing system. These results are considered significant because they demonstrate the feasibility of chemically converting on a batch basis all the nonvolatile test chamber exhaust products to pure UF_6 using a single reactant.

Follow-on tests included using a flowing preheated UF_4/fluorine system (argon dc arc plasma torch) to investigate the effect of temperature and fluorine flow configuration on the UF_4 to UF_6 conversion process. The fraction of UF_4 converted was found to increase to as high as 55 percent as temperatures within the reaction chamber approached 800 K. In some tests, gaseous fluorine was injected into the reaction chamber through a porous Monel duct without degradation of the duct structural properties. These results indicated the option now exists for future tests wherein a very large fraction of the total UF_6 injected into the rf plasma test chamber may be continously converted to pure UF_6 using a flowing gaseous fluorine system. Another significant result from these tests was obtained using the T.O.F. on-line exhaust gas sampling system: negligible concentrations (<100 ppm) of UF_6 were detected in the axial bypass duct. This provided a quantitative on-line measurement of the effective uranium confinement characteristics of the vortex flow employed in the plasma test chamber.

This research report presents results of the continuing rf-heated uranium plasma experiments using a flowing high-pressure, high-temperature fluorine system to regenerate on-line, pure UF_6 from the effluent uranium compounds in the plasma exhaust. The dedicated on-line T.O.F. gas sampling system was used to determine the overall efficiency of the system. These results will aid in establishing the reliability of a hot, pressurized UF_6 handling and regeneration system that is applicable to future closed-cycle UF_6 PCR experiments.

DESCRIPTION OF PRINCIPAL EQUIPMENT

Fluorine Test Facility for UF_4/F_2 Flowing UF_6 Regeneration Tests

Figure 2 is a schematic of the components used in the flowing high temperature UF_4/F_2 to UF_6 regeneration tests. The main components, shown by the dashed outline in Fig. 2, are (1) the fluorine supply with vent and nitrogen purge system, (2) the large vacuum test tank, remote control fluorine flow control system, argon dc arc plasma torch, and reaction chamber system, and (3) the UF_6 regeneration/cryogenic exhaust trap system.

Figure 3 is a photograph showing the overall fluorine test facility. For personnel safety, the fluorine test tank, reaction chamber test section, and exhaust gas system were located within a separated sealed and ventilated test cell. The tests were conducted from the remote master control console shown on the left in Fig. 3. This console also contained the fluorine leak detection and alarm systems. The entire test tank was maintained under vacuum during the tests and was vented to a large spherical vacuum chamber located outside the laboratory, allowing rapid scavenging of the test gases in the event of a component failure. The large (1.5-m-dia) dome to the test tank is shown removed in Fig. 3 to better illustrate the location of the test section. The cryogenic exhaust/trap system is shown located to the left of the fluorine test tank.

Figure 4 is a photograph of the test components located within the steel vacuum tank. The main components were (1) the fluorine supply and flow metering system, (2) the UF_4 powder feeder system, (3) the dc arc plasma torch system, (4) the fluorine injection manifold and reaction test chamber, (5) the uranium compound cryogenic trap system, and (6) the post-test UF_6 regeneration/conversion trap system.

As illustrated in Fig. 2, the main fluorine supply was located outside the laboratory. A fluorine pump system was used to transfer and pressurize the laboratory fluorine cylinders. A flow metering venturi was designed and fabricated to measure the fluorine injection flow rate. An optional in-line NaF trap was provided to remove HF impurities from the fluorine supply. The fluorine vent system went through a charcoal trap prior to being discharged to the laboratory roof.

To provide a uniform and controlled feed of UF_4 powder, a powder feeder system used in a previous NASA research program (Ref. 12) was modified for use in these tests. The feeder operated on a volumetric feed/entrained flow principle. Prefiltered argon gas was used as the carrier in all tests. The feeder was adapted to the plasma torch system (see Fig. 5) to provide a

positive feed at repeatable rates (typically 0.15 g/s). Laboratory pure UF_4 powder ranging in size from about 10-100-μm-dia was used. A deagglomerator was located downstream of the UF_4 feeder to prevent the UF_4 seed material leaving the feed canister from reagglomerating; it also acted as a pulsation damper. For seed mass flow calibration purposes, a ball valve was used downstream of the deagglomerator to allow the seeded stream to be directed into either the plasma torch chamber or a seed collection system (for determination of time-averaged seed flow rate.

The plasma torch, shown at the far right in Fig. 4, provided the high temperature argon plasma stream into which the UF_4 powder was injected. The basic plasma heater system consisted of the argon dc arc plasma torch, high-frequency starter, dc power supply, master control console, and associated water cooling and gas flow systems. The torch was a modified commercial plasma torch (Thermal Dynamics H-50). The torch contained a water-cooled thoriated-tungsten pin cathode and a hollow water-cooled cylindrical anode. To aid in maintaining sputter-free operation, prepurified argon gas was fed into the annulus between the two electrodes. The arc was ignited using a 15 kHz, high-voltage (18 kV peak-to-peak) starter system. Immediately upon ignition, the starter was deactivated and the argon flow and arc current level were adjusted to provide the desired test conditions. The current to the torch electrodes was adjusted by varying a power-control reheostat. The torch master control console contained all the necessary control operating components, electrical meters, and flow metering system. Immediately downstream of the plasma torch was a nickel mixing plenum. Downstream of the plenum was a 15-cm-long x 1.6-cm-ID nickel inlet section which was connected to the fluorine injector manifold.

Figure 6 is a schematic which illustrates the fluorine injection assembly used in the tests. This fluorine injection assembly was designed and fabricated of Nickel 200 (selected based on its resistance to corrosion by UF_6/F_2 at elevated temperatures). As shown in Fig. 6, the assembly could utilize several injector ring configurations which can be used individually or in combination within the manifold to provide various flow patterns. Included were swirl flow, straight radial injection, and radial injection with a 30 deg upstream component. This assembly permitted injection of controlled amounts of fluorine ranging from approximately 0.1-0.3 g/s. A 30-cm-long by 1.6-cm-ID Nickel 200 reaction chamber was located downstream of the reaction chamber on the centerline location to provide an on-line measurement of the exit temperature. A pressure transducer was used to monitor the pressure in the reaction test chamber. Cooling and seal modifications were made to the plasma torch system, the nickel mixing plenum section, and the downstream nickel reaction chamber to permit operation for extended time periods at the relatively high temperatures. All the components fabricated from Nickel 200 were chemically cleaned prior to passivation with fluorine.

As shown in Fig. 5, the cryogenic trap system was located downstream of the reaction chamber, but outside of the fluorine test tank. Two cryogenic trap systems were employed, as shown in Fig. 2: one used liquid argon and the other used liquid nitrogen. The liquid nitrogen system was used to convert the UF_6 that was generated in the reaction test chamber and subsequently trapped in the upstream liquid argon trap to sodium metauranate (Na_2UO_4) for post-test analysis. The following equation describes the net reaction: $UF_6+8NaOH \rightarrow Na_2UO_4+6NaF+4H_2O$. For this net reaction, the following two sub-reactions are also involved: $UF_6+4NaOH \rightarrow Na_2UO_4+4HF+2NaF$ and $4HF+4NaOH \rightarrow 4NaF+4H_2O$. The traps were isolated from one another by appropriate valves, as shown in Fig. 2. The effluent exhaust trap system was sized to permit quantitative determination of the amount of UF_4 converted to UF_6. To reclaim the UF_6 from the UF_6/argon cold trap, its temperature was raised (using a heat gun) to slightly above 373 K. The complete recovery and post-test procedure was conducted slowly since the reaction of the desorbed UF_6 with sodium hydroxide solution (1.9 Molar) produced a brilliant yellow precipitate and some HF vapor. The yellow precipitate (Na_2UO_4) formed upon the reaction of the UF_6 with sodium hydroxide solution was highly insoluble and was readily filtered, washed, dried, and weighed. The thoroughly washed precipitate was oven dried at 350 K and accurately weighed on an electronic balance prior to any post-test chemical analysis to determine uranium content. From the post-test chemical analysis, the equivalent mass of UF_6 was readily calculated.

Fluorine Preheater Assembly Used in UF_4/F_2 Flowing UF_6 Regeneration Tests

Figure 2 shows the location of the fluorine preheater assembly used in the UF_4/F_2 flowing UF_6 regeneration tests. Figure 7 is a schematic of the fluorine heater. The preheater unit was of welded nickel construction and was capable of providing a continuous flow of up to approximately 0.25 g/s of fluorine at temperatures up to approximately 1200 K. This preheater was designed to permit investigating the effect of fluorine atoms (F) on the UF_4/UF_6 conversion process. The system was fabricated from electrolytic grade Nickel 200; the 200 type is the most resistant to fluorine attack at elevated temperatures. The core of the heater is shown in view A-A of Fig. 7. It consisted of a cylindrical bar of Nickel 200, 3.1-cm-dia, with a series of six parallel slots (each slot 2.5 mm x 1.1 mm) equally spaced along a diameter of the bar. The entire assembly was carefully welded, x-rayed, and pressure checked at 50 atm.

The heater core (8-cm-dia by 1-m-long) was surrounded by a Lindberg Model 50042 electrical resistance heater assembly rated at 2.8 kW and capable of continuous operation at temperatures up to approximately 1475 K. The resistance heater was powered by a 220 V variable power supply. Because of

the high heat losses associated with operation of this type heater at the high temperatures, a radiation heat shield was fabricated (see Fig. 7) that completely surrounded both the heater assembly and the adjacent fluorine injection manifold. To further reduce the heat losses when operating under nonvacuum conditions, Fiberfrax insulation material was also placed around the heat shield. Prior experience in tests with fluorine has revealed that sharp bends in transfer lines, surface irregularities, or sharp edges can become focal points for fluorine attack; therefore, smooth, large radius turns were used throughout the entire system. An example is the smooth 90 deg bend connecting the exit of the heater to the injection manifold as shown in Fig. 7.

Figure 8 is a photograph of the test components used in the flowing high temperature UF_4/preheated fluorine to UF_6 regeneration tests. The Fiberfrax insulation material is visible surrounding the fluorine preheater. The preheater assembly was instrumented with thermocouples at several locations, including a thermocouple to measure the flowing fluorine gas temperature within the injection manifold. Shakedown calibration tests with the heater were conducted using nitrogen as the simulated reaction gas; the results of these tests indicated the design flow rates and temperatures could be achieved. From calibration tests, it was determined that about 2½ hours was required for the heater to reach a complete equilibrium temperature of about 1200 K with approximately 1.6 kW input power to the heater core. Heat sinking to adjacent components and connecting lines was the most significant factor in the long heat-up time. These heat transfer results were in agreement with complementary analytical heat transfer estimates of the system. Extreme caution was exercised in conducting all the follow-on hot flow tests with pure fluorine due to potential material property limits of nickel at elevated temperatures in the presence of fluorine.

The literature (Ref. 13) indicates unalloyed nickel to be the best common metal or alloy capable of withstanding a high temperature fluorine environment. It is limited to temperatures below about 1200 K because of severe loss in strength and the onset of extensive chemical attack (Ref. 14). The onset of nickel corrosion as temperature is increased appears to be caused by the breakdown of the nickel fluoride film formed initially at low temperatures. Because of this, a complete chemical cleaning followed by an extensive fluorine passivation (statically prepassivated with pure fluorine at room temperature for one hour at 7.5 atm) was used prior to the tests using the preheater with high temperature pure fluorine. In addition, electron beam welding was used on the assembly joints to alleviate the requirement for seals which would degrade under exposure to high pressure, high temperature fluorine. The entire preheater assembly was suspended in a cradle assembly to allow for the effect of thermal expansion.

To provide an indication of the type of corrosive attack generated by preheated fluorine, an exploratory test series was conducted using a mockup of the nickel preheater assembly and inlet feed line. The special Nickel 200 tubing designated for use at the inlet to the fluorine preheater, due to shipment delay, was replaced with a 4.6-mm-ID stainless steel 304 tube (375 μm in wall thickness)(see sketch at top of Fig. 9). The complete preheater assembly was located in the large vacuum test tank (see Fig. 8) and connected to the fluorine feed supply. The heater assembly was operated at temperatures of about 1000 K and exposed to the fluorine environment for controlled test times of about three hours. After several such tests, detailed inspection of the inlet region revealed a circumferential crack in the stainless steel near the interface between the stainless steel inlet line and the main body of the fluorine preheater (see fig. 9). Several cross section cuts were made of the assembly to determine the degree of attack. The results are illustrated in the three photomicrographs in Fig. 9. The results indicate that in the lower temperature region away from the main heater, no corrosion occurred. At the higher temperature region near to the failure, distinct grain boundary attack is evident. At the failure region, a distinct bulk diffusion failure mode at the interface was found. The rate of corrosion for the stainless steel 304 in the failure region was determined to be approximately 10^3-$5x10^3$ μm/hr. This information emphasized why nickel material was selected for all components where high temperature fluorine is used.

A heat transfer/flow analysis of the fluorine preheater assembly was also completed, including parametric calculations of the mole fraction of fluorine atoms (F) available for the UF_6 regeneration as a function of temperature and pressure. For reference, at a temperature of about 1000 K and fluorine atom (F) pressures of 0.05 atm (typical of operating regime in these experiments), the mole fraction of F atoms present is about 40 percent.

Fluorine Test Facility Used in Flowing High-Temperature UF_6 Regeneration Tests Conducted in 1.2 MW RF Uranium Plasma Facility

Figure 10 is a schematic of the fluorine supply, flow control, and trap system that was designed, fabricated, and installed at the 1.2 MW rf uranium plasma test facility. The system incorporates many of the features and techniques developed in the flowing fluorine/UF_6 regeneration tests using the dc plasma torch system (see prior discussion). The major components included (1) the fluorine supply, enclosure vessel, and charcoal trap system located outside the rf uranium plasma laboratory, (2) the jacketed trough for safely routing the main fluorine supply line to a location adjacent to the exhaust section of the rf plasma test configuration, (3) calibrated venturis and pressure monitoring equipment located within a secondary sealed chamber, (4) a portable remote master control console including switches, interlocks,

and activation/warning lights, (5) a fluorine leak detection/alarm system, and (6) a stainless steel vessel containing two main compartments: in one compartment was located the fluorine preheater assembly, the fluorine sonic injection manifold, and the reaction/UF_6 regeneration test chamber; in a lower compartment was a dual cryogenic trap system and the corresponding set of post-test UF_6 conversion cold trap systems.

As shown by the dark lines in Fig. 10, several interconnected but isolated and sealed aluminum and stainless steel chambers were used to contain the fluorine system. The fluorine was supplied from two cylinders located outside the laboratory test area. Each cylinder was pressurized to 28 atm and contained a maximum of 2.2 kgs of fluorine. The maximum fluorine pressure used inside the laboratory, based on safety considerations, was always limited by pressure regulators to a maximum of 7 atm. Pressure regulator 1 (see Fig. 10) controlled the fluorine flow through the flow metering venturi, preheater assembly, and sonic injection manifold. Pressure regulator 2 controlled the fluorine flow through a second flow metering venturi and the porous Monel duct assembly (when in use). A burn wire was installed on all the fluorine transfer lines; any failure or break in the line or burn wire automatically closed the main fluorine valve and activated a high flow of nitrogen gas purge through the entire system. During all tests, the fluorine preheater assembly enclosure was normally kept under vacuum.

During the design phase, considerable effort was directed to the various safety aspects of the fluorine gas-handling, supply systems, components, and detection systems. The fluorine supply cylinder was stored in a steel enclosure with provision for nitrogen gas purge through a charcoal trap should a leak develop in the gas cylinder or shutoff valves. An additional safety feature was the fabrication of a double-walled supply line which had a constant flow of nitrogen purge gas between the fluorine-carrying line and the atmosphere. The double-walled line was also vented to atmosphere through a charcoal trap which would react with any fluorine to produce a nontoxic gas. All the additional enclosures shown in Fig. 10 were also under constant nitrogen purge and vented through the trap. To further ensure the safe handling of the fluorine gas, remote detectors were located at five critical locations in the system (see the starred locations in Fig. 10). Figure 11 is a photograph of the fluorine leak detection/alarm system that was designed, fabricated, and installed adjacent to the 1.2 MW rf plasma test tank. This fluorine detection system was connected to an automatic alarm to allow instantaneous indication should a hazardous condition develop. The system was calibrated prior to the hot flow test series and was capable of detecting concentrations of fluorine of 0.5 ppm (0.00005%). Upon activation, the system was designed to automatically close all the main fluorine feed valves and initiate a full nitrogen gas purge to all components. In prior UF_6 regeneration tests using the dc plasma torch facility and the UF_4/F_2 system, the entire fluorine test tank,

reaction chamber test tank, and exhaust gas system were located within a separate sealed and ventilated test cell. This was not possible to do in the tests using the 1.2 MW rf uranium plasma test facility; therefore, because of the presence of hot, pressurized fluorine in the immediate vicinity of personnel with the rf laboratory test area, considerable effort was directed, as evident from the preceding discussion, to the safety aspects of the fluorine supply, transfer, metering, and detection system.

Figure 12 is a photograph of the assembled components within the fluorine test chamber. (The stainless steel top cover was removed in Fig. 12 to show the components.) The interface seal assembly, which connects the exhaust system from the 1.2 MW rf uranium plasma test chamber to the fluorine test chamber is shown located in the upper portion of the test chamber. The fluorine sonic injection manifold assembly was an integral part (welded) of the exhaust system and is shown in the lower right portion of Fig. 12. It was also surrounded by a radiation heat shield. Immediately downstream of the injection manifold assembly was the nickel reaction chamber (1.6-cm-ID x 33-cm-long). To permit continuous monitoring of the temperature of the key components, thermocouples were located within the fluorine test chamber. One thermocouple was located on the centerline of the exhaust duct immediately downstream of the regeneration chamber (see Fig. 12). This was the key reference temperature used in the fluorine/UF_6 regeneration tests.

The cryogenic trap system and post-test UF_6 regeneration conversion trap system were located in a separate sealed chamber below the main fluorine test chamber. Figure 13 is a photograph illustrating the location of the key components. (Not shown is the front cover plate and seal assembly used to isolate this chamber from the main fluorine chamber.) A dual parallel trap system was used. This permitted conducting two different tests within a given hot flow test series and/or to provide backup in the event one trap system clogged, or malfunctioned due to improper control valve sequencing. The liquid argon traps were designed with sufficient heat sinking capability to permit continuous hot flow testing for time intervals up to about ten minutes. The two liquid nitrogen post-test conversion traps shown in Fig. 13 incorporated an improved design. An earlier version used a completely closed collection vessel which contained 9.0 Molar NaOH solution used to convert to Na_2UO_4, the UF_6 that was cryopumped into the vessel from the liquid argon cold trap. The present design permitted slowly adding controlled amounts of the basic solution from outside the trap assembly. Separate tests have shown this was necessary to reduce the possibility of contamination and surface reactions within the trap.

At the downstream end of the nickel reaction chamber, provision was made to interface with either an additional 1.6-cm-ID nickel exhaust duct or a porous Monel (approximately 5 μm-dia nominal pore size) duct assembly. Figure

14 is a photograph of the porous Monel duct assembly used in selected tests. (Refer to Ref. 2 for additional details on the porous duct design, material properties, and operating characteristics.) In selected prior tests (Ref. 2) employing a similar porous duct assembly with argon transpiration flow, the absolute level of uranium compound residue found on the surface of the duct in post-test analysis was reduced approximately three (3) orders of magnitude (to typically hundreds of microgram range --- equivalent to about 3 $\mu g/cm^2$ of exposed surface). In future closed-loop PCR systems, this technique may significantly reduce wall coatings and, consequently, minimize the complexity of the exhaust gas reprocessing systems.

Basic RF Plasma Test Chamber Configuration

Figure 15 is a sketch showing a simplified cross section of the basic rf plasma test chamber configuration employed in the rf plasma/UF_6 reconstitution tests. The selection of this configuration was based on the test results reported in Ref. 1; several desirable features were incorporated in this configuration which included the ability to independently vary the distribution of exhaust gas flow (axial bypass). The peripheral wall was comprised of a concentric set of water-cooled fused-silica tubes. The argon vortex was driven from the right endwall only by a set of vortex injectors located tangent to the periphery of the endwall. The axial distance between endwalls was 10 cm. The rotationally symmetric rf argon plasma was initiated using a vacuum start technique to eliminate possible contamination. The rf power was coupled into the plasma via a pair (9-cm-dia) single turn, water-cooled silver plated work coils. Each coil was connected to a vacuum capacitor array; two arrays of ten vacuum capacitors each comprised the entire resonator section. (Refer to Ref. 1 for a detailed description of the rf induction heater system.) The rf operating frequency used in these experiments was approximately 5.4 MHz.

To inject the pure UF_6 into the rf plasma, a UF_6 injector assembly was located on-axis and concentrically within the right endwall. It was fabricated from a 50-cm-long three concentric copper tube assembly. The injector tip protruded 2 cm into the test chamber from the face of the endwall. High pressure water heated via a steam heat exchanger system was used to control the temperature of the injector, thus eliminating any solidification of UF_6 in the injector transfer lines. Reference 1 contains additional details of the UF_6 supply and transfer system used in these tests to provide the controlled and steady flow of heated UF_6 at temperatures up to about 450 K.

Diagnostic Equipment Used in Exhaust Gas Analysis

Figure 16 is a photograph containing the custom built ruggedized T.O.F. mass spectrometer system used in the exhaust gas sampling tests. In this photograph it is shown located adjacent to the rf uranium plasma test tanks (front dome removed) and the fluorine test chamber. Refer to Ref. 2 for a detailed description of the unique design, operating characteristics, and calibration procedures of this diagnostic tool and the associated data acquisition reduction system. Partially visible in Fig. 16 is the vacuum system comprised of the 10-cm-dia diffusion pump with high speed valves and baffles to provide a net flow of 400 ℓ/s. On the top is shown a portion of the electronic subsystem, ion source, and inlet system (cover plates installed), the flight tube and instrumentation for the detectors and focusing grids. Incorporated is a cryopumped ion source cold finger method system and fabricated to reduce drift tube and detector contamination by UF_6 and related halogenates. Figure 17 is a photograph showing the remote master control console (remote operation up to a distance of about 7 m) and data system developed for use with the T.O.F. system for the UF_6 exhaust gas analysis tests. The main components were a Northern Scientific NS575A signal averager and a seven-track magnetic tape system. Figure 18 is a schematic of the exhaust gas sampling, data acquisition, and data processing system as used in the exhaust gas analysis experiments. A 0.5 ℓ Monel canister containing filtered UF_6 was used to calibrate the instrument. The UF_6 data obtained with the signal averager and recorded on the seven-track magnetic tape was, in turn, transferred and processed on a PDP-6 computer system using a previously developed UTRC spectral data reduction program. As shown in Fig. 18, several 1-mm-ID Nickel sampling probes were used to extract samples of the effluent exhaust gas during the hot flow tests with pure UF_6 and fluorine injection. A sampling probe was positioned at three different locations: (1) on the centerline of the axial bypass exhaust duct just downstream of the rf plasma test chamber; (2) on the centerline of the exhaust duct downstream of the liquid argon cold trap; and (3) on a traversible assembly located in the main exhaust thru-flow duct immediately downstream of the porous Monel duct assembly. (See Fig. 19 for a photograph of this traversible T.O.F. sampling probe assembly removed from the exhaust duct system -- see Fig. 18 for a schematic of the relative location of the sampling probes). The sampling line lengths were made as short as possible to enhance the response time of the system. Electric resistance heater tape was wrapped around all the nickel transfer lines and maintained at approximately 450 K to eliminate possible condensation of the gaseous uranium compounds on the walls. All the nickel transfer lines in the entire system were prepassivated with pure fluorine (7.5 atm for one hour at room temperature) prior to introduction of UF_6.

Diagnostic Instrumentation Used in Analysis of Post-Test Uranium Compound Residue

Several different complementary diagnostic methods were used in the post-test residue analysis for identifying and quantifying the small amounts of uranium compounds deposited onto the different components of the test chamber, exhaust gas, and trap/regeneration systems. These techniques included the use of the electron microprobe, scanning electron microprobe, IR spectrophotometer, ion scattering spectrometer, secondary ion mass spectrometer, and photoacoustic spectrometer. Refer to Refs. 1 and 2 for additional details on this diagnostic instrumentation and methods of operation. Also included in Ref. 2 is the extended compilation of uranium compound reference standards used in these tests and for future post-test residue compound identification. The majority of these standards included the uranium-oxygen-fluorine compounds, laboratory prepared uranium compounds, and samples of residue actually removed from different test configuration components. The documented IR absorption spectrum were obtained using an IR spectrophotometer system.

DISCUSSION OF RESULTS

The overall objective of this research effort was continued development of UF_6 injection, confinement, handling, and reprocessing open-cycle systems applicable to the rf-heated uranium plasma experiments. Successful design and operation of such a system would provide a basis for the scaled up design of UF_6 handling, reprocessing, and recirculation systems directly applicable to future high temperature cavity reactor experiments. These experiments are directed toward establishing the feasibility of future closed-cycle gaseous-fueled nuclear reactors. Some of the technology is also applicable to nuclear pumped laser systems. In the results reported herein, particular emphasis has been placed on the UF_6 regeneration aspects using a flowing, high-temperature, high-pressure fluorine system, including the application of on-line exhaust gas sampling diagnostic techniques. Simultaneous with the above has been the requirement to maintain the test chamber and exhaust duct systems relatively free of uranium compound deposition.

Test Results Using DC Plasma Torch System With Flowing UF_4/Fluorine for UF_6 Regeneration (No F_2 Preheat)

A series of tests were conducted using the test facility described in the "Description of Principal Equipment" section. Refer to Fig. 2 for a schematic of the system and Fig. 3 for a photograph of the overall facility. These tests were directed toward investigating the potential for converting, on-line, solid UF_4 (the major uranium compound constituent in the plasma exhaust duct) to gaseous UF_6 using flowing fluorine within a reaction test section. Previous test results (Ref. 3) employing a static batch-type UF_4/F_2 system indicated conversion efficiencies, η_c, (defined as the fraction of solid UF_4 converted to gaseous UF_6) up to 100 percent were achieved. This result was considered significant because it demonstrated the feasibility of chemically converting on a batch basis all the nonvolatile exhaust products to UF_6 using a single reactant. Temperatures >650 K, fluorine pressures of 1 atm, and residence times of 0.2-5 minutes were required to achieve these high conversion efficiencies. Higher temperatures were required to affect complete conversion if the sample residue contained other uranium compounds representative of those found in the exhaust of the rf uranium plasma system (e.g., UO_2F_2, UO_2). The majority of tests in the flowing system were conducted at operating conditions similar to those anticipated in the rf uranium plasma exhaust system; thus a test matrix could be established to determine the effect of temperature (dominant parameter determined from prior tests) on the overall UF_6 conversion efficiency.

The results of exploratory tests indicated the importance of reducing all sources of impurities and the requirement to adequately passivate all systems with pure fluorine prior to initiation of the hot flow tests. An example of the measured conversion data is shown in Fig. 20. TABLE I contains a summary of the range of test conditions. No fluorine preheat was employed in any of these tests. For reference, prior regeneration test results obtained using a standard configuration (Ref. 3) are shown by the circle symbols. In these exploratory tests, a maximum conversion efficiency of approximately 55 percent was achieved at a centerline reference temperature of about 880 K. No conversion was noted at temperatures less than about 650 K. In all tests using the fluorine sonic injection assembly and improved UF_6 conversion trap, a fixed test time of 20 s was used. The test conditions were comparable for the prior tests with the exception of the dc plasma torch input power and UF_4 argon carrier feed rate; these were adjusted to achieve the higher temperatures at the centerline exit of the reaction chamber. The fluorine flow rate was maintained constant at 0.2 g/s; the reaction chamber pressure was 1.5 atm. Note that at these conditions, an excess of fluorine gas was present based on stoichiometric equilibrium calculations ($\approx$10X based on mole fraction). This was preselected to enhance the conversion in the event that the bulk mixing was not as efficient as estimated (an overkill of fluorine was used).

As in prior regeneration tests (reported in Ref. 3), the amount of UF_6 regenerated was determined from post-test analysis of the mass of Na_2UO_4 formed from the UF_6 transferred into the cryogenic NaOH conversion trap (see Figs. 2 and 5). Separate absorption measurements using an IR spectrophotometer were used to verify purity level; post-test chemical analysis was also used to determine the uranium weight percent of Na_2UO_4. The triangle symbols illustrate the effect of increasing temperature on conversion efficiency. The highest conversion efficiency achieved was approximately 78 percent and occurred at a centerline temperature at the exit of the reaction chamber of 990 K.

As noted in Fig. 20, for the tests conducted at centerline reference temperatures of approximately 925 K, H_2O contamination was present (confirmed by the dominance of UO_2F_2 in the exhaust system during post-test examination). Several attempts to eliminate this impurity were unsuccessful; therefore, the entire system, including the dc arc plasma torch assembly was disassembled and all O-rings, seals, and water cooling connections were replaced. The argon supply was also replaced with a new purified argon supply bottle. The source of the contamination was attributed to a defective seal in the torch water cooling system; these results served to indicate the pronounced effect impurities have on the UF_6 regeneration reaction. If extrapolated, these results indicate that using the given configuration but employing a fluorine preheater system and operating the plasma torch system near to its highest power level limit may permit achieving flowing on-line UF_4/fluorine to UF_6

conversion efficiencies within the 90-100 percent range at reference centerline temperatures of about 1100-1200 K.

Test Results Using DC Plasma Torch System With Flowing UF_4/Preheated Fluorine for UF_6 Regeneration

Using the test configuration shown in Fig. 2 and including the use of the optional fluorine preheater assembly shown in Fig. 7, a follow-on set of tests was conducted. It was anticipated that operation at centerline reference temperatures above about 1000 K should produce enhanced conversion efficiencies. However, at temperatures of about 1000 K or greater, severe degradaon of material properties due to fluorine attack can occur. The severity of attack is influenced by many factors: temperature, pressure, fluorine species present, reaction time, contamination, surface coating, material composition, and prepassivation. Available information is very limited on the detailed corrosion rates for the various fluorine species present over the wide range of operating conditions employed in these tests. Therefore, extreme care was taken to insure safety in all tests operated in the higher temperature regime (>950 K). Refer to Ref. 2 - Appendix A for an additional discussion and supporting information on the corrosion/contamination aspects of UF_6 and associated reactant species.

Based on the results of exploratory tests using the different fluorine injector manifolds (see Fig. 6), a final manifold design was selected for use with the preheated fluorine which contained twenty-four (0.1-mm-dia) orifices uniformly spaced around the circumference of the injection ring. The orifice sonic flow was directed radially inward toward the duct centerline axis. To verify system integrity and to calibrate the venturi flow meter system, a set of calibration tests were conducted using nitrogen as the reactant gas. Concurrently, a series of tests were conducted to verify the reproducibility and efficiency of the post-test cold trap collection procedure. This procedure was used to determine the quantitative conversion efficiency values.

Three different uranium compounds, including uranyl fluoride (UO_2F_2), uranyl sulfate ($UO_2SO_4 \cdot 3H_2O$), and uranyl nitrate ($UO_2(NO_3) \cdot 6H_2O$), were tested using the same operating procedure as when the standard reference Na_2UO_4 was used. Using the same post-test analysis procedures (including 9.0 molar NaOH solution, oven dried filter paper, and sequenced drying and washing with 300 mℓ distilled H_2O), the overall collection efficiencies agreed within 2 percent. Following this sequence, chemical analyses were performed to determine the moisture content that may be present in the sodium metauranate (i.e., $Na_2UO_4 \cdot xH_2O$). Both Differential Scanning Calorimetry (DSC) and Differential Thermal Analysis (DTA) tests of the residue indicated very small amounts (negligible) of moisture.

Prior to conducting the set of hot flow tests with the fluorine preheater, a set of calibration measurements were also conducted. A water-cooled calorimeter assembly and several sets of thermocouples attached to the walls of the main test components at different axial locations were used to determine the power losses from the different components of the system at different stations downstream of the plasma torch. Figure 21 is a schematic illustrating the key components. This information was used in the supporting flow and heat transfer analysis summarized in APPENDIX A.

As illustrated in Fig. 22, of the total of twenty-six tests completed, eleven were conducted using the fluorine preheater assembly. TABLE II is a summary of the operating ranges. The two square symbols shown correspond to two additional no-preheat fluorine tests, at exhaust temperatures greater than 1000 K. The improved UF_6 conversion trap was employed in these tests along with additional plasma torch modifications. At an exit centerline temperature of 1070 K, the conversion efficiency was extended to 82 percent. The solid diamond symbols correspond to the tests employing the fluorine preheater. With the fluorine preheater assembly operating at about 900 K ($\leq$40 percent F atoms present at a fluorine species pressure of about 0.05 atm -- see Fig. 23) an approximate 10 percent enhancement in the conversion efficiency was noted in the temperature range of about 950-1000 K. This enhancement is believed to be partly due to the highly reactive F atoms in the injected gas. Two key factors are influential in determining the rate of conversion of the UF_4 to UF_6 due to either the F_2 or F. One is the reaction rate of the particular species (rate constant, k, for F > rate constant k_1, for F_2) and the other is the diffusion rate (i.e., bulk mixing) of the particular species. The diffusion rates are proportional to the square of the molecular weights; therefore the rate for F is about 1.4 times faster than for F_2. Both these factors are present and in this particular test configuration both would tend to increase the rate of conversion within a given test time (or test chamber reaction length). A detailed analysis beyond the scope of this program, involving considerable complex uranium chemistry, and be required to quantify these effects.

At 1108 K, a conversion efficiency of 93.9 percent was reached; extending the temperature to the maximum possible with the existing equipment (power supply operated at overload) resulted in a conversion efficiency of 94.8 percent which corresponded to an exit centerline temperature of 1180 K. A post-test uranium weight percent analysis of the Na_2UO_4 obtained for several of these high conversion efficiency tests indicated agreement to within 3 percent of the theoretical expected value of 68.3 percent.

These test results are considered significant and indicate that using a flowing hot fluorine/UF_6 regeneration system, conversion efficiencies approaching 95 percent can be achieved with reaction temperatures in the 1000-2000 K

range and residence times within the reaction test chamber of typically tens of milliseconds.

Test Results Using 1.2 MW RF Uranium Plasma Facility With Flowing High-Temperature Fluorine/UF_6 Regeneration

Figure 10 is a schematic of the components used in the 1.2 MW rf uranium plasma tests using flowing fluorine for UF_6 regeneration in the open-cycle exhaust duct system. The results of the tests are illustrated in Fig. 24. The measured conversion efficiency, η_c, is shown as a function of the reference centerline temperature measured at the exit of the 33-cm-long nickel reaction chamber. TABLE III is a summary of the operating conditions corresponding to these tests. In all tests the rf was operated at a frequency of about 5.42 MHz. This was selected based on prior test experience that indicated good coupling and a relatively stable discharge. (For reference, the unloaded resonator frequency was approximately 5.40 MHz for this test series.) As can be seen in Fig. 24, at the relatively low reaction chamber exit centerline temperatures of about 900 K, approximately 50 percent conversion efficiency was achieved. The majority of the tests in this temperature regime were conducted for a test time of about five minutes. At an exit centerline temperature of about 940 K, a set of tests was conducted on two separate days to determine the degree of reproducibility for comparable test conditions. The data for these tests indicate good reproducibility was achieved. For a higher test temperature of 970 K, a test (#6) was conducted using preheated fluorine. A slight enhancement ($\approx$9 percent) was noted. As in the prior tests conducted with the plasma torch system, the conversion efficiency enhancement was achieved with the inclusion of the added safety aspects associated with operating fluorine at high preheat temperatures. In all the fluorine tests conducted in this program, only one safety related problem occurred. This involved an automatic activation of the fluorine detector alarm system followed by an emergency shutdown procedure; simultaneous with this was the automatic activation of the fast nitrogen purge. The entire emergency shutdown procedure occurred with no complications. Post-test inspection revealed that during the reassembly procedure for that particular test, additional silicon rubber sealant was used on one of the fluorine tank enclosure gaskets and had not completely cured. The vapors emitted under the high temperature operation were sufficient to trigger the remote fluorine detection sensor.

At this time, it is not clear if the preheated fluorine approach is warranted. However, in a still higher temperature regime within the reaction test chamber and for the relatively short residence times of these tests (order of tens of milliseconds), preheating the fluorine may have a more pronounced effect when both the higher reaction rate and diffusion rate of fluorine atoms (F) relative to fluorine molecules (F_2) is taken into account.

From this aspect, no experimental data were found in the literature and little, if any, rate constant data are available in this range of test conditions.

To determine the effect of injecting fluorine (nonpreheated) at the downstream porous duct location, both with and without fluorine being simultaneously injected through the sonic injection manifold system, two additional tests (Nos. 8 and 10) were conducted. The effect of introducing the additional 0.322 g/s of fluorine at the downstream porous duct location increased the conversion efficiency from 72 percent to 78 percent; a possible indication that complete mixing of the fluorine with the uranium compounds had not taken place at the entrance to the porous duct assembly particularly in the boundary region within the penetration depth of the fluorine flow. A very distinct drop in conversion efficiency was noted for case #10 which employed the porous duct only. An approximate factor of two (2X) reduction in conversion efficiency occurred, thus indicating that insufficient mixing occurred at the downstream location even though the reference temperature for this case was 50 K higher than in the prior test case. This minimal degree of penetration was illustrated in APPENDIX B of Ref. 2 which showed that the diffusion of uranium compounds toward the wall of the porous duct can be counter-balanced by the radial transpiration injection of argon bleed gas through the porous wall (≤ 20 percent penetration at relatively high mass flow rates).

To verify that regeneration, back to the pure UF_6, of the uranium compounds in the exhaust occurs within the duct and not during a post-test reaction with residue material on the wall reacting with fluorine, a separate controlled test was conducted. The result is illustrated as test #9 in Fig. 24. A negligible amount of UF_6 was detected in the cryotrap system. This test was conducted at a reference temperature of 1020 K and immediately after a prior argon/UF_6 only test wherein no post-test disassembly/residue removal was conducted.

The final two data points shown in Fig. 24 illustrate the effect of fluorine preheat on the conversion efficiency with corresponding reference centerline temperatures up to a maximum of approximately 1200 K. Based on safety considerations, this was determined to be the maximum fluorine preheat permitted within the constraints of this apparatus and range of test conditions. For test case #12, a maximum conversion efficiency of 87.6 percent was achieved; the corresponding test time was five minutes. TABLE III contains a summary of the corresponding test conditions for all the tests. Refer to APPENDIX A for a supporting analysis of the heat and mass transfer aspects of the uranium plasma exhaust system. The following section discusses the complete post-test analysis of Test #12.

Results of Post-Test Analysis Completed After Long Run Time Test Using Flowing Preheated Fluorine/UF_6 Regeneration System in the 1.2 MW RF Uranium Plasma Test Facility

To provide an estimate of the overall efficiency of the fluorine/UF_6 regeneration system employed in these exhaust gas reprocessing tests, a complete post-test analysis was conducted upon completion of Test #12. Figure 25 is a photograph of the majority of the key test components examined. Not shown are the rf test chamber components (i.e., fused-silica peripheral wall, right endwall assembly including the UF_6 injector, and the left endwall assembly. These were shown previously in Figs. 15 and 16.) Figure 26 is a photograph showing the fused-silica peripheral wall of the test chamber before and after Test #12. TABLE IV summarizes the test results. Each component examined is listed consecutively with the corresponding letter codes for its location (also see Fig. 18). The weight of the residue (in grams) removed from each key component is shown in the second column of TABLE IV. Based on the UF_6 mass flow rate for this test, the total weight of UF_6 injected into the rf plasma test chamber was 11.1 gms. The numbers in parentheses after the second column of TABLE IV are the corresponding residue mass deposition per unit area for the key test components. (Test time five minutes.) These ranged from a low of 2 $\mu g/cm^2$ for the UF_6 injector assembly to a high of 760 $\mu g/cm^2$ for the UF_6 injector assembly. The total amount of post-test residue collected and weighed on an electronic balance was 4.014×10^{-1} g. This represents about 3.6 percent of the total UF_6 injected into the rf test chamber that was not available for potential regeneration. Within the confines of the rf test chamber, the total weight of residue deposited was approximately 19.5×10^{-3} g; this represents about 0.18 percent of the total mass of UF_6 injected. A technique that could be employed in future tests to reduce the level to near zero, would be to fabricate the test chamber endwalls themselves of a porous material (e.g., nickel) and introduce a small bleed flow through the porous wall. This might permit achieving deposition levels comparable to those obtained for the porous duct assembly shown in TABLE IV (i.e., 1.0×10^{-4} g = 0.001 percent of total UF_6).

The sum of the weight of UF_6 regenerated and the total residue deposition was 10.12 gms. This represents about 91 percent of the total UF_6 injected into the test chamber for this test. The remainder is assumed to be due to a combination of: experimental error in the measurement of the UF_6 flow rate (± 5 percent); experimental error in the collection and weighing of the residue from the different test components (± 3 percent); and, possible additional residue material remaining on several of the test components (especially valve assemblies where complete disassembly and material removal is difficult). This last item alone could conceivably account for up to 0.5 gms. Based on the T.O.F. exhaust gas analysis measurements described in the following section, no entrainment of UF_6 through the cryogenic trap system was shown to occur

within the accuracy of the exhaust gas composition measurements (measurements down to about 50 ppm on a molar basis).

The last column in TABLE IV lists the major compounds identified during the post-test residue analysis using the different complementary diagnostic equipment previously described in "Description of Principal Equipment" section. References 2 and 3 contain additional details on the operation, calibration, and limitations of these various diagnostics techniques.

Results of Complementary Measurements Made With T.O.F. Mass Spectrometer Exhaust Gas Analysis Section

Figure 18 shows the test configuration used in the flowing fluorine/UF_6 regeneration tests employing exhaust gas sampling and conducted in the 1.2 MW rf uranium plasma test facility. These tests were included in order to gain some insight into the understanding of the complex chemical processes occurring from the point of UF_6 injection into the rf argon plasma to the final exhaust duct system downstream of the UF_6 regeneration components. It is not possible at this time to develop a kinetic model that can be used to accurately describe the chemical processes. Several reasons include: (1) lack of fundamental data (e.g., heats of formation); (2) competing simultaneous homogeneous/heterogeneous reactions and complex mixing/aerodynamic flow conditions. Reference 3 describes details of an on-line mass spectrometric method used to study the exhaust products that remain in the gas phase from room temperature up to a maximum temperature compatible with nickel probe operation of about 2000 K. The method included development of a noncommercially available T.O.F. mass spectrometer that could be exposed to significant amounts of $UF_6/(F_2)$ without serious damage to the ion optics and vacuum chamber. The ability to operate correctly in a strong rf environment was another operating constraint that was satisfied.

The data acquisition system (see Fig. 17) permitted taking the spectrometer scans (12 atomic mass units to 425 atomic mass units obtained in about six seconds) and processing the information on a digital tape/computer system. The major portions of the computer software used included (1) a fast Fourier transform routine to analyze the noise content of the spectra, (2) a digital filter to smooth the data, (3) a baseline subtraction routine, (4) a mass marker routine, (5) a peak height and area routine, and (6) a deconvolution routine for unfolding overlapping peaks.

The fragmentation pattern of molecules under bombardment by electrons in the ion source of the T.O.F. instrument is important for accurate reduction of spectra, especially in regions of spectral overlap. Reference 3 contains details of this fragmentation pattern for UF_6 at an ionizing electron energy

of 75 eV. Also included are the sensitivity factors and their comparison with other published data. The precision of the data was within 5 percent. This comparison showed that the UTRC T.O.F. spectrometer sensitivity for UF_6 was approximately 3X greater than that of any commercial T.O.F. spectrometer.

In this research effort, only the UF_5^+ peak, which is the dominant ion, was employed to estimate the UF_6 concentration. The precision of this peak is typically 1 percent. For the data included in this report, the inlet pressure was maintained at approximately 20 Torr and the spectrometer pressure was typically $1x10^{-6}$ Torr. The noise equivalent concentration of UF_6, as measured by the UF_5^+ ion after averaging the spectra in the rf environment, was approximately 30 ppm. This is approximately an order of magnitude greater than the sensitivity of any commercially available unit. During all the measurements taken in this study, the instrument required no service. In the prior study (Ref. 3), the CuO/BeO dynode electron multiplier required replacement.

Examples of several representative mass spectral relative intensities obtained throughout this research effort are shown in Figs. 27 through 30. These plots were obtained directly from a computer visual display. Figure 27 is a good example of the instrument in detecting impurities (note the HF^+ and fragments of C_2Cl_3H (trichloroethylene) in addition to the O_2^+ and N_2^+.) Figures 28 through 30 show examples of the spectra obtained from measurements with the sampling probe located at the different locations illustrated in Fig. 18 (i.e., axial bypass station (1), downstream of the cryogenic trap station (3), and upstream of the cryogenic trap station (2)). TABLE III summarizes the results obtained using the T.O.F. sampling probe system that corresponds to the data shown in Fig. 24. In no test conducted was the concentration of UF_6 (molar basis) found in the axial bypass duct greater than 100 ppm (0.01 percent). This result quantitatively confirms estimates of the good uranium confinement characteristics of the radial inflow vortex employed in the plasma test chamber.

Measured concentrations less than 50 ppm (0.005 percent) of UF_6 were found downstream of the liquid argon cold trap assembly used to collect the UF_6; thus demonstrating that essentially all the UF_6 was efficiently collected and none was entrained downstream. For the test case corresponding to the complete post-test exhaust gas residue analysis (Test #12), the upstream UF_6 concentration was determined to be 1180 ppm. This compares to a calculated value of 1396 ppm for the UF_6 initially injected into the rf test chamber and assuming complete mixing.

To provide an indication of the possible mixing pattern existing in the exhaust duct, a set of sampling probe radial traverses were conducted. Some difficulties were experienced in this test series due to a partial seizing of the traversing mechanism (see Fig. 19) used to drive the probe assembly from

the centerline position to the near wall location. Therefore, a complete radial profile with a secondary reproducibility check as originally planned was not possible. TABLE V summarizes the results obtained and provided a first time indication that a radial concentration gradient of UF_6 exists in the exhaust duct system. More experimental measurements of this type over a wide range of test conditions are required before a complete analysis of the gaseous species concentration in the exhaust duct can be formulated.

The overall results to date have provided much worthwhile information toward furthering the understanding of the on-line fluorine/UF_6 regeneration process. The results also suggest that this particular ruggedized T.O.F. mass spectrometer will prove most useful in future fundamental studies, such as UF_4 vapor pressure measurements, and appearance potential measurements for all the halide ions of uranium. These measurement methods are also suited for composition measurements required in the study of future nuclear pumped laser systems.

REFERENCES

1. Roman, W. C.: Laboratory-Scale Uranium RF Plasma Confinement Experiments. United Technologies Research Center Report R76-912205, Sept. 1976. Also Issued as NASA CR-145049, Sept. 1976.

2. Roman, W. C.: High Temperature UF_6 RF Plasma Experiments Applicable to Uranium Plasma Core Reactors. NASA CR-159159, 1979.

3. Roman, W. C.: Argon/UF_6 Plasma Experiments: UF_6 Regeneration and Product Analysis. United Technologies Research Center Report R79-914533, July 1979 (to be issued as NASA CR).

4. Rodgers, R. J., et al.: Investigation of Applications for High-Power, Self-Critical Fissioning Uranium Plasma Reactors. NASA CR-145048, Sept. 1976.

5. Thom, K. and F. C. Schwenk: Gaseous Fuel Reactor System for Aerospace Applications. AIAA Conference on the Future of Aerospace Power Systems, Paper No. 77-513, St. Louis, MO., March 1977.

6. Kendall, J. S. and R. J. Rodgers: Gaseous Fuel Reactors for Power Systems. Paper Presented at 12th Intersociety Energy Conversion Engineering Conference, Washington, D.C., 29 August-2 September 1977.

7. Rodgers, R. J.: Initial Conceptual Design Study of Self-Critical Nuclear Pumped Laser Systems. NASA CR-3128, April 1979.

8. Rodgers, R. J., et al.: Analyses of Low-Power and Plasma Core Cavity Reactor Experiments. United Technologies Research Center Report R75-911908-1, May 1975.

9. Thom, K., et al.: Gaseous-Fuel Nuclear Reactor Research for Multimegawatt Power in Space. International Astronautical Federation XXVIIIth Congress, Prague, 25 Sept.-1 Oct. 1977.

10. Barton, D. M., et al.: Plasma Core Reactor Experiments. Paper 3D-13, 1977 IEEE International Conference on Plasma Science, RPI, Troy, N.Y., May 1977.

REFERENCES (Concluded)

11. Mensing, A. E. and J. S. Kendall: Experimental Investigation of Containment of a Heavy Gas in a Jet-Driven Light-Gas Vortex. United Technologies Research Center Report D-910091-4, Mar. 1965. Also Issued as NASA CR-68926.

12. Roman, W. C. and J. F. Jaminet: Development of RF Plasma Simulations of In-Reactor Tests of Small Models of the Nuclear Light Bulb Fuel Region. United Technologies Research Center Report L-910900-12, Sept. 1972.

13. Brown, M. H.: Resistance of Materials with Fluorine and Hydrogen Fluoride. AEC Report No. MDDC-144, 1952.

14. Steindler, M. J. and R. D. Vogel: Corrosion of Materials in the Presence of Fluorine at Elevated Temperatures. Argonne National Laboratory Report ANL-5662, Jan. 1957.

15. Skrivan, J. F. and W. VonJaskowsky: Heat Transfer from Plasmas to Water-Cooled Tubes. Industrial and Engineering Chemistry Process Design and Development, Vol. 4, No. 4, Oct. 1965.

16. Thorsen, R. and F. Landis: Friction and Heat Transfer Characteristics in Turbulent Swirl Flow Subjected to Large Transverse Temperature Gradients. Trans. ASME J. of Heat Transfer, Paper No. 67-HI-24, 1967.

LIST OF SYMBOLS

f	RF operating frequency, MHz
h	Enthalpy, kW s/g
ℓ	Liters
$\dot{m}_{Ar}$	Argon buffer gas flow rate, g/s
$\dot{m}_{Ax}$	Axial bypass flow rate, g/s
$\dot{m}_{D}$	Argon diluent gas flow rate, g/s
$\dot{m}_{F_2}$	Fluorine flow rate, g/s
$\dot{m}_{F_{2PD}}$	Fluorine flow rate through porous duct assembly, g/s
$\dot{m}_{F_{2SI}}$	Fluorine flow rate through sonic injector assembly, g/s
$\dot{m}_{SC}$	Argon carrier flow rate for UF_4 seed, g/s
$\dot{m}_{UF_6}$	Uranium hexafluoride flow rate, g/s
$\dot{m}_{UF_4}$	Uranium tetrafluoride flow rate, g/s
N	Number density, cm^{-3}
P	Pressure, atm, mmHg, or Torr
P_c	Chamber pressure, atm
Q	Power, kW
Q_T	Total rf discharge power, kW
R	Radius, cm
r	Radial distance, cm
T_p	Fluorine preheat temperature, deg K
T	Temperature, deg K

LIST OF SYMBOLS (Concluded)

$T_{\mathbb{C}}$	Centerline temperature, deg K
t	Time, minutes (m) or seconds (s)
W	Weight of residue material, mg
X	Mole fraction, dimensionless
λ	Wavelength, nm; wavenumber, cm^{-1}
η_c	Conversion efficiency, percent

APPENDIX A*: SUPPORT ANALYSIS OF HEAT AND MASS TRANSFER ASPECTS OF URANIUM PLASMA EXHAUST SYSTEM

A heat transfer analysis was conducted to provide complementary data on the exhaust gas UF_6 regeneration system connected to the 1.2 MW rf plasma facility. The function of the exhaust gas UF_6 regeneration system was to condition the effluent exhaust gas from the plasma chamber so as to convert a high degree of the plasma dissociated UF_6 and any existing uranium compounds back to gaseous UF_6.

Exploratory tests were conducted in the easily accessible and readily disassembled UTRC plasma torch facility to provide some of this design data. This could then be used as design input for the UF_6 conversion system to be used with the relatively complex 1.2 MW rf facility. A schematic of the key components of the plasma torch exhaust system is shown in Fig. 31. Prepurifield argon gas was heated in the torch. Provision was made to inject UF_4 powder entrained in an argon carrier stream into the torch's heated exhaust, such that the combined flows were uniformly mixed in a mixing plenum. Station I was the location of the mixing plenum exit. The flow proceeded through an uncooled 12.7-cm-long nickel duct to Station II where provision was made for preheated fluorine at a temperature of approximately 922 K to be added to the flow stream. A calorimetric measurement indicated that approximately 0.38 kW of power was removed from the torch flow stream in traversing the duct between Stations I and II. An uncooled 33-cm-long nickel tube duct connected Station II to Station III. This was the reference reaction chamber within which the UF_4 and fluorine gases were reacted to convert the UF_4 powder to UF_6. Approximately 0.33 kW was removed from the flow via the reaction chamber wall. A final 91.5-cm-long transition section was attached to the exhaust system and was located between Stations III and IV. Beyond Station IV the flow was ducted to a UF_6 cold trap (liquid argon). Calorimeter measurements indicated approximately 0.66 kW was removed from the flow stream via convective heat transfer to the duct walls, between Stations III and IV.

Representative results for the torch test are shown in TABLE VI for a similar set of test conditions in which the argon torch flow (1.82 g/s), preheated fluorine flow (0.21 g/s/922 K), argon UF_4 carrier flow (0.41 g/s), and UF_4 flow (0.15 g/s) rates were sequentially introduced into the system. The torch power with argon only flow was 6.68 kW; with the addition of the fluorine the power coupling was slightly different (due to slight pressure increase), resulting in a torch power of 7.3 kW. At the mixing plenum exit (Station I),

*Assistance in analysis provided by Richard Rodgers/Susanne Orr.

bulk gas temperatures in the range of 2035 to 2824 K were calculated for total power levels, associated with the gas flow, between 2.1 and 2.39 kW. At Station II the bulk gas flow temperature dropped significantly, principally due to the dissociation energy requirement of molecular fluorine to atomic fluorine. Also, approximately 0.2 kW of heat addition was included at Station II to account for the fluorine preheated to approximately 922 K. Bulk gas temperatures varied between 2184 K and 1260 K at Station II. As the flow stream proceeded through the reaction duct (between Stations II and III) and the transition section (between Stations III and IV), the temperature continued to decrease to the range between 1142 K to 815 K, from the argon only flow condition to the argon, UF_4, argon carrier, and fluorine combined flow condition. The results for the flow condition with fluorine included, have a smaller temperature decrease than the argon only flow between Stations II and IV because of the exothermic heat release due to fluorine recombination. The results of these tests indicated the range of flow rates and expected temperatures which would be applicable to the rf exhaust system as well as the range of heat transfer requirements.

In the 1.2 MW rf plasma facility pure UF_6 was initially injected into the plasma test chamber where it was dissociated into uranium and fluorine species which were both ionized and nonionized (Ref. 1). The UF_6 plasma was confined in the plasma chamber within an argon vortex buffer gas. Most of the argon ($\approx 2/3$) was extracted from the chamber along with the UF_6 decomposition species through a centerline port in the exhaust endwall of the chamber (see Fig. 15). The remaining argon was removed via an annular bypass duct at the outer periphery of the exhaust endwall.

A schematic of the key components of the exhaust gas UF_6 conversion system is shown in Fig. 31, and has been described in the "Description of Principal Equipment" section. The heat transfer analysis treats the exhaust gas effluent as it exits the rf plasma chamber (Station I) to the inlet of the UF_6 cold trap (Station VII). The gas effluent is a swirling flow as it enters the exhaust system. For this example approximately 7.4 kW of power was associated with the gas flow. This condition corresponded to a high power rf opearting condition with the discharge operating with argon gas. A 12.7-cm-long interstage exhaust duct with high pressure water cooling was employed to remove approximately 3.1 kW. The heat transfer to the walls of the interstage exhaust duct was determined calorimetrically for an argon plasma by entraining the entire exhaust flow at Stations I and II, respectively, in separate complementary tests at the same operating conditions. These results compared well with analytical convective heat transfer calculations for which heat transfer enhancement due to swirling flow conditions in the 12.7-cm-long interstage exhaust duct was considered. At the operating conditions of the plasma exhaust system, an enhancement factor of approximately 3 was predicted (Refs. 15 and 16) for the ratio of convective heat transfer with swirl flow

relative to convective heat transfer without swirl flow. At Station II (Fig. 31) a capability for adding argon diluent flow at approximately 0.5 g/s was provided. Additional exhaust gas calorimetric measurements were made to estimate the heat transfer loss from the gas effluent exhaust duct section between Stations II and III. This section of duct also had high pressure water cooling which removed approximately 2.2 kW of power from the effluent flow. The injection of the argon diluent flow and increasing separation from the plasma chamber exhaust exit resulted in a steadily decreasing swirl effect on the convective heat transfer to the exhaust system walls as the flow proceeded through this section of the duct. Results of the calorimetric measurements of the exhaust flow agreed within approximately 5 percent when compared with the analytic calculations of the convective heat transfer to the section walls when no enhancement due to swirl flow was considered.

Between Stations III and IV, no heat transfer was assumed. Location IV was the location where the preheated fluorine flow was added to the exhaust gas flow to augment the conversion of uranium species to gaseous UF_6 within the nickel reaction chamber which was located between Stations IV and V (Fig. 31). A porous duct assembly with fluorine bleed flow (or in some tests, a nickel exhaust duct section) followed the reaction chamber and was located between Stations V and VI. In selected tests a T.O.F. mass spectrometer sampling probe was inserted into the exhaust flow stream at Station VI. An L-shaped exhaust duct section then connected the exhaust system at Station VI to the UF_6 cold trap at Station VII. The heat transfer losses from Station IV to Station VII were calculated assuming analytic convective heat transfer from the gas to the duct walls and assuming no enhancement due to swirl flow. This was based on the agreement between the calorimetric results and the analytic results in exhaust sections between Stations I and II and Stations II and III, respectively.

The results of the heat transfer analysis of the exhaust duct system are presented in TABLE VII for a representative set of test conditions between Stations I and VII. The argon flow rate from the plasma chamber into the exhaust system was 2.6 g/s and the UF_6 injected flow rate into the plasma chamber is 0.032 g/s. Essentially all of the UF_6 injected was withdrawn into the main on-axis exhaust duct system. Separate measurements using the T.O.F. exhaust gas analysis system indicated negligible amounts of UF_6 were in the axial bypass. The total power chosen for the argon and UF_6 decomposition species flow at the entrance to the exhaust conversion system (Station I) was 7.4 kW assuming an argon injection temperature of 300 K into the plasma chamber. At Station I a bulk gas temperature of 5499 K was calculated assuming constant specific heat at constant pressure for the argon and temperature dependent thermodynamic data for UF_6 thermal equilibrium decomposition species distribution (see Fig. 32). Argon diluent flow of 0.50 g/s was added to the exhaust duct flow at Station II. A bulk gas temperature of approxi-

mately 2907 K was calculated at Station II with the argon diluent added for a calorimetrically determined heat transfer loss of 3.1 kW from the gas to the duct walls. Also included at Station II was a 0.22 kW exothermic step heat addition due to the reconversion of uranium and fluorine species to primarily UF_4 and atomic fluorine as the gas temperature approaches 4000 K as indicated in Fig. 33. The second water-cooled exhaust duct reduced the effluent gas temperature to approximately 1592 K at Station III and 2.2 kW power was removed. At Station IV, 0.25 g/s of fluorine gas preheated to a temperature of approximately 1034 K was added to the exhaust duct flow via the ring manifold series of sonic injectors. Approximately 0.90 kW was added to the exhaust gas stream due to the heated fluorine at Station IV. The exothermic heat of reaction for the reconversion of primarily UF_4 and atomic fluorine to UF_6 based on the UF_6 decomposition species calculations was also included as a step addition of approximately 0.063 kW at Station IV, to simplify the calculations. This was based on the UF_6 enthalpy calculations which are shown in Fig. 33. The UF_6 thermal decomposition species distributions in the temperature range of 1000 K to 4000 K are shown in Fig. 32, and correspond in this range to the enthalpy calculations presented in Fig. 33. A bulk gas temperature of 1246 K was calculated at Station IV. Additional convective heat transfer calculations were performed to estimate the losses to the walls at Stations V, VI, and VII. Calculated losses of 0.26, 0.07, and 0.7 kW between Stations IV and V, V and VI, and VI and VII, respectively, resulted in bulk gas temperatures of 1203 K, 1065 K, and 916 K, at Stations V, VI, and VII, respectively. A preliminary estimate of the heat transfer aspects associated with the liquid argon cold trap also indicated reasonable agreement with the calorimeter measurements and boil-off rates noted. This information will prove valuable in future estimates directed toward scale-up of fluorine/UF_6 regeneration systems applicable to closed-loop uranium plasma core systems and/or nuclear pumped laser systems.

TABLE I

SUMMARY OF OPERATING RANGES FOR FLOWING HIGH TEMPERATURE UF_4/FLUORINE TO UF_6 REGENERATION TESTS CONDUCTED WITH DC ARC PLASMA TORCH SYSTEM

See Fig. 2 for Schematic of Test Configuration
See Fig. 20 for Example of Measured Conversion Data

$2.21 \leq \dot{m}_{Ar} \leq 2.52$ g/s
$\dot{m}_{F_2} = 0.2$ g/s
$\dot{m}_{UF_6} = 0.15$ g/s
$1.3 \leq P_c \leq 1.5$ atm
$10 \leq$ Test Time ≤ 20 s
$700 \leq T_{\text{℄}_{exit}} \leq 990$ K
$22 \leq \eta_c \leq 79\%$

TABLE II

SUMMARY OF OPERATING RANGES FOR FLOWING HIGH TEMPERATURE UF_4/PREHEATED FLUORINE TO UF_6 REGENERATION TESTS CONDUCTED WITH DC ARC PLASMA TORCH SYSTEM

See Fig. 2 for Schematic of Test Configuration
See Fig. 22 for Example of Measured Conversion Data

$2.23 \leq \dot{m}_{Ar} \leq 2.64$ g/s
$0.1 \leq \dot{m}_{F_2} \leq 0.3$ g/s
$965 \leq F_2$ Preheat Temperature ≤ 1020 K
$0.14 \leq \dot{m}_{UF_4} \leq 0.15$ g/s
$1.3 \leq P_c \leq 2.1$ atm
$19.9 \leq$ Test Time ≤ 20.3 s
$961 \leq T_{\text{℄}_{exit}} \leq 1180$ K
$57 \leq \eta_c \leq 94.8\%$

TABLE III

SUMMARY OF TEST CONDITIONS CORRESPONDING TO PURE FLUORINE/UF_6 REGENERATION TESTS CONDUCTED IN 1.2 MW RF URANIUM PLASMA TEST FACILITY

See Fig. 10 for Schematic of Components

See Fig. 24 for Plot of Test Results

TEST CASE	RF OPERATING FREQUENCY (MHz)	$\dot{m}_{Ar}$ (g/s)	$\dot{m}_{AX}$ (g/s)	$\dot{m}_{UF_6}$ (g/s)	$\dot{m}_D$ (g/s)	$\dot{m}_{F_2}$ SI (g/s)	Preheat Temp. if used (°K)	P_c (atm)	$\dot{m}_{F_2}$ (Porous Duct)	T_{exit} (°K)	T.O.F. Sampling Probe Location	UF_6 conc. (ppm)	Test Time t(min)	η_c (%)
1	5.4256	3.7	0.84	0.024	0.60	0.2	-	1.48	-	895	AB*	<100	6	51
2	5.4267	3.6	0.84	0.018	0.55	0.18	-	1.68	-	905	AB*	<100	5	49
3	5.4242	3.7	0.92	0.018	0.55	0.15	-	1.94	-	915	AB*	<100	1	58
4	5.4251	3.5	0.84	0.027	0.50	0.2	-	1.55	-	940	AB*	<100	7	64
5	5.4268	3.5	0.84	0.028	0.50	0.2	-	1.49	-	945	D**	< 50	6	62
6	5.4253	3.5	0.84	0.024	0.50	0.2	936	1.41	-	975	D**	< 50	6	72
7	5.4246	3.5	1.10	0.018	0.52	0.22	-	1.81	-	1020	URP***	see Table V	1	72
8	5.4279	3.5	1.14	0.018	0.52	0.2	-	2.02	0.322 (519 K)	1020	D**	< 50	1	78
9	5.4244	3.5	1.14	--	0.52	0.25	-	1.41	-	1020	-	-	6	1
10	5.4285	3.6	0.84	0.024	0.50	0.00	-	2.49	0.322 (535 K)	1070	D**	< 50	1	41
11	5.4268	3.45	1.14	0.032	0.50	0.2	997	1.82	-	1160	AB*	<100	5	83
12	5.4271	3.52	0.92	0.037	0.50	0.25	1034	2.72	0.322 (517 K)	1202	Upstream	1180	5	88

*Axial Bypass

**Downstream of Trap

***Upstream Radial Profile

See Fig. 13 for Schematic of Test Configuration

TABLE IV

SUMMARY OF POST-TEST ANALYSIS COMPLETED AFTER LONG RUN TIME TEST USING FLOWING PREHEATED FLUORINE/UF_6 REGENERATION SYSTEM AND CONDUSTED IN 1.2 MW RF URANIUM PLASMA TEST FACILITY

See Fig. 10 for Schematic of Test Configuration
See TABLE III for Summary of Test Conditions Corresponding to Long Run Time Test No. 12
See Fig. 25 for Photograph of Disassembled Major Test Components Analyzed
See Fig. 26 for Photograph of Fused-Silica Tube Peripheral Wall Before and After Test
Numbers in Parentheses are Equivalent Mass Deposition per Unit Area for Several Key Test Components ($\mu g/cm^2$)
Total UF_6 Mass Injected for this Test = 11.1 gms

COMPONENT	WEIGHT OF RESIDUE (g)	CONSTITUENTS
5.7-cm-IDx12.2-cm-long Fused-Silica Peripheral Wall (A)	8.03×10^{-3} (45)	UO_2F_2, UF_4, UO_2
UF_6 Injector (B)	5.07×10^{-3} (760)	UO_2F_2, UF_4, UO_2
Right Endwall (C)	4.10×10^{-3} (210)	UO_2F_2, UF_4
Left Endwall (D)	2.27×10^{-3} (121)	UO_2F_2, UF_4
Axial Bypass Duct (E)	4.34×10^{-3} (28)	UO_2F_2, UF_4
Interstage Exhaust Duct (F)	1.07×10^{-3} (18)	UO_2F_2, UF_4
Diluent Gas Injector (G)	2.2×10^{-4}	UO_2F_2, UF_4
Water-Cooled Exhaust Duct (H)	1.6219×10^{-1} (100)	UO_2F_2, UF_4
Flange Junction (J)	1.2999×10^{-1}	UO_2F_2, UF_4
Fluorine Injector Manifold (J)	2.16×10^{-3}	UO_2F_2, UF_4
Nickel Reaction Chamber (K)	7.122×10^{-2} (429)	UO_2F_2, UF_4
Coupling Assembly for T.C. (L)	1.0×10^{-5}	UO_2F_2, UF_4
Porous Duct Assembly (Monel) (M)	1.0×10^{-4} (2)	UO_2F_2, UF_4
T.O.F. Traversing Probe Assembly (N)	5.60×10^{-3}	UO_2F_2, UF_4
Tee-Assembly and Line to Trap (O)	1.52×10^{-3}	UO_2F_2, UF_4
Cryogenic Trap Assembly (P)	4.7×10^{-4}	UO_2F_2
Return Line From Trap (Q)	5.2×10^{-4}	UO_2F_2
Remote Control Nupro Valve and Tee (R)	4.3×10^{-4}	UO_2F_2
Nupro Valve and Downstream T.O.F. Sampling Probe (S)	2.3×10^{-4}	UO_2F_2
Bellows, Elbow (T)	1.9×10^{-3}	UO_2F_2
TOTAL	4.014×10^{-1}	

TABLE V

EXAMPLE OF RESULTS OBTAINED FOR RADIAL UF_6 CONCENTRATION PROFILE USING ON-LINE EXHAUST GAS SAMPLING SYSTEM IN FLOWING FLUORINE/UF_6 REGENERATION TESTS CONDUCTED IN 1.2 MW RF URANIUM PLASMA TEST FACILITY

See Fig. 18 for Schematic of Test Configuration
See Fig. 19 for Photograph of Traversible Sampling Probe Assembly
See Fig. 30 for Example of Mass Spectral Relative Intensities Used in Determining Concentration
Test Case 7 - see TABLE III for Additional Test Conditions

T.O.F. Mass Spectrometer Operating Conditions

Filaments - 2.6
Emission - 5.3
Electron Energy - 88 ev
$P_{T.O.F.}$ - 5×10^{-6} Torr
Number of Passes - 32
Gain - X2
Filter - 100 μs
Input Attentuation - 1 v
Sample Time Sensitivity - X1
Time Base - 280 x 10 μs

T.O.F. SAMPLE PROBE LOCATION	UF_6 CONCENTRATION (ppm molar)
Centerline r/R = 0 Location	485
r/R = 0.25	505
r/R = 0.75	582

NOTE: r/R = 1 = wall location, R = 0.8 cm

TABLE VI

EXAMPLE SUMMARY OF HEAT TRANSFER ANALYSIS OF UF_4/UF_6 REGENERATION TEST USING PURE FLUORINE INJECTION CONDUCTED WITH PLASMA TORCH SYSTEM

Example Representative of Maximum Conversion Test Case Shown in Fig. 22
See Fig. 21 for Schematic of Components and Exhaust Stations I-IV Used in Analysis
Refer to APPENDIX A for Description of Analysis

	Q_T (kW)	6.68	7.3	7.3	7.3
	$\dot{m}_{Ar}$ (g/s)	1.82	1.82	1.82	1.82
	$\dot{m}_{SC}$ (g/s)	0	0	0.41	0.41
	$\dot{m}_{F_2}$ (g/s)	0	0.21	0.21	0.21
	$\dot{m}_{UF_4}$ (g/s)	0	0	0	0.15
Station I	T_I (K) Q_I (kW)	2584 2.17	2824 2.39	2361 2.39	2035 2.1
Station II	T_{II} (K) Q_{II} (kW)	2184 1.79	1430 2.18	1325 2.18	1260 2.01
Station III	T_{III} (K) Q_{III} (kW)	1836 1.46	1225 1.68	1165 1.68	1120 1.51
Station IV	T_{IV} (K) Q_{IV} (kW)	1142 0.8	985 0.91	925 0.91	815 0.74

TABLE VII

EXAMPLE SUMMARY OF HEAT TRANSFER ANALYSIS APPLICABLE TO FLUORINE/UF_6 REGENERATION TESTS CONDUCTED IN 1.2 MW RF URANIUM PLASMA TEST FACILITY

See Fig. 31 for Schematic of Key Components and Corresponding Exhaust Stations Used in Analysis

STATION	I	II	III	IV	V	VI	VII
$\dot{m}_{Ar}$ (g/s)	2.60	3.10	3.10	3.10	3.10	3.10	3.10
$\dot{m}_{UF_6}$ (g/s)	0.032	0.032	0.032	0.032	0.032	0.032	0.032
$\dot{m}_{F_2}$ (g/s)	0	0	0	0.25	0.25	0.25	0.25
T (K)	5499	2907	1592	1246	1203	1065	916
$Q_{(300\ K)}$ (kW)	7.4	4.3	2.1	2.5	2.2	2.2	1.4

PLASMA CORE REACTOR UNIT CELL CONFIGURATION

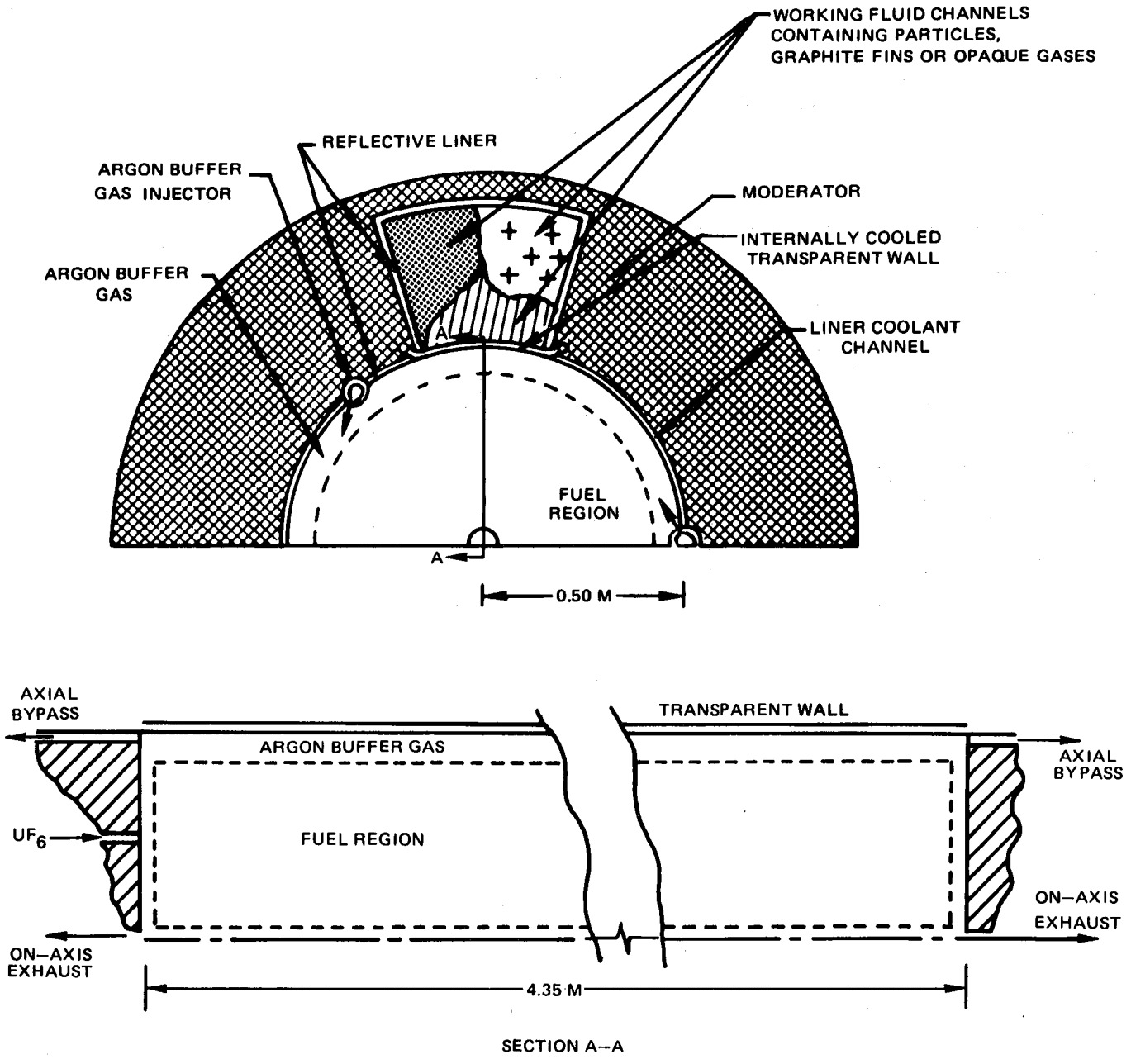

SECTION A–A

SCHEMATIC OF COMPONENTS USED IN FLOWING HIGH TEMPERATURE UF_4/ PREHEATED F_2 TO UF_6 REGENERATION TESTS

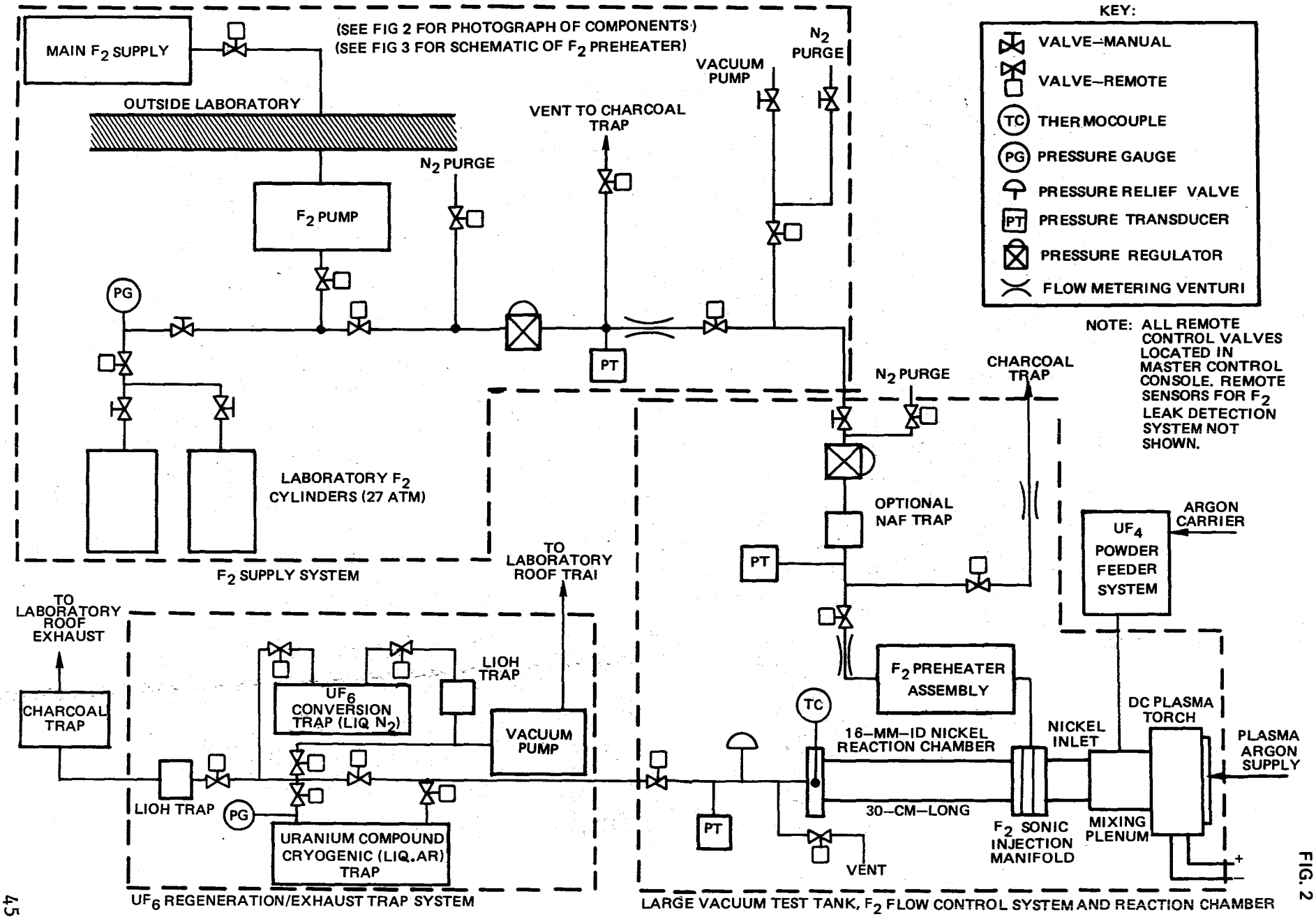

FIG. 2

PHOTOGRAPH OF FLUORINE TEST FACILITY USED IN UF_4/F_2 FLOWING UF_6 REGENERATION TESTS

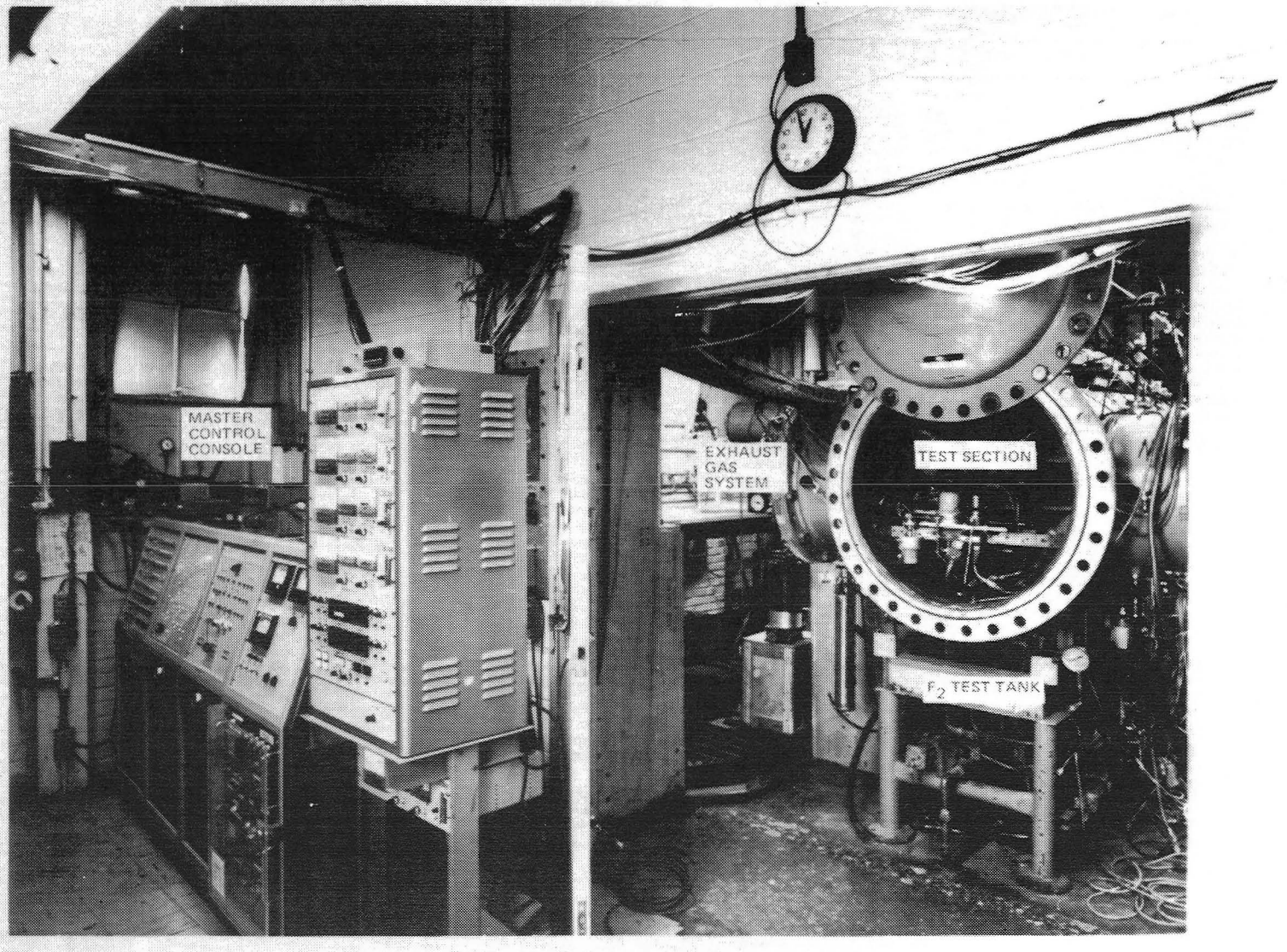

FIG. 3

PHOTOGRAPH OF TEST COMPONENTS USED IN UF_4/F_2 FLOWING UF_6 REGENERATION TESTS

(FRONT DOME REMOVED
CHAMBER DIA~1.5M)

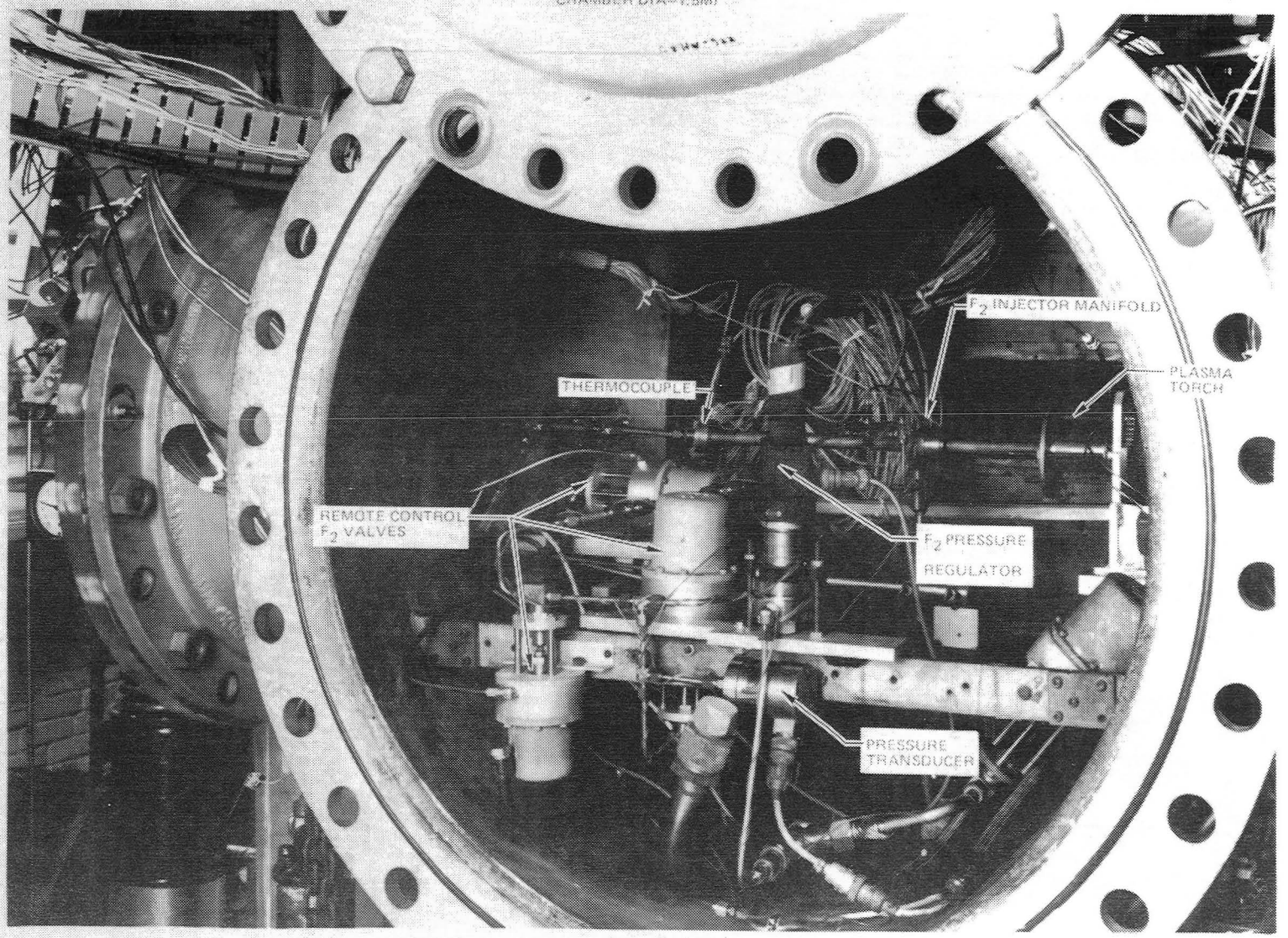

FIG. 5

PHOTOGRAPH OF EXHAUST GAS TRAP SYSTEM USED IN UF_4/F_2 FLOWING UF_6 REGENERATION TESTS

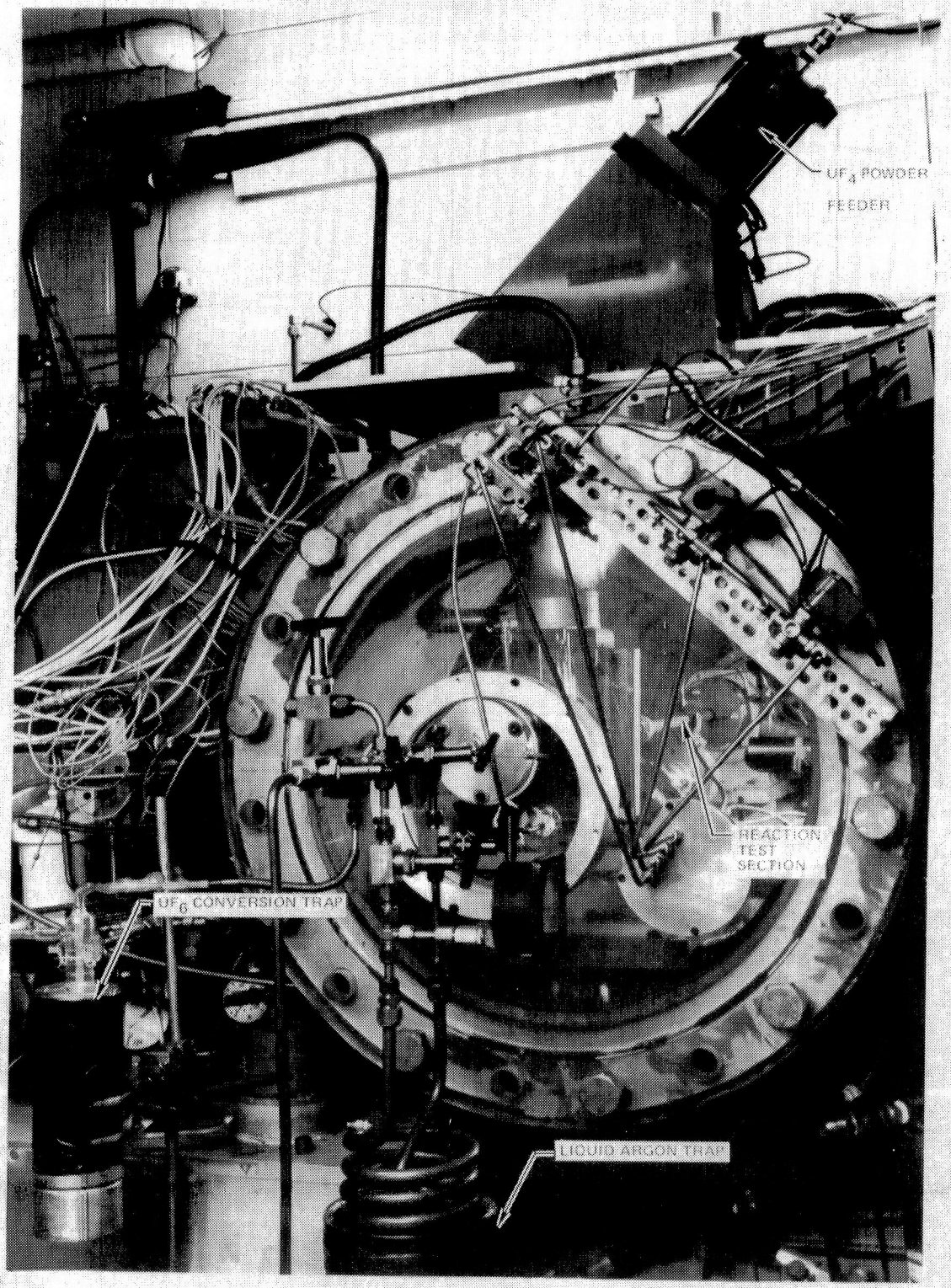

SCHEMATIC OF FLUORINE INJECTION ASSEMBLY FOR UF_6 REGENERATION TESTS

(NOT TO SCALE)

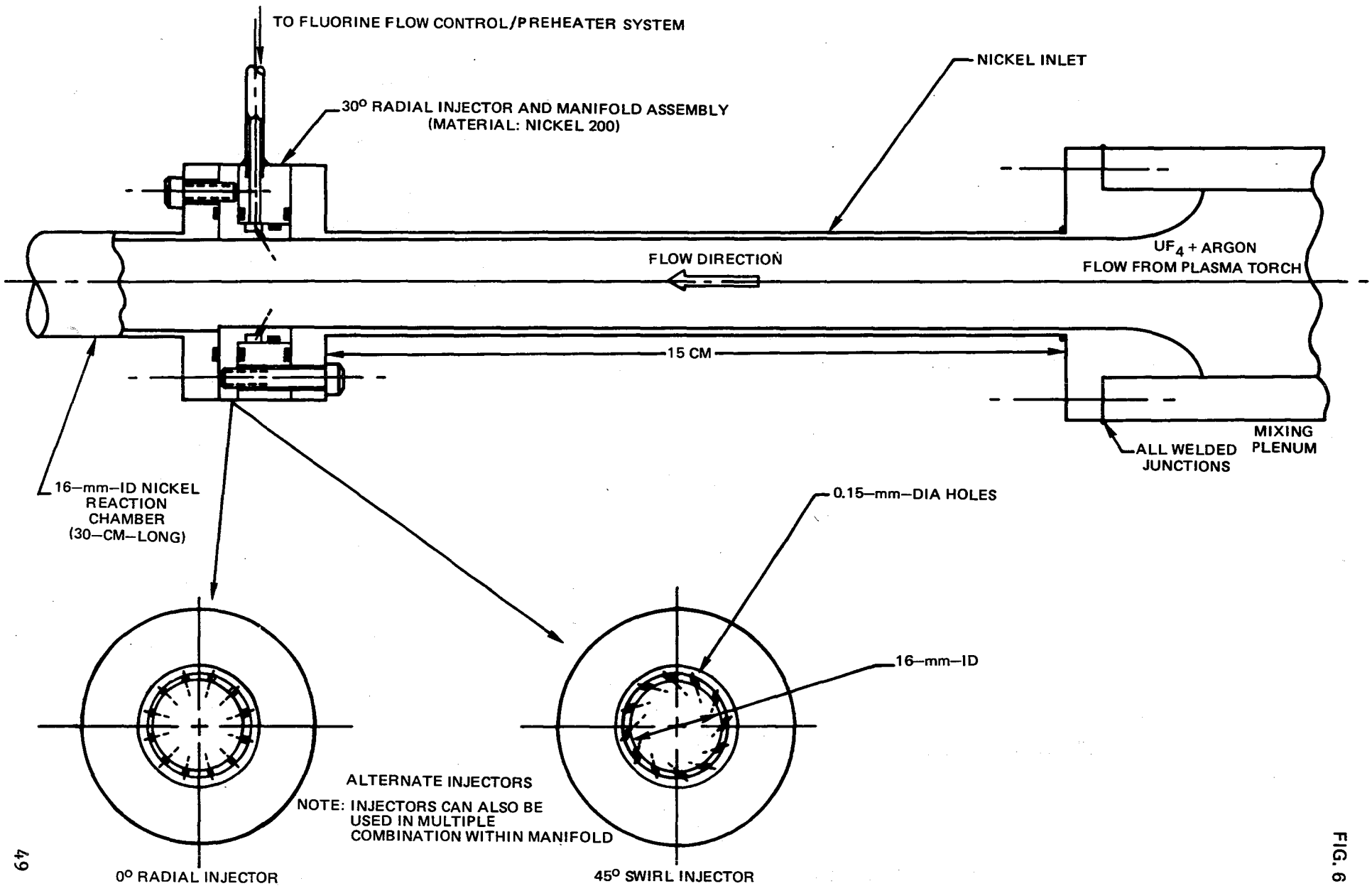

FIG. 6

SCHEMATIC OF F_2 PREHEATER ASSEMBLY USED IN UF_6 REGENERATION TESTS

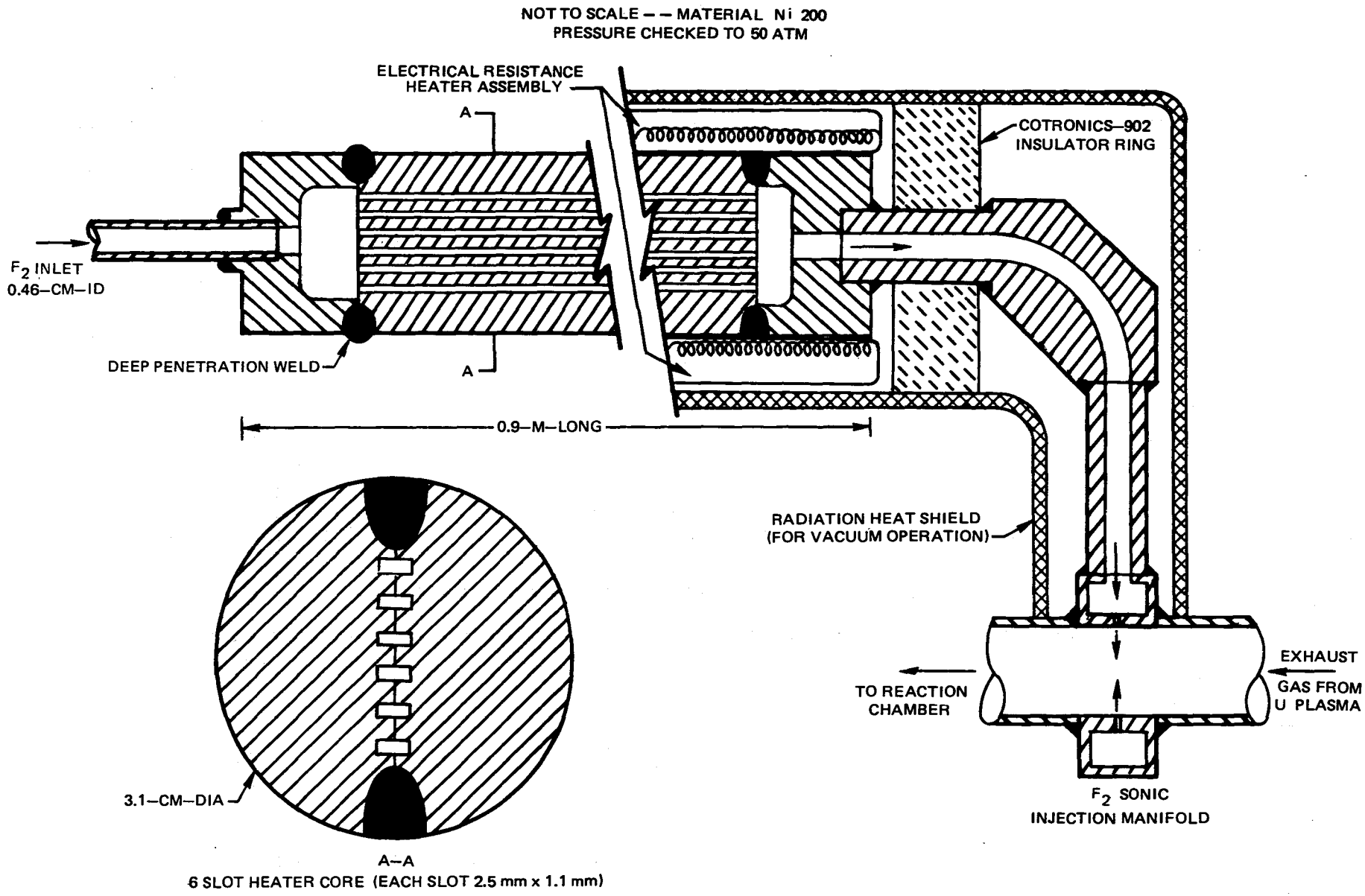

FIG. 7

PHOTOGRAPH OF TEST COMPONENTS USED IN FLOWING HIGH TEMPERATURE UF_4/PREHEATED F_2 TO UF_6 REGENERATION TESTS

(FRONT DOME REMOVED – CHAMBER DIA.–1.5 m)

SEE FIG. 2 FOR SCHEMATIC OF COMPONENTS SEE FIG. 7 FOR SCHEMATIC OF F_2 PREHEATER

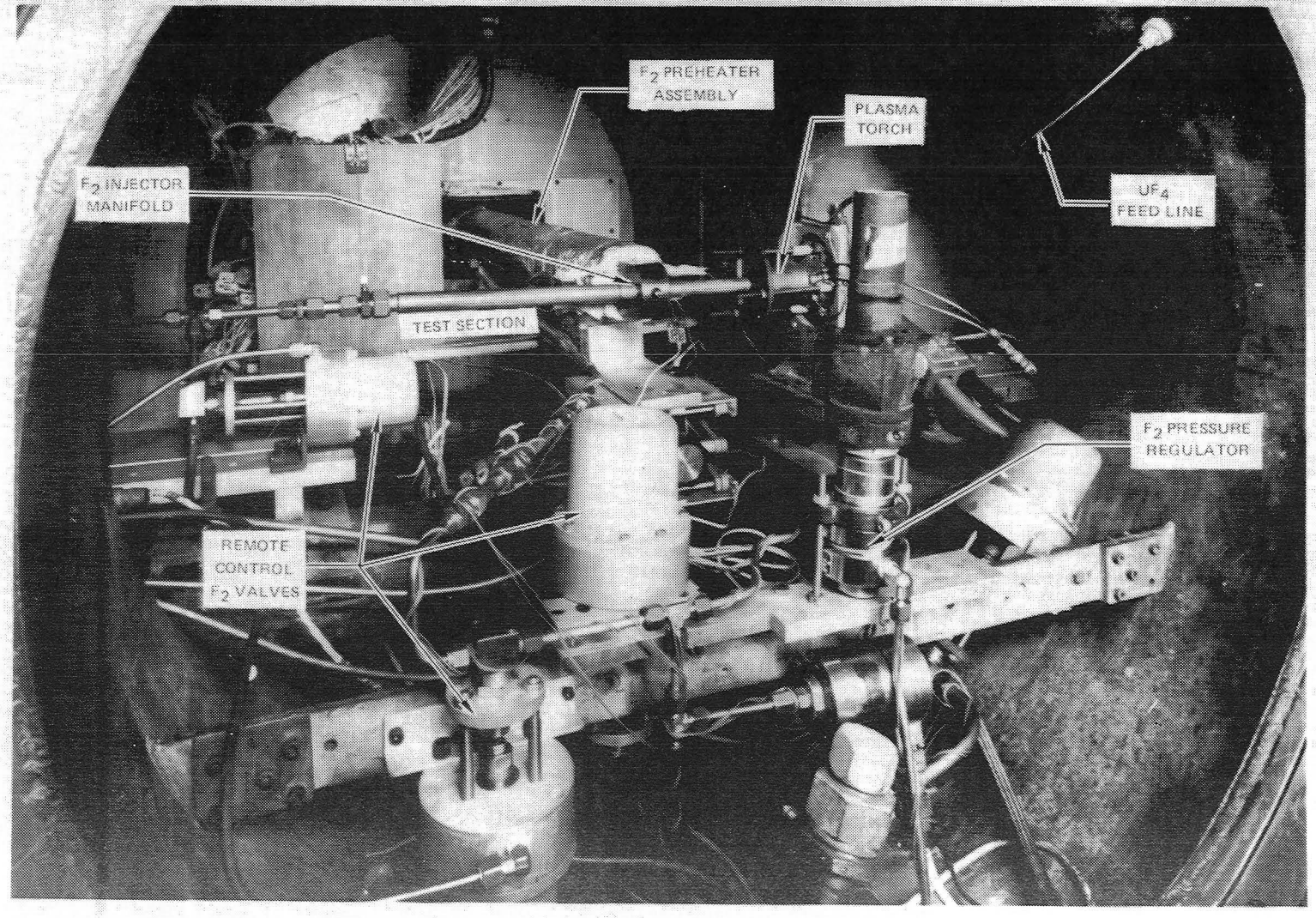

FIG. 8

EXAMPLE OF PHOTOMICROGRAPHS ILLUSTRATING CORROSION ATTACK BY FLUORINE

ALL PHOTOS TAKEN AT 1250X MAGNIFICATION
SEE FIG. 7 FOR SCHEMATIC OF F_2 PREHEATER ASSEMBLY

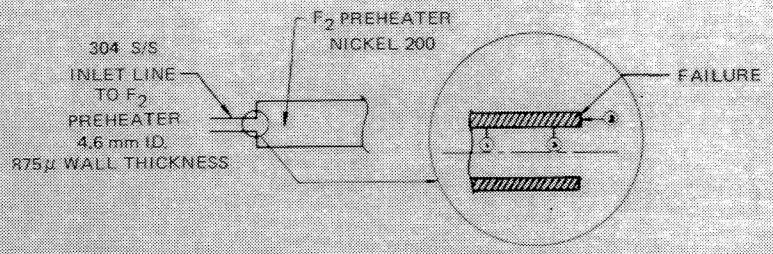

1. CROSS-SECTION AWAY FROM FAILURE REGION – LOWER TEMP. REGION – NO DAMAGE

2. CROSS-SECTION NEAR TO FAILURE REGION – MODERATE TEMP. REGION – GRAIN BOUNDARY ATTACK

3. CROSS-SECTION AT FAILURE – HIGH TEMP. REGION – BULK DIFFUSION FAILURE MODE AT INTERFACE

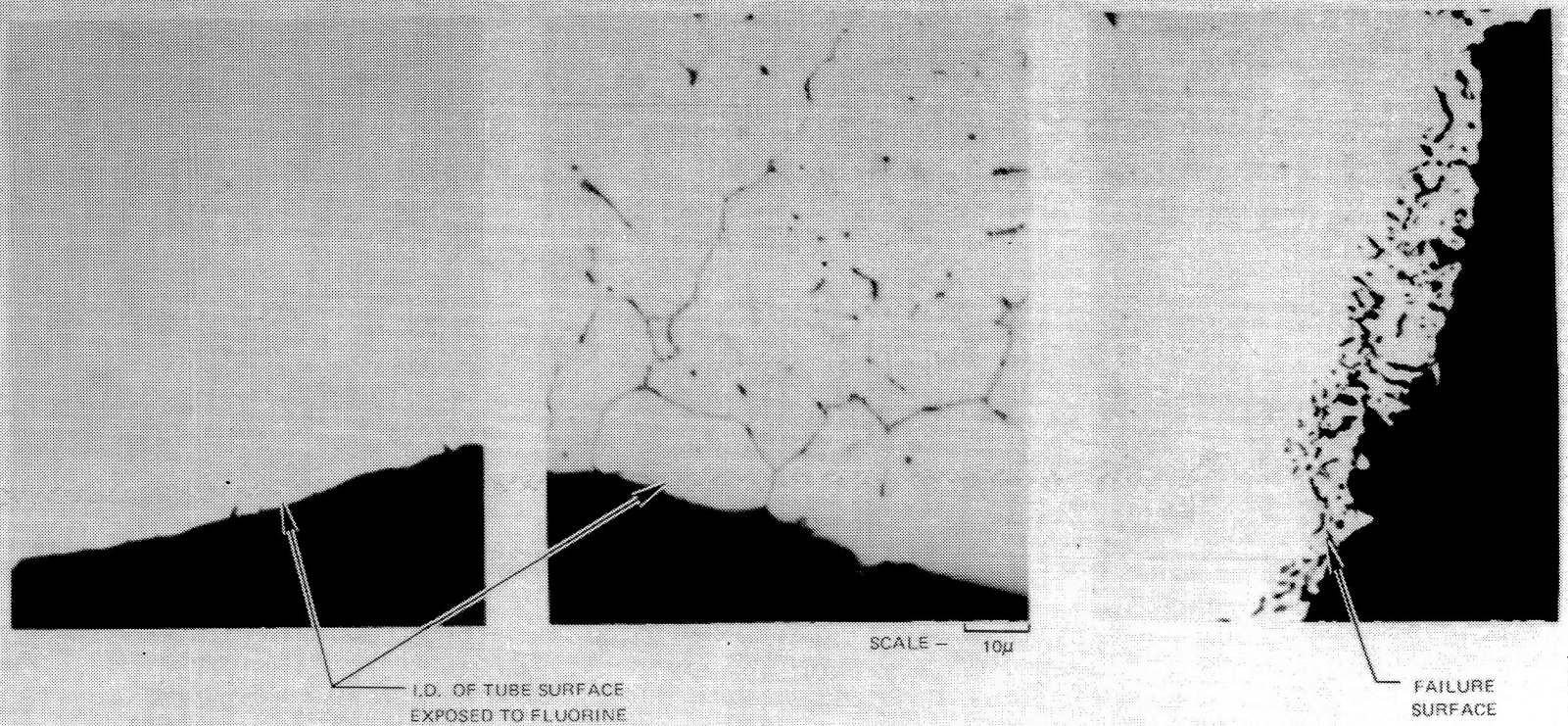

FIG. 9

SCHEMATIC OF COMPONENTS USED IN FLOWING HIGH TEMPERATURE F_2/– UF_6 REGENERATION TESTS CONDUCTED IN 1.2 MW RF PLASMA FACILITY

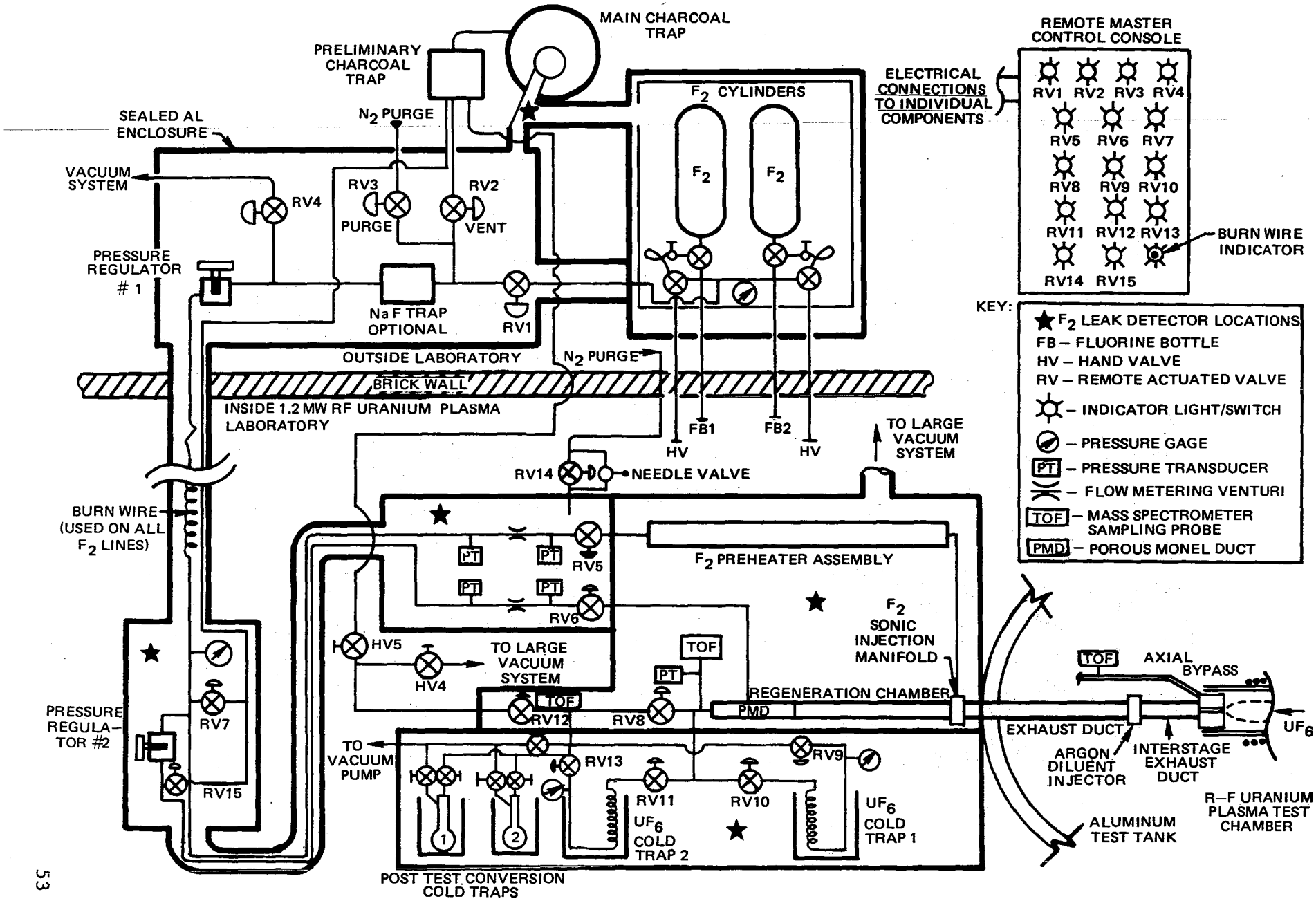

FIG. 10

PHOTOGRAPH OF FLUORINE SYSTEM CONTROL CONSOLE AND LEAK DETECTION/ALARM SYSTEM USED IN FLOWING F_2–UF_6 REGENERATION TESTS IN 1.2 MW RF URANIUM PLASMA TEST FACILITY

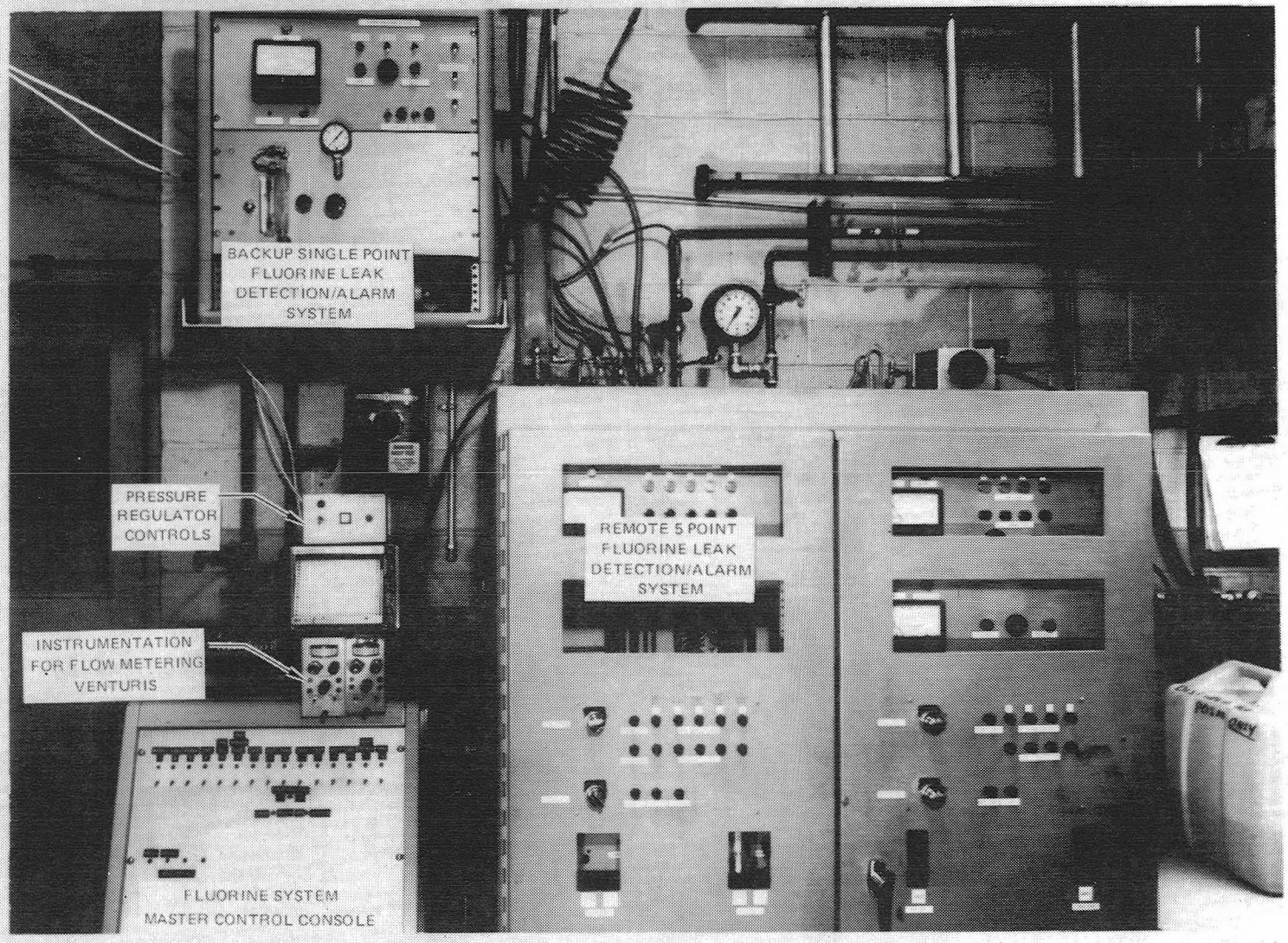

FIG. 11

PHOTOGRAPH OF FLUORINE TEST CHAMBER COMPONENTS USED IN FLOWING F_2–UF_6 REGENERATION TESTS CONDUCTED IN 1.2 MW RF URANIUM PLASMA TEST FACILITY

(TOP COVER REMOVED– CHAMBER LENGTH– 1.4 M)
SEE FIG. 10 FOR SCHEMATIC OF COMPONENTS

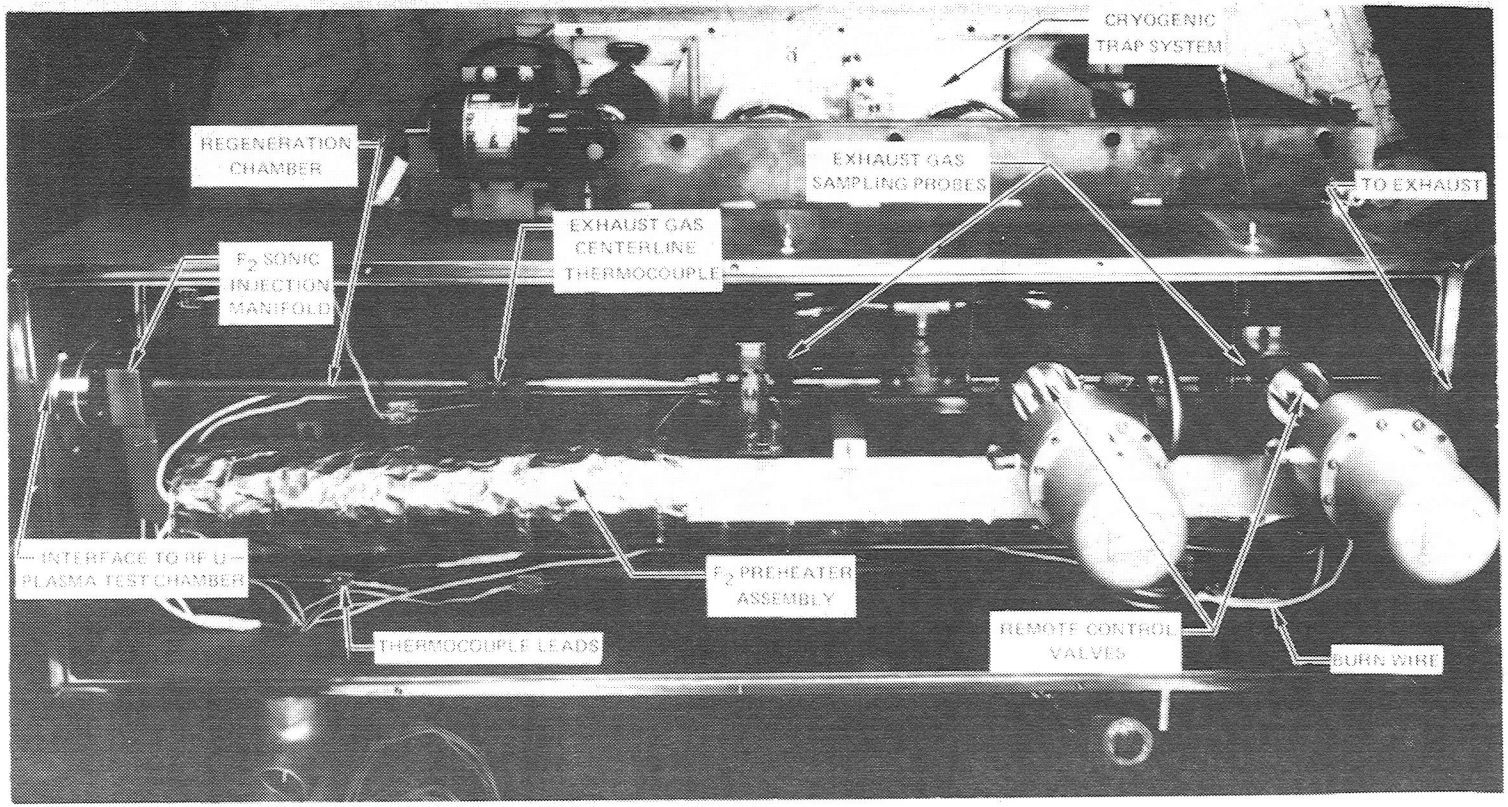

FIG 11

PHOTOGRAPH OF CRYOGENIC COLD TRAPS AND POST TEST CONVERSION TRAPS USED IN F_2–UF_6 REGENERATION TESTS

SEE FIG. 10 FOR SCHEMATIC OF COMPONENTS

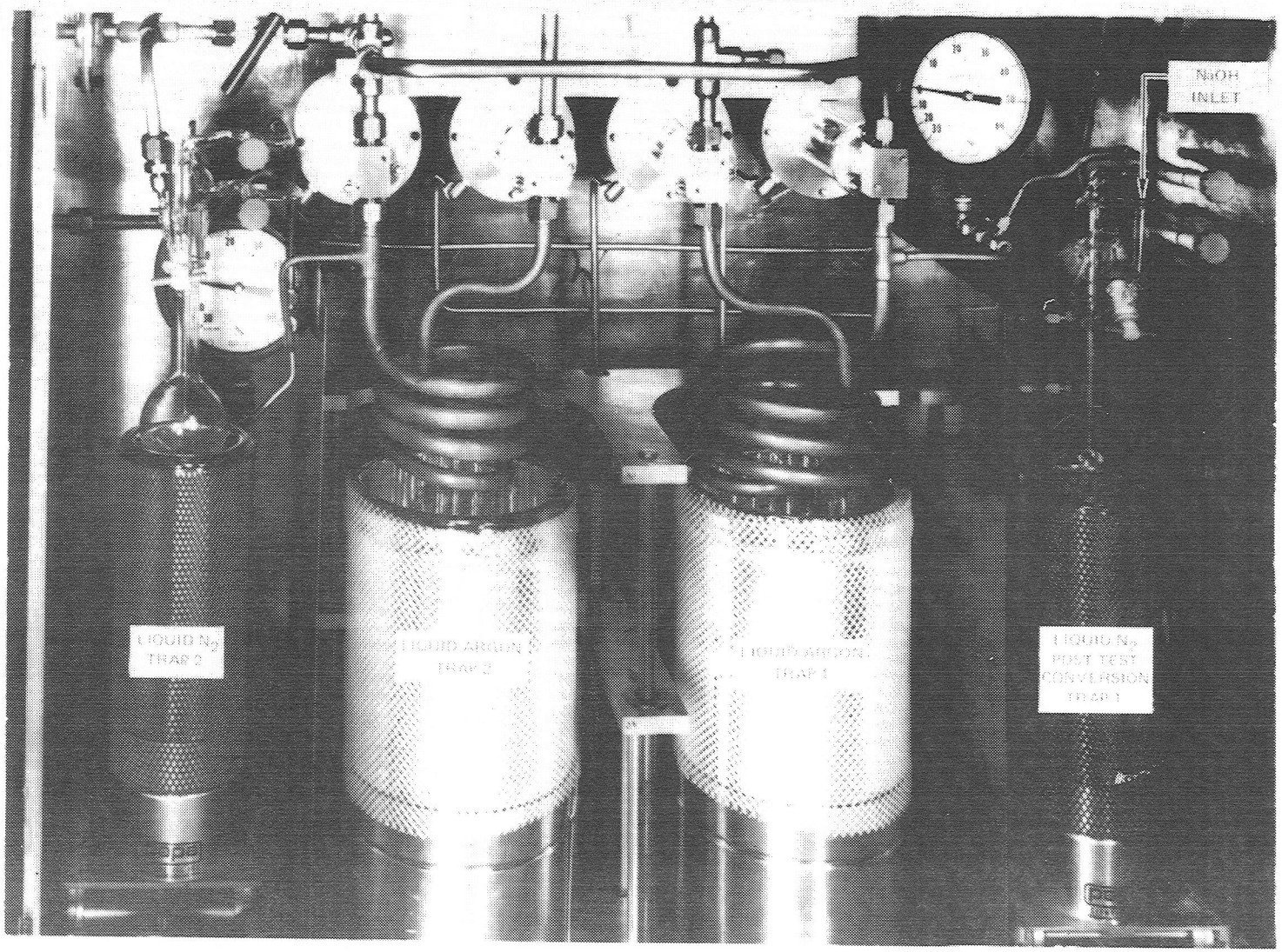

PHOTOGRAPH OF POROUS MONEL EXHAUST DUCT ASSEMBLY USED IN FLOWING FLUORINE/UF_6 REGENERATION TESTS CONDUCTED IN 1.2 MW RF URANIUM PLASMA TEST FACILITY

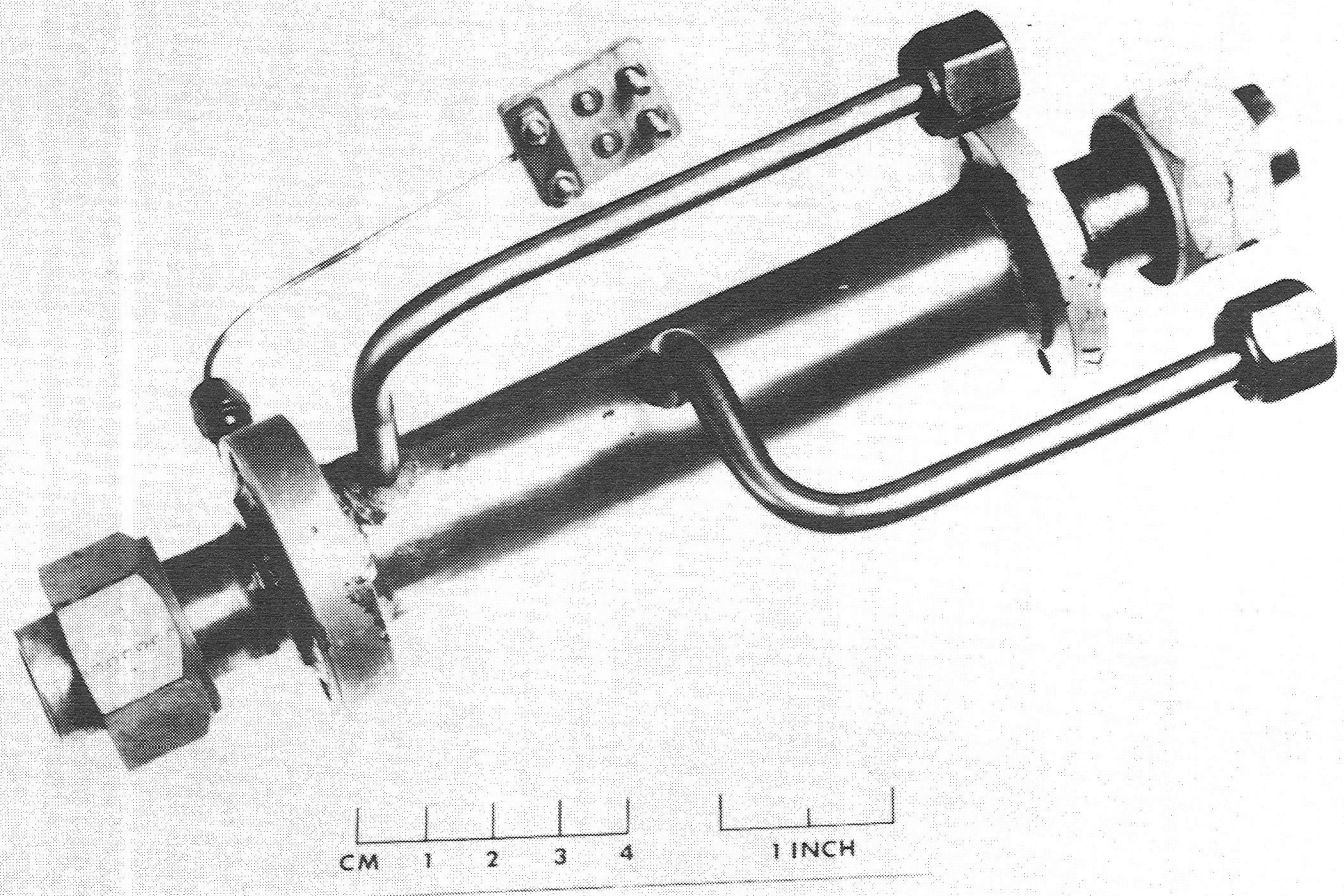

FIG. 14

SKETCH OF BASIC TEST CHAMBER CONFIGURATION USED IN RF PLASMA/UF_6 REGENERATION TESTS

(SEE FIG. 16 FOR PHOTOGRAPH OF TEST CHAMBER CONFIGURATION INSTALLED IN 1.2MW RF INDUCTION HEATER TEST TANK)

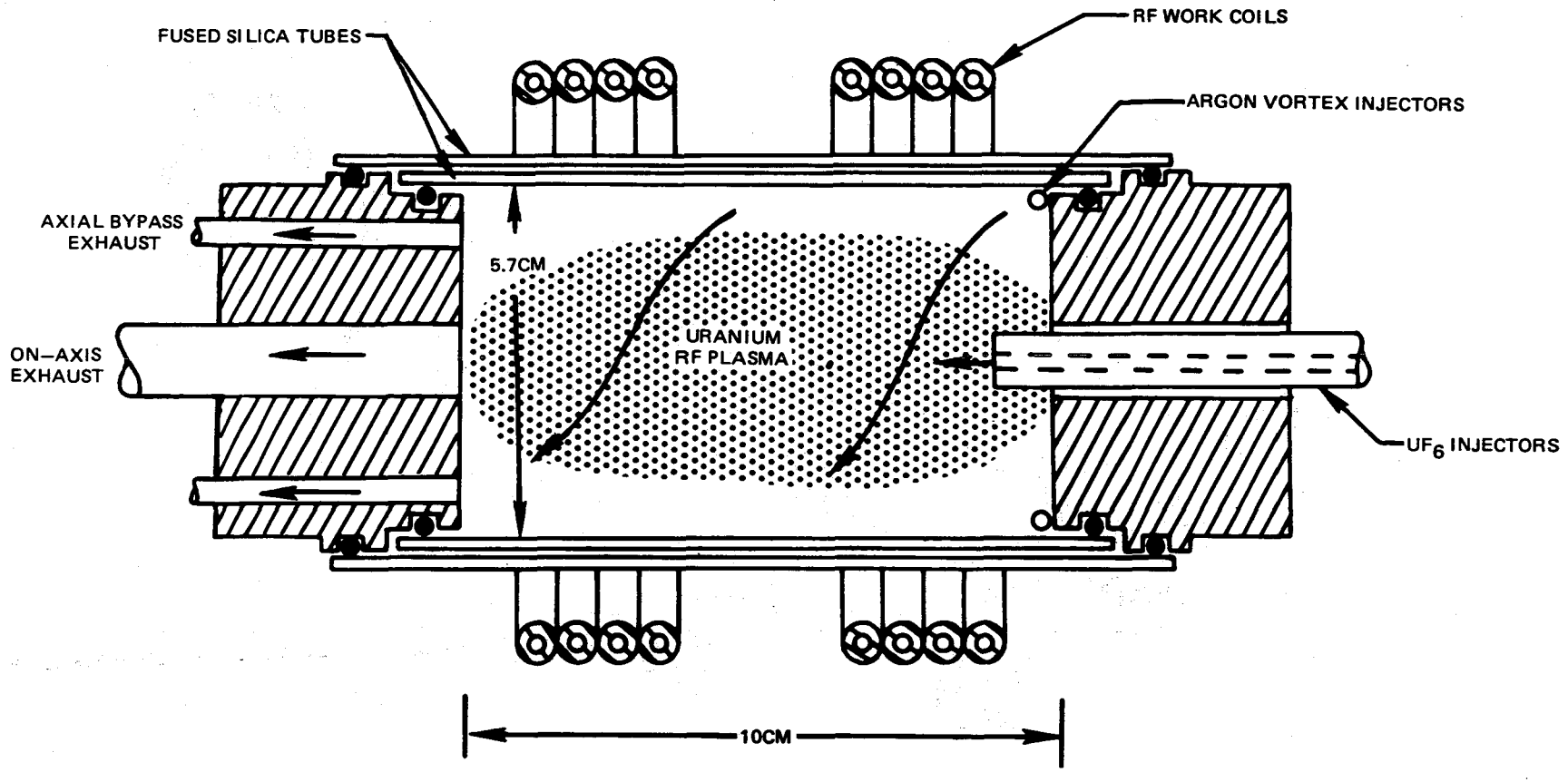

(NOT TO SCALE)

FIG. 15

PHOTOGRAPH OF TEST COMPONENTS USED IN FLOWING F_2–UF_6 REGENERATION TESTS IN 1.2 MW RF URANIUM PLASMA TEST FACILITY

(RF CHAMBER FRONT DOME REMOVED—DIA. 1.7 M)

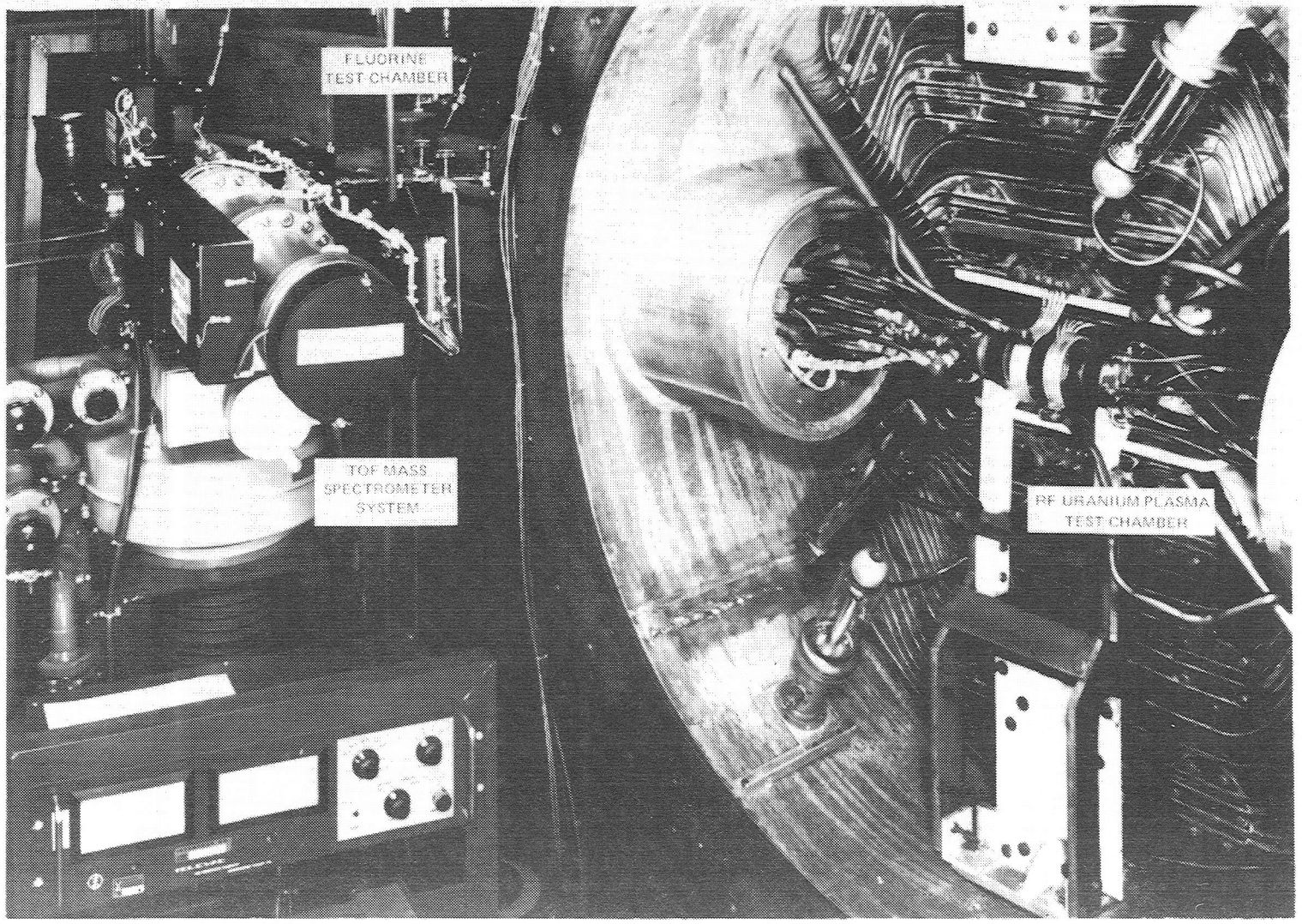

FIG. 17

PHOTOGRAPH OF DATA SYSTEM EMPLOYED WITH RUGGEDIZED TOF MASS SPECTROMETER SYSTEM IN RF URANIUM PLASMA EXHAUST GAS ANALYSIS TESTS

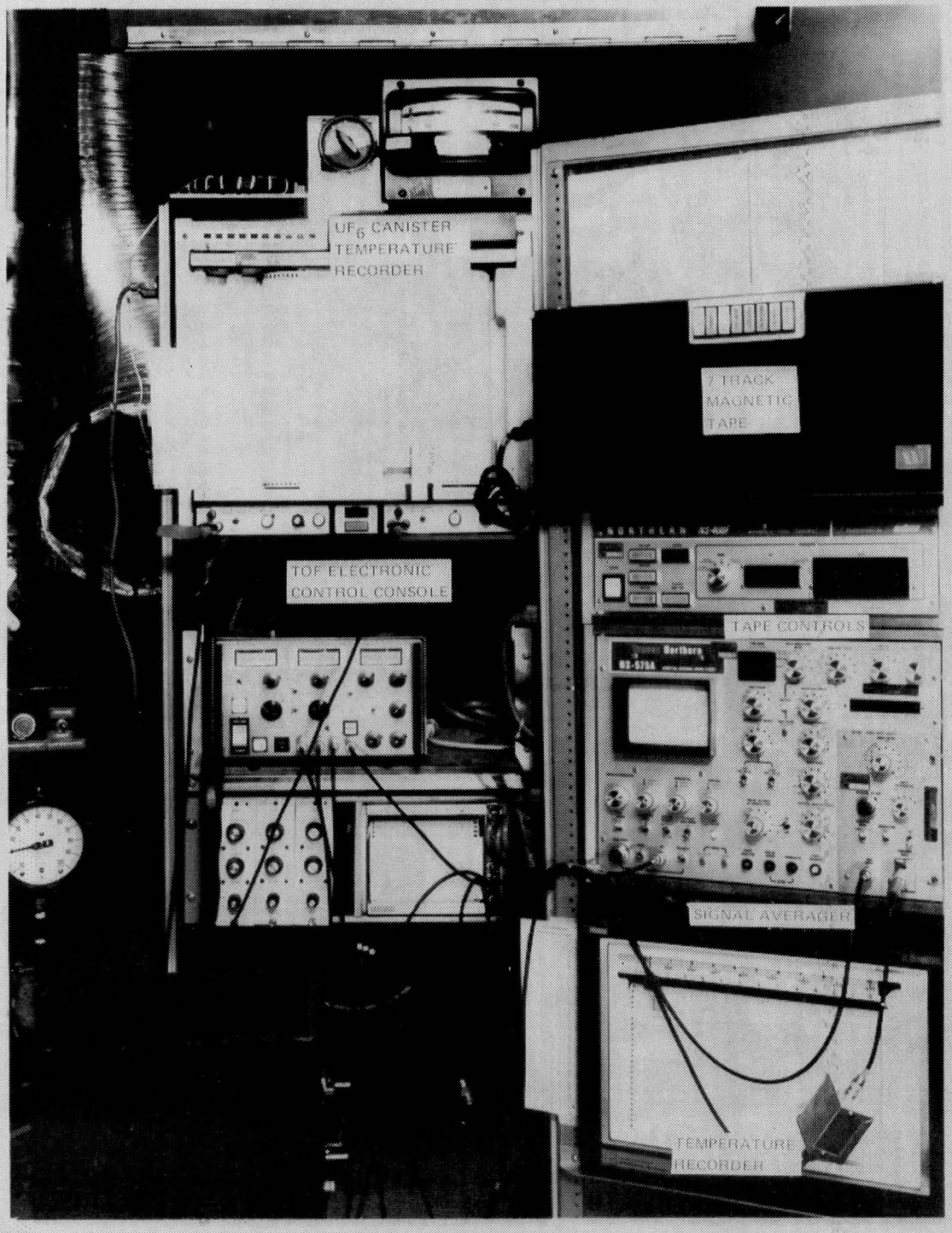

SCHEMATIC OF TEST CONFIGURATION USED IN FLOWING HIGH TEMPERATURE FLUORINE/UF6 REGENERATION TESTS EMPLOYING EXHAUST GAS SAMPLING AND CONDUCTED IN 1.2 MW RF URANIUM PLASMA FACILITY

NOT TO SCALE

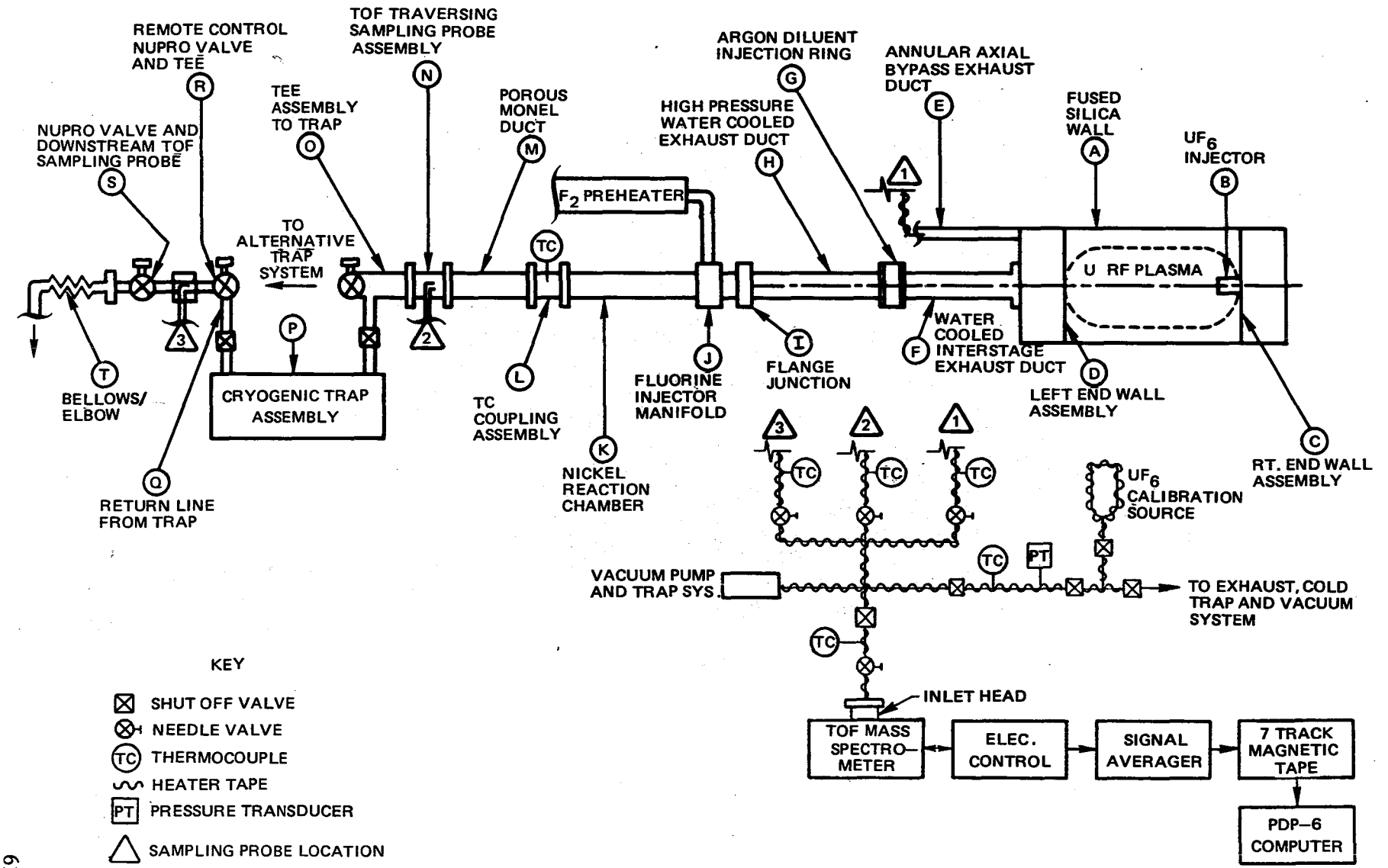

FIG. 18

FIG. 19

PHOTOGRAPH OF TRAVERSIBLE SAMPLING PROBE ASSEMBLY USED WITH T.O.F. MASS SPECTROMETER SYSTEM IN FLOWING URANIUM PLASMA–FLUORINE/UF_6 REGENERATION TESTS CONDUCTED IN 1.2 MW RF URANIUM PLASMA FACILITY.

SEE FIG. 18 FOR SCHEMATIC OF TEST CONFIGURATION

SEE TABLE V FOR EXAMPLE OF TEST RESULTS

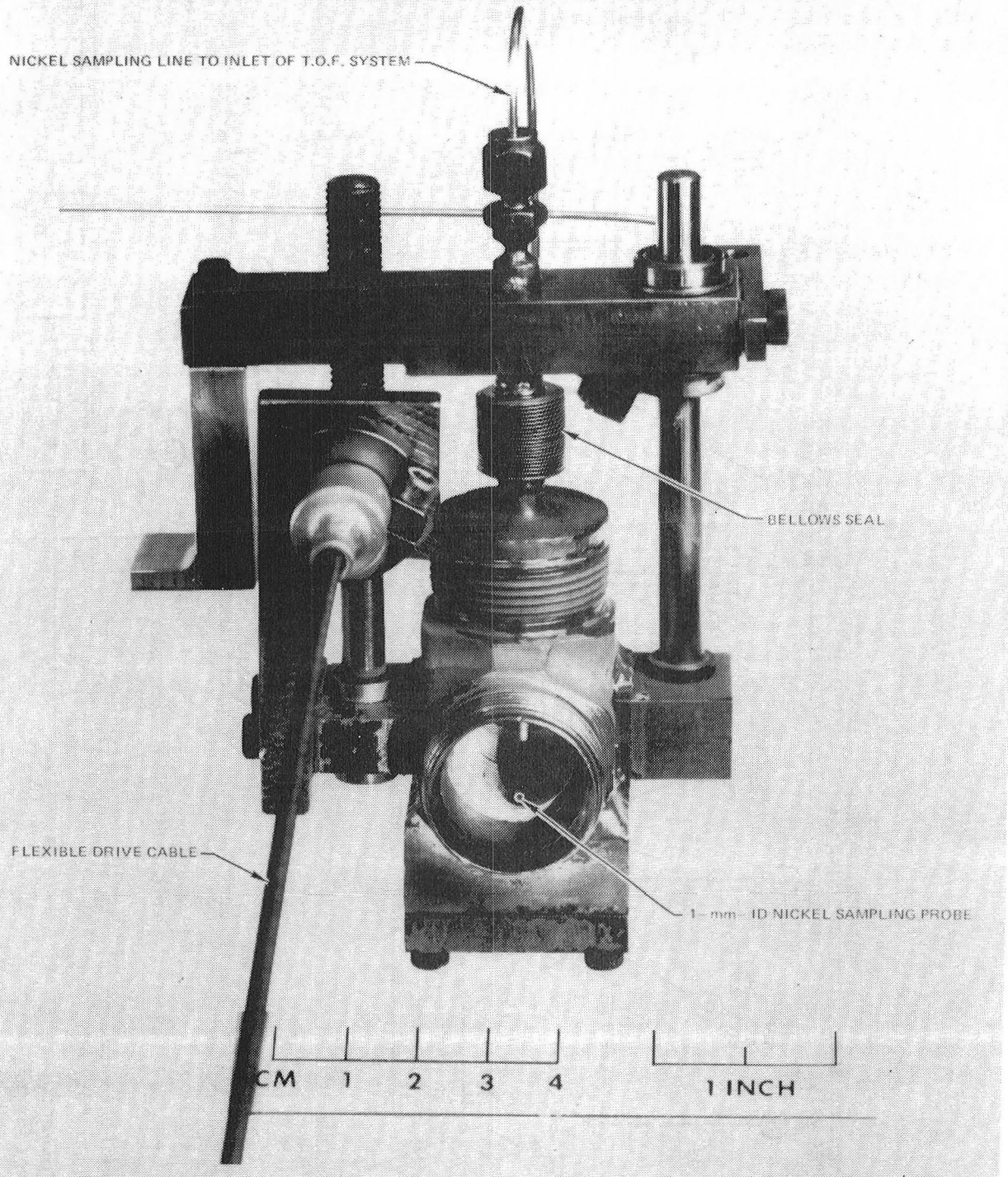

EXAMPLE OF MEASURED CONVERSION DATA OBTAINED FROM FLOWING HIGH TEMPERATURE UF_4/F_2 TO UF_6 REGENERATION TESTS

NO FLUORINE PREHEAT USED IN THESE TESTS

SEE FIG. 2 FOR SCHEMATIC OF TEST CONFIGURATION

SEE TABLE I FOR RANGE OF TEST CONDITIONS

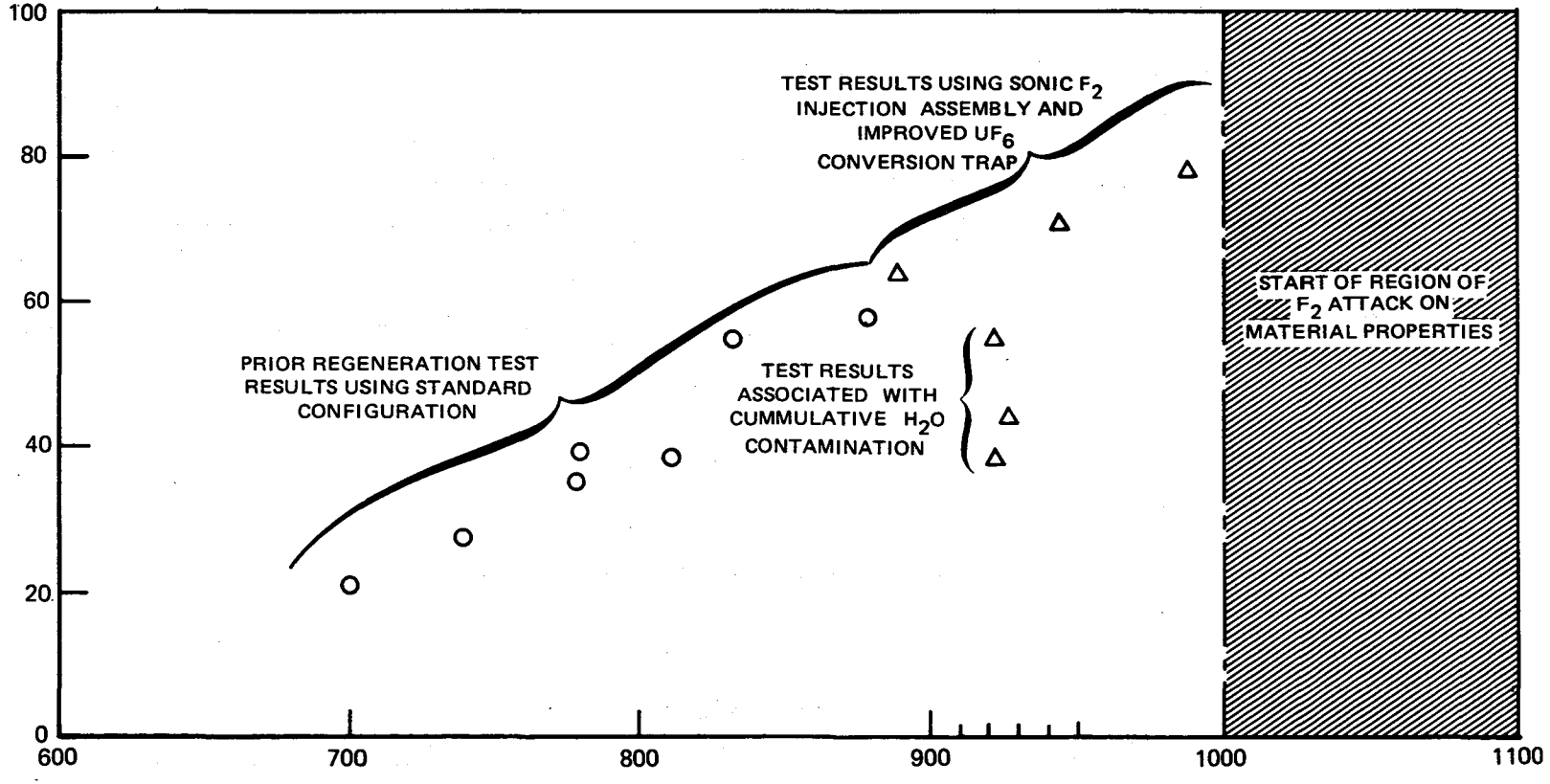

FIG. 20

SCHEMATIC OF KEY COMPONENTS USED IN HEAT TRANSFER ANALYSIS OF FLOWING HIGH TEMPERATURE UF_4/PREHEATED FLUORINE TO UF_6 REGENERATION TESTS CONDUCTED WITH DC ARC PLASMA TORCH SYSTEM

(NOT TO SCALE)

SEE TABLE II FOR ADDITIONAL TEST CONDITIONS

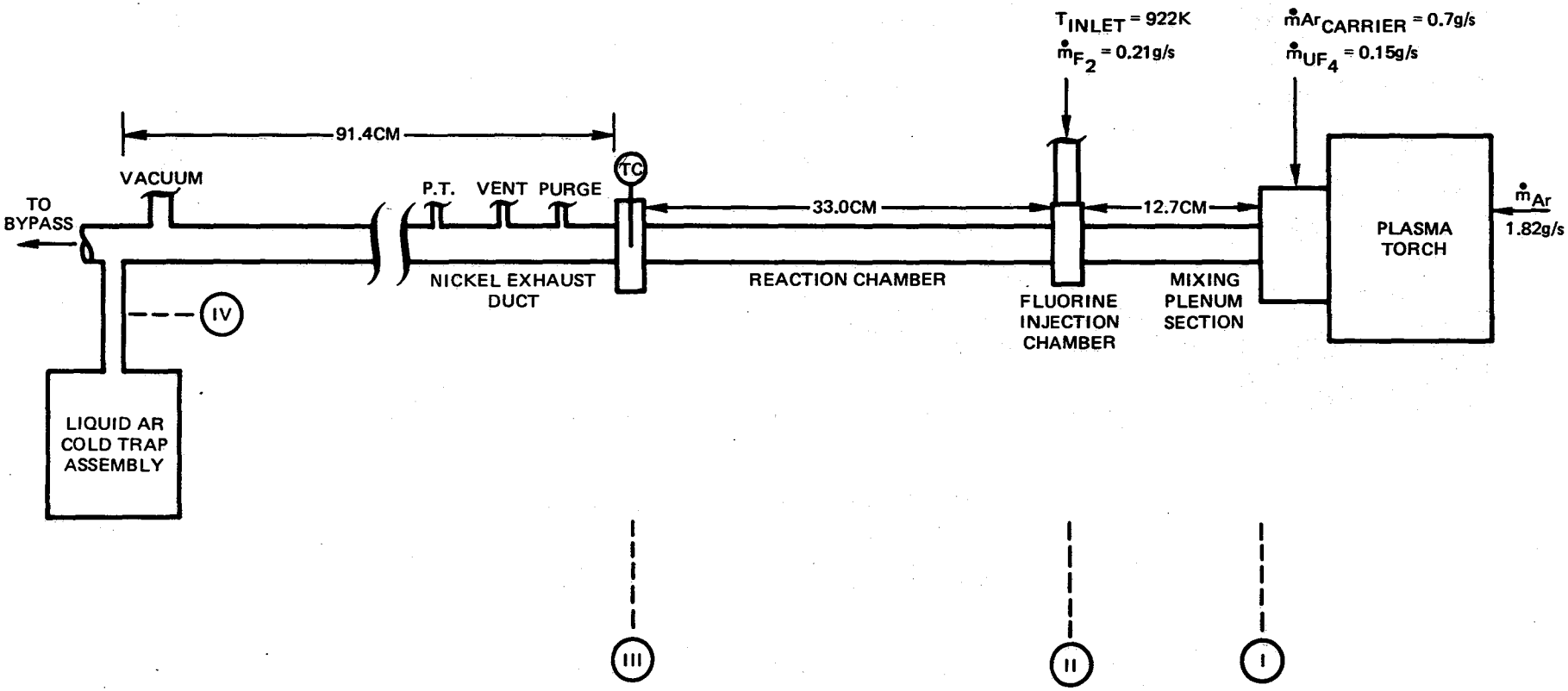

FIG. 21

EXAMPLE OF MEASURED CONVERSION DATA OBTAINED FROM FLOWING HIGH TEMPERATURE UF_4/PREHEATED F_2 TO UF_6 REGENERATION TESTS

SEE FIG. 2 FOR SCHEMATIC OF CONFIGURATION
SEE FIG. 8 FOR PHOTOGRAPH OF TEST COMPONENTS

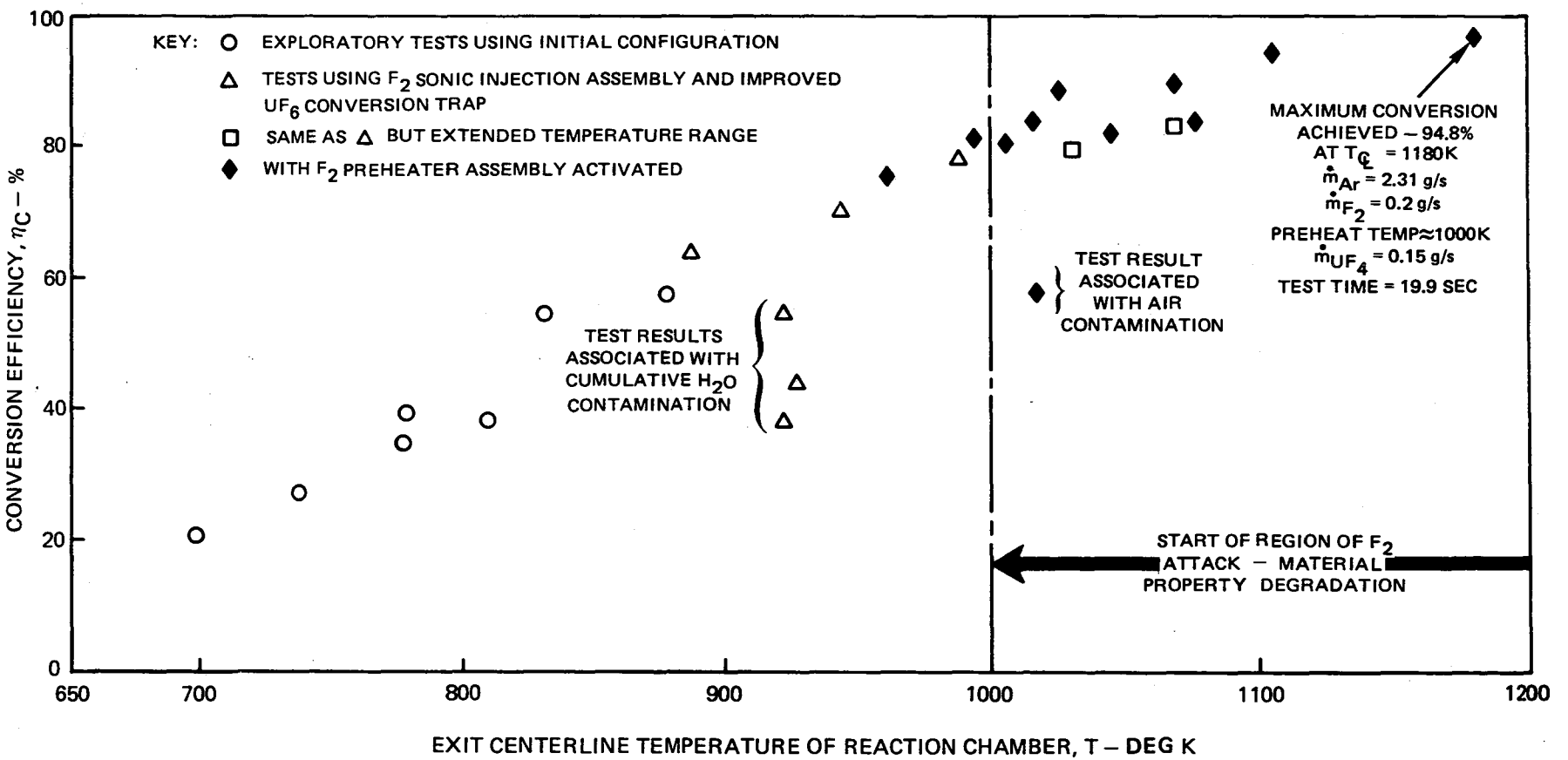

FIG. 22

FIG. 23

EFFECT OF TEMPERATURE ON MOLE FRACTION OF FLUORINE ATOM (F)

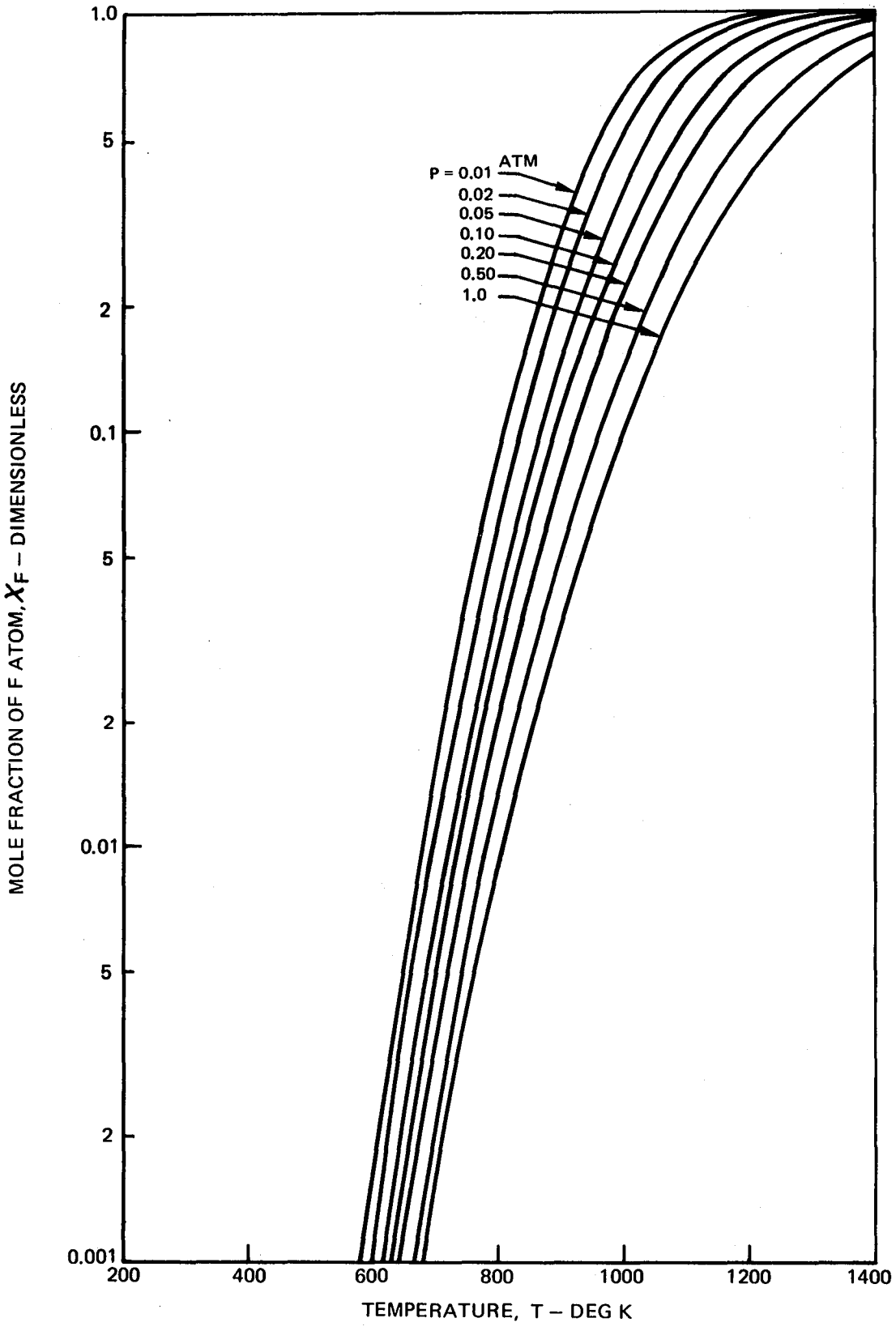

EXAMPLE OF MEASURED CONVERSION DATA OBTAINED FROM FLOWING HIGH TEMPERATURE F_2/UF_6 REGENERATION TESTS CONDUCTED IN 1.2 MW RF URANIUM PLASMA FACILITY

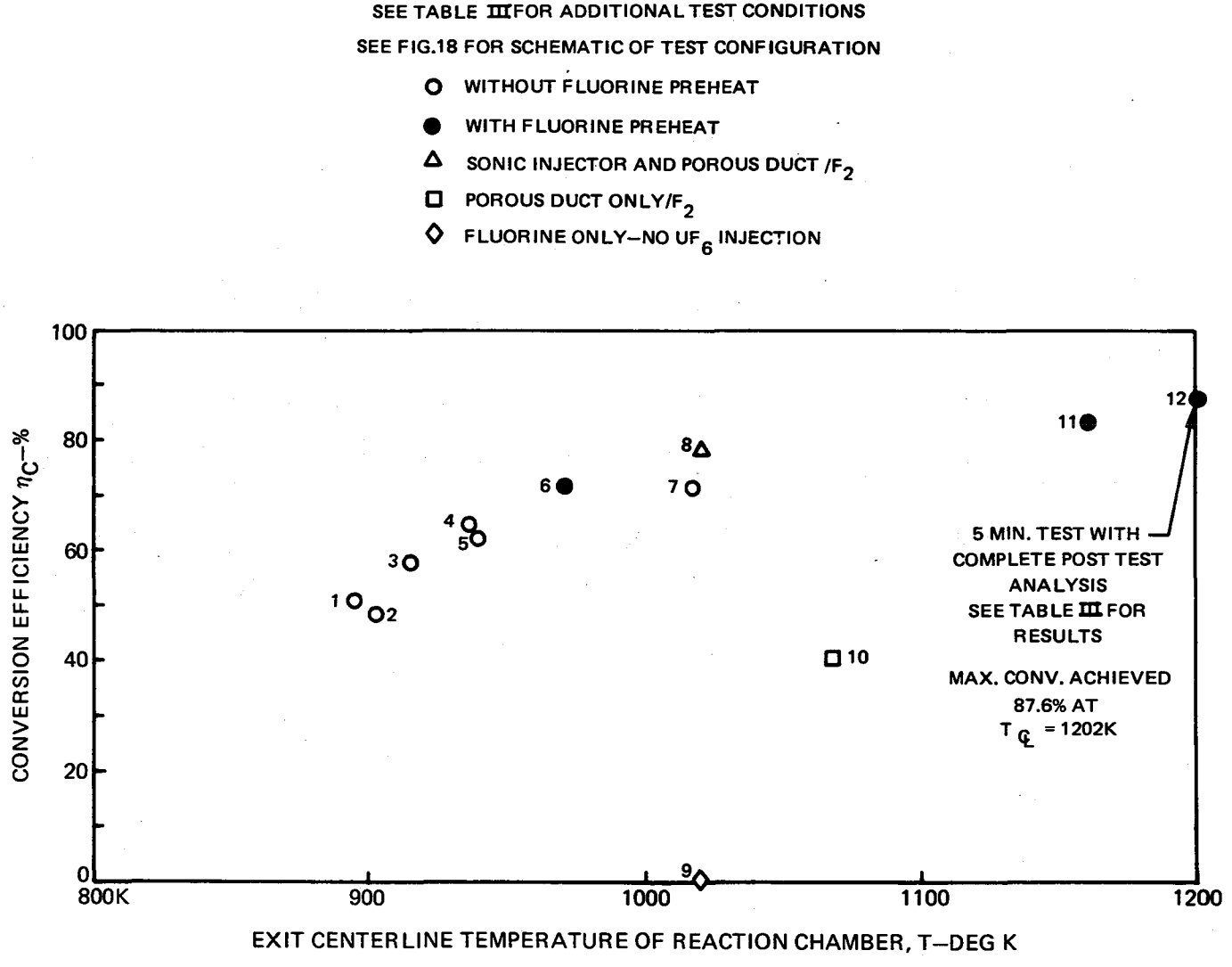

FIG. 24

PHOTOGRAPH OF DISASSEMBLED KEY TEST COMPONENTS USED IN FLOWING FLUORINE/UF_6 REGENERATION TESTS CONDUCTED IN 1.2 MW RF URANIUM PLASMA TEST FACILITY

SEE FIG. 18 FOR SCHEMATIC OF TEST COMPONENTS
SEE TABLE IV FOR SUMMARY OF POST TEST RESIDUE ANALYSIS

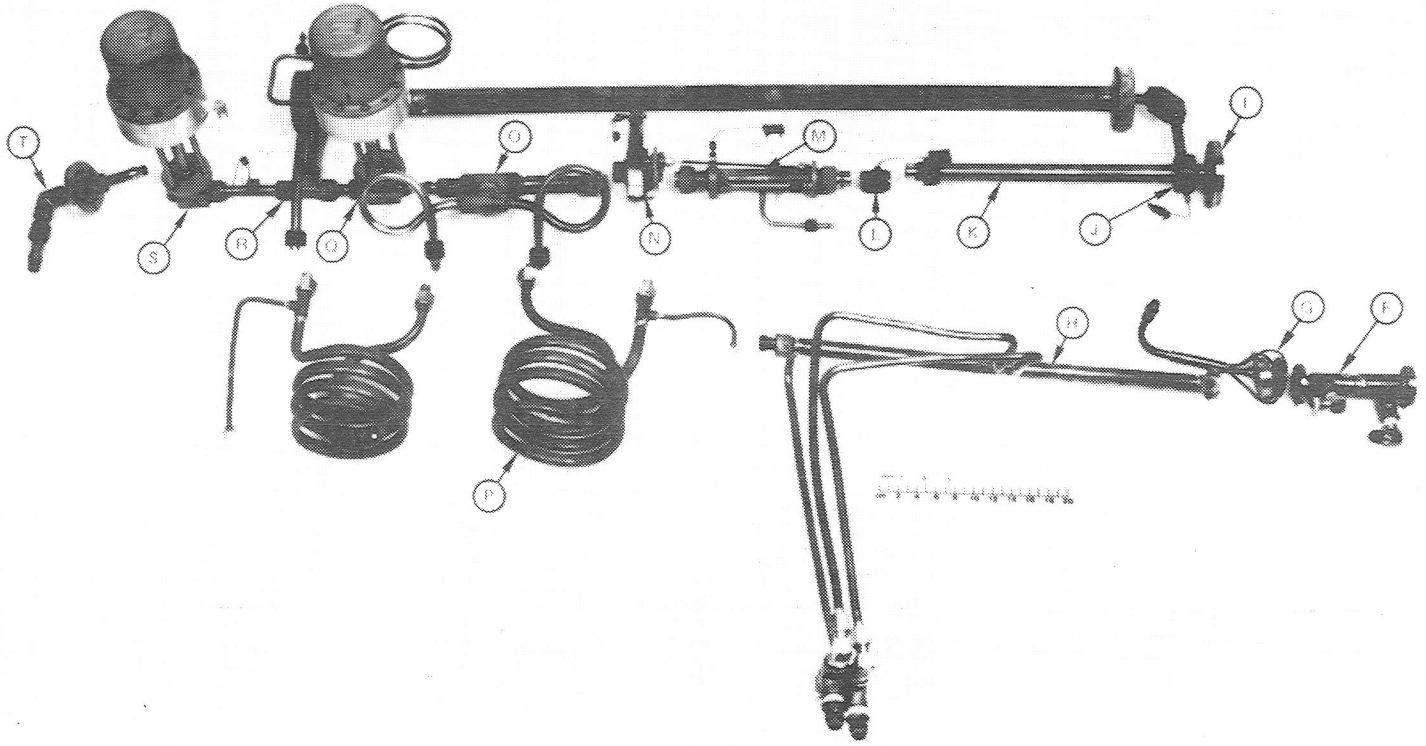

FIG. 25

FIG. 26

PHOTOGRAPH OF FUSED–SILICA TUBES USED IN FLOWING RF URANIUM PLASMA FLUORINE/UF_6 REGENERATION TESTS

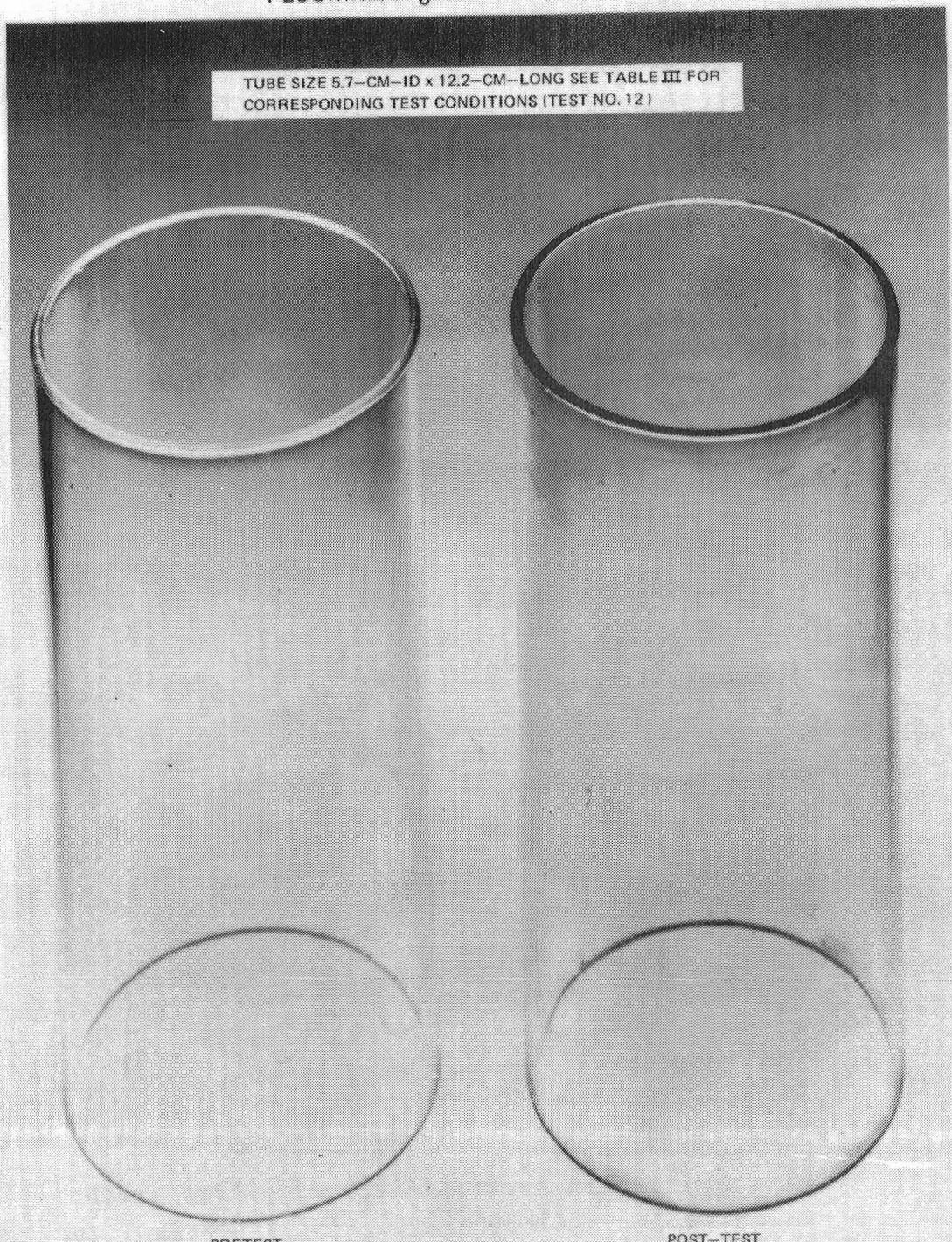

FIG. 27

EXAMPLE OF UF_6 MASS SPECTRAL RELATIVE INTENSITIES USED IN CALIBRATION OF RF URANIUM PLASMA FLUORINE/UF_6 REGENERATION TESTS

(DATA POINT NUMBER EQUIVALENT TO ADDRESS NUMBER IN MULTICHANNEL SCALER)

SEE FIG. 18 FOR SCHEMATIC OF EXHAUST GAS SAMPLING SYSTEM

SEE FIG. 16 FOR PHOTOGRAPH OF EQUIPMENT

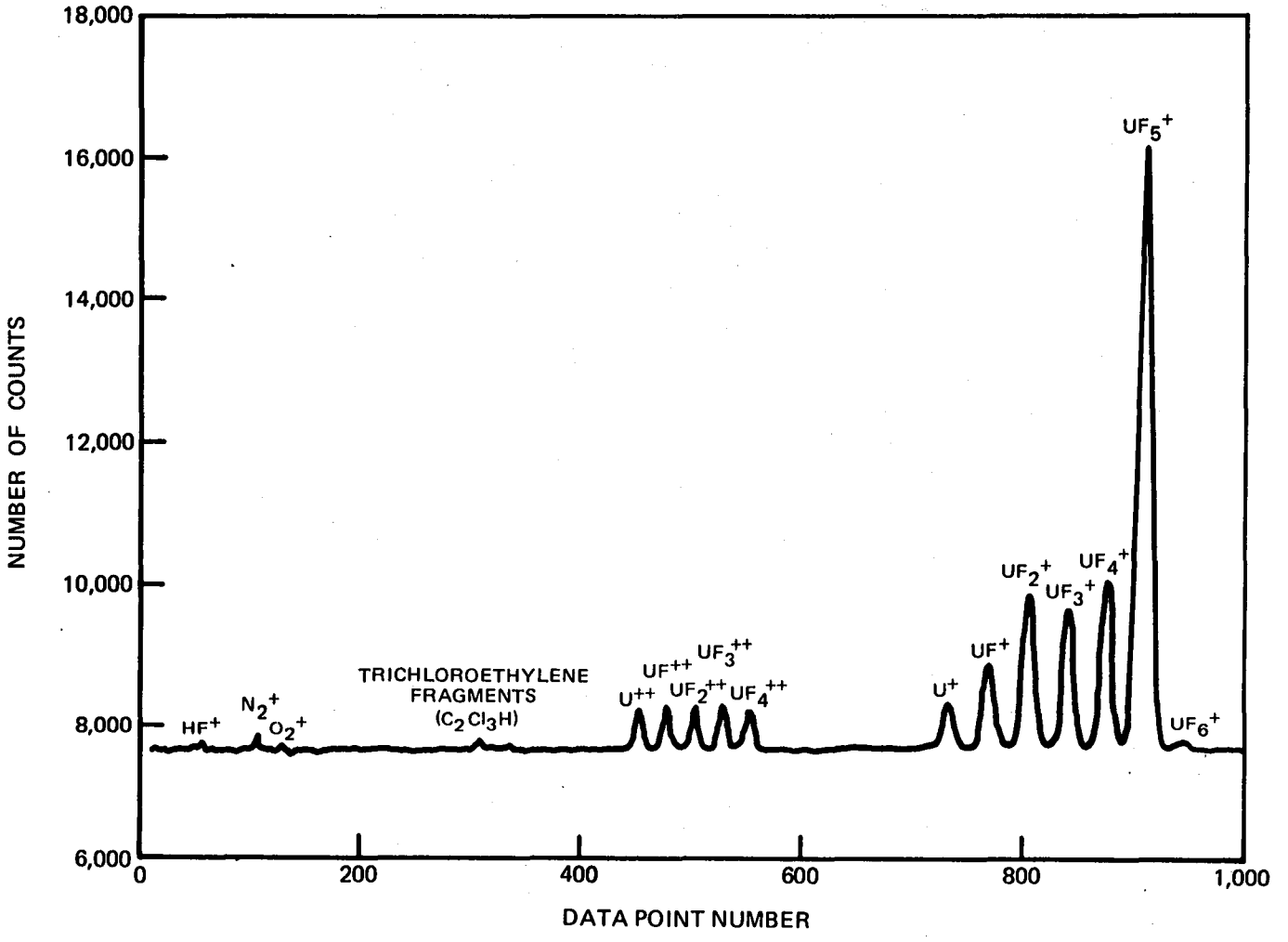

FIG. 28

EXAMPLE OF MASS SPECTRAL RELATIVE INTENSITIES OBTAINED WITH SAMPLING PROBE LOCATED AT AXIAL BYPASS STATION (1) IN 1.2 MW RF URANIUM PLASMA FLUORINE/UF_6 REGENERATION TESTS

(DATA POINT NUMBER EQUIVALENT TO ADDRESS NUMBER IN MULTICHANNEL SCALER)

SEE FIG. 18 FOR SCHEMATIC OF EXHAUST GAS SAMPLING SYSTEM

SEE FIG. 16 FOR PHOTOGRAPH OF EQUIPMENT DOUBLET

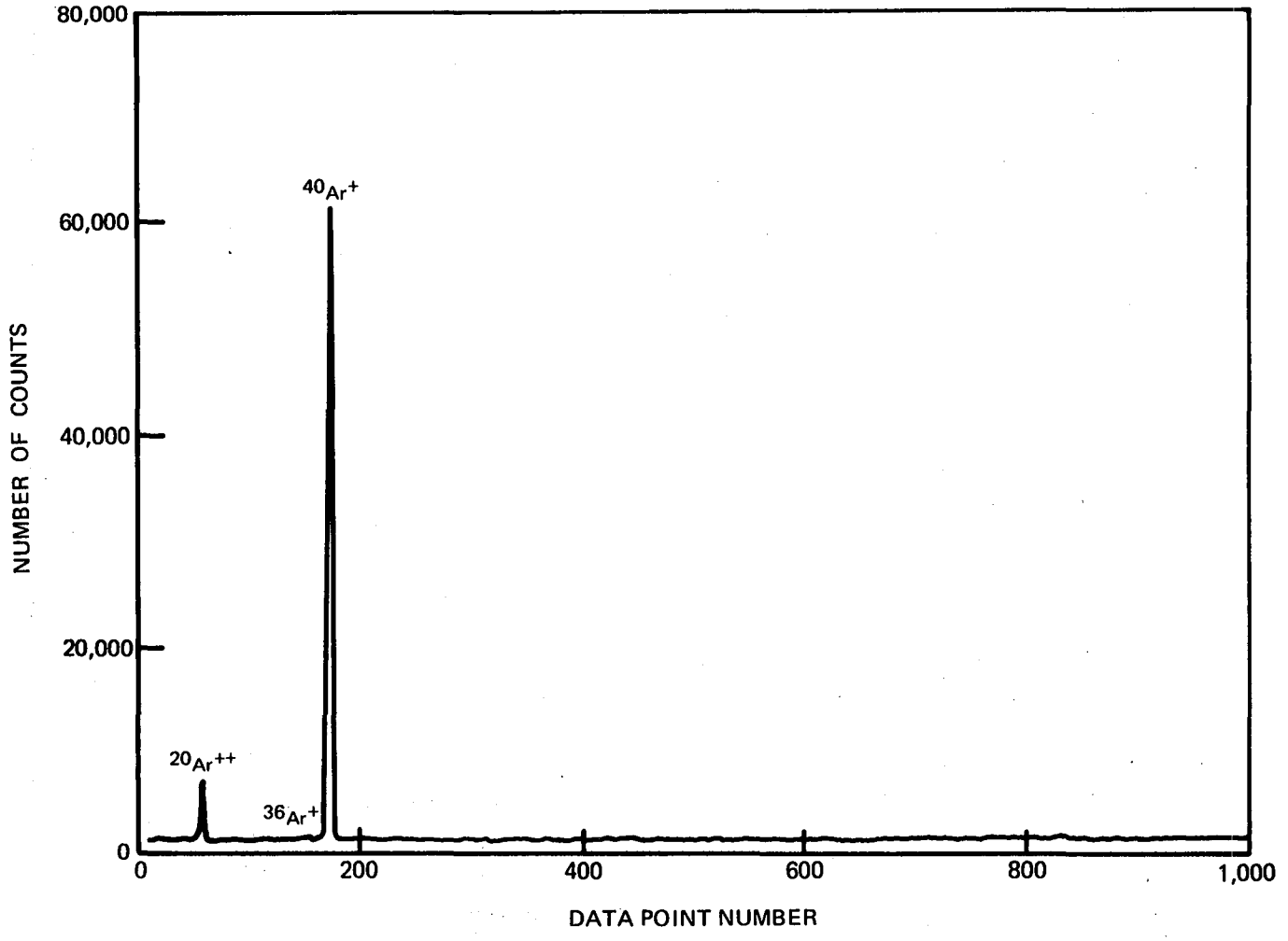

FIG. 29

EXAMPLE OF MASS SPECTRAL RELATIVE INTENSITIES OBTAINED WITH SAMPLING PROBE LOCATED AT DOWNSTREAM STATION (3) IN 1.2 MW RF URANIUM PLASMA FLUORINE/UF_6 REGENERATION TESTS

(DATA POINT NUMBER EQUIVALENT TO ADDRESS NUMBER IN MULTICHANNEL SCALER)

SEE FIG. 18 FOR SCHEMATIC OF EXHAUST GAS SAMPLING SYSTEM

SEE FIG. 16 FOR PHOTOGRAPH OF EQUIPMENT

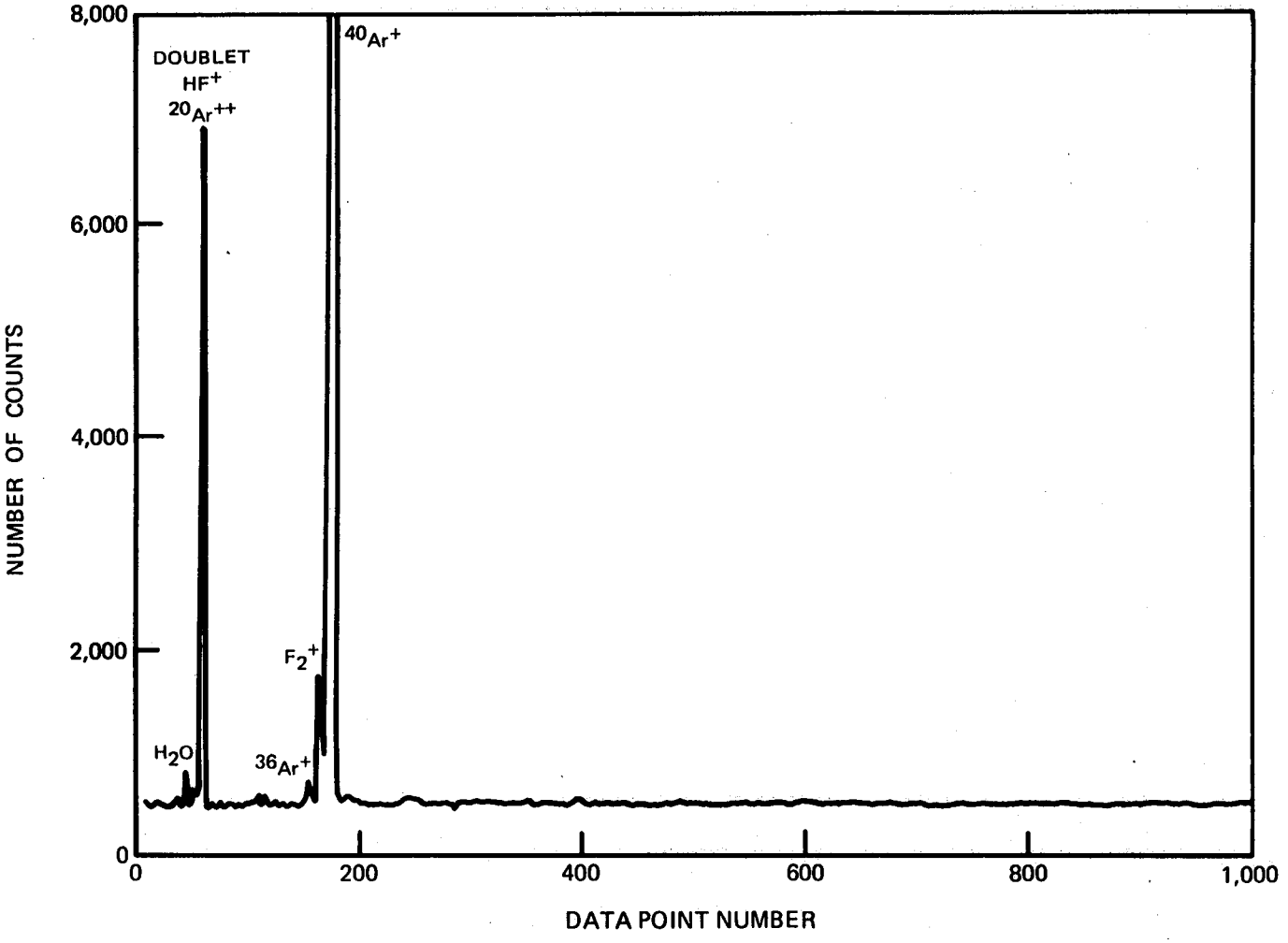

FIG. 30

EXAMPLE OF MASS SPECTRAL RELATIVE INTENSITIES OBTAINED WITH SAMPLING PROBE LOCATED AT UPSTREAM STATION (2) IN 1.2 MW RF URANIUM PLASMA FLUORINE/UF_6 REGENERATION TESTS

(DATA POINT NUMBER EQUIVALENT TO ADDRESS NUMBER IN MULTICHANNEL SCALER)

SEE FIG. 18 FOR SCHEMATIC OF EXHAUST GAS SAMPLING SYSTEM

SEE FIG. 16 FOR PHOTOGRAPH OF EQUIPMENT

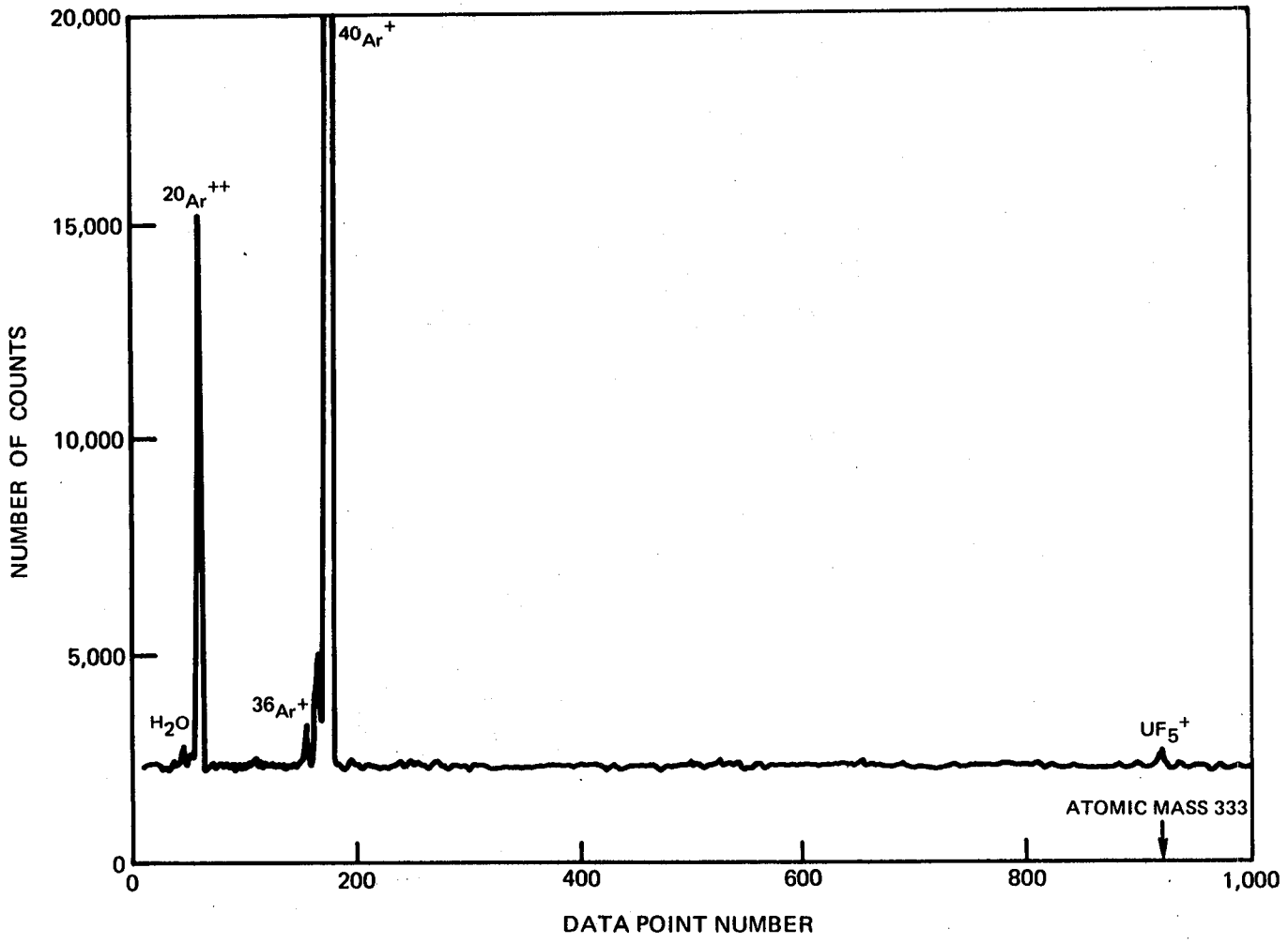

SCHEMATIC OF KEY COMPONENTS USED IN HEAT TRANSFER ANALYSIS OF FLOWING HIGH TEMPERATURE RF PLASMA EXHAUST/PREHEATED FLUORINE TO UF_6 REGENERATION TESTS CONDUCTED USING 1.2 MW RF URANIUM PLASMA TEST FACILITY

(NOT TO SCALE)

SEE APPENDIX A AND TABLE VII FOR ADDITIONAL TEST CONDITIONS AND HEAT BALANCE

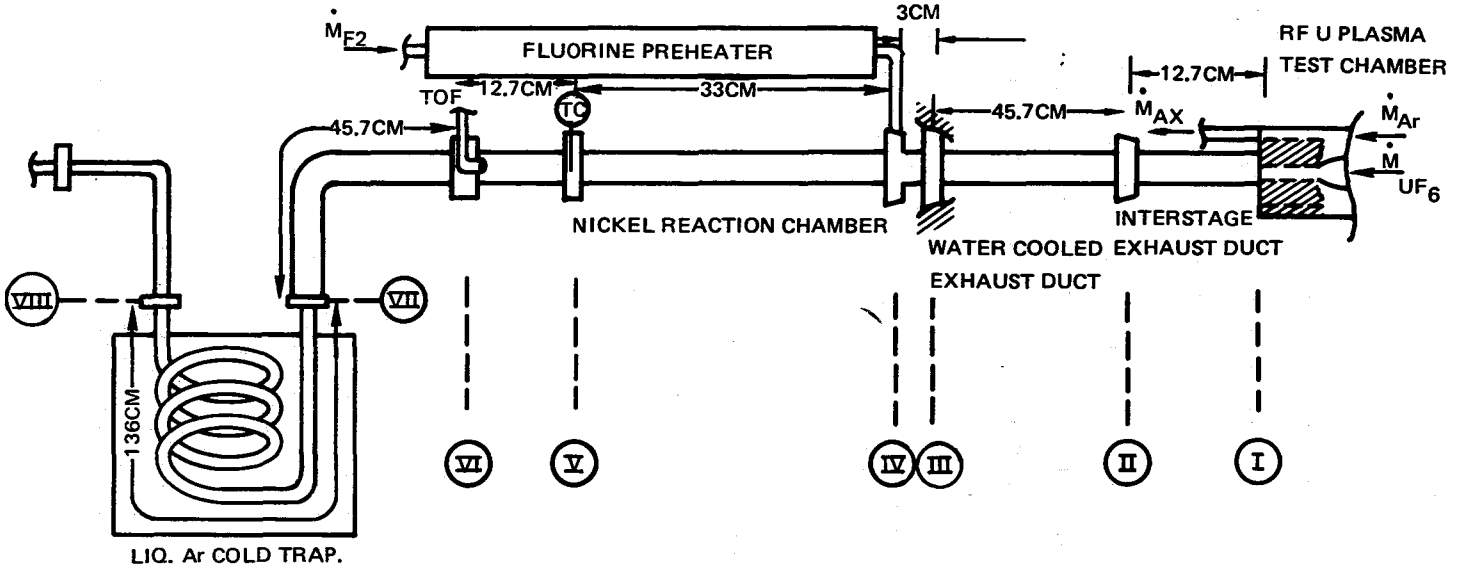

FIG. 31

COMPOSITION OF UF_6/ARGON MIXTURE AS A FUNCTION OF TEMPERATURE

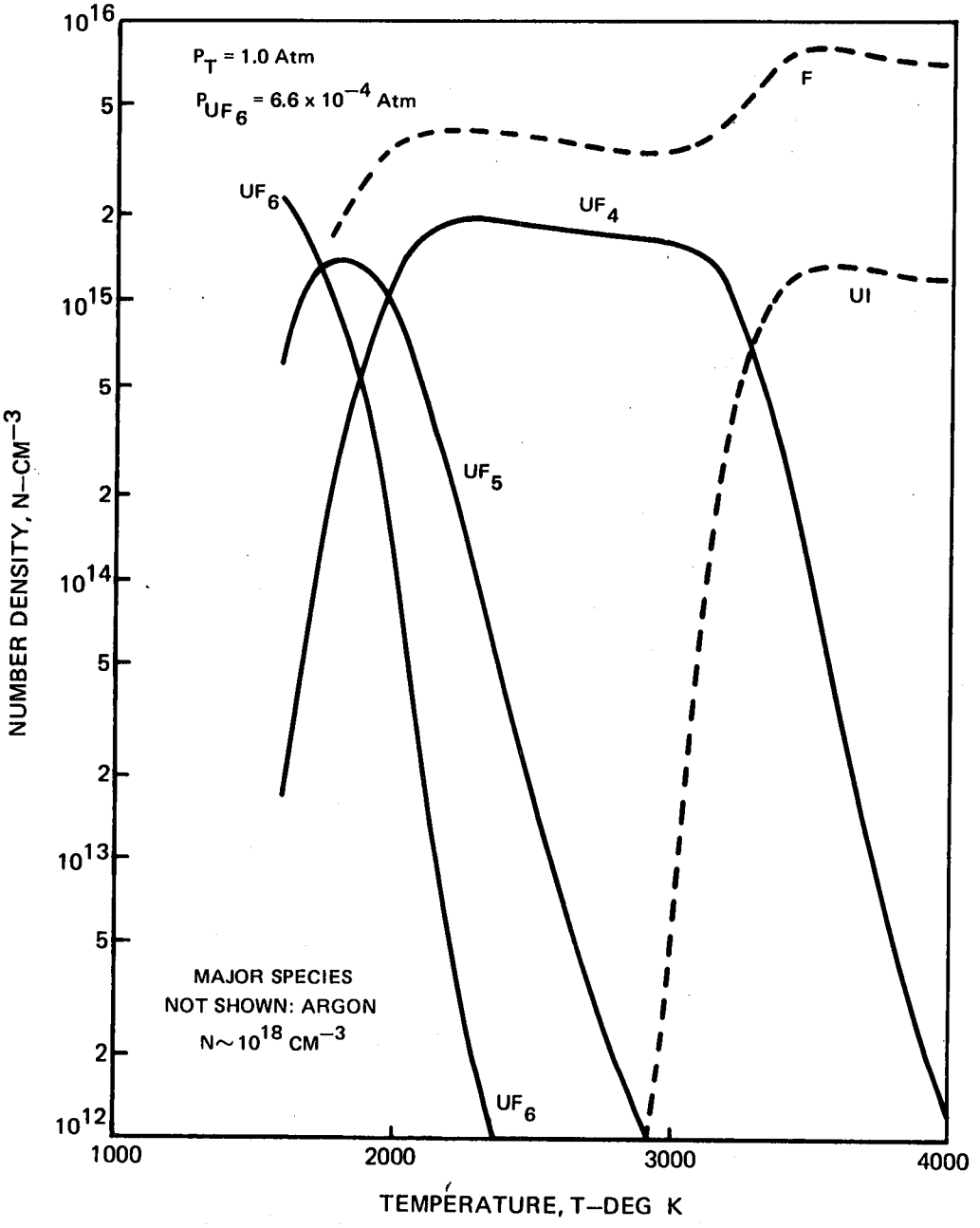

CALCULATED VARIATION OF ENTHALPY WITH TEMPERATURE FOR UF_6 AND ITS THERMAL DECOMPOSITION SPECIES

SEE FIG. 32 FOR EXAMPLE OF EQUILIBRIUM COMPOSITION

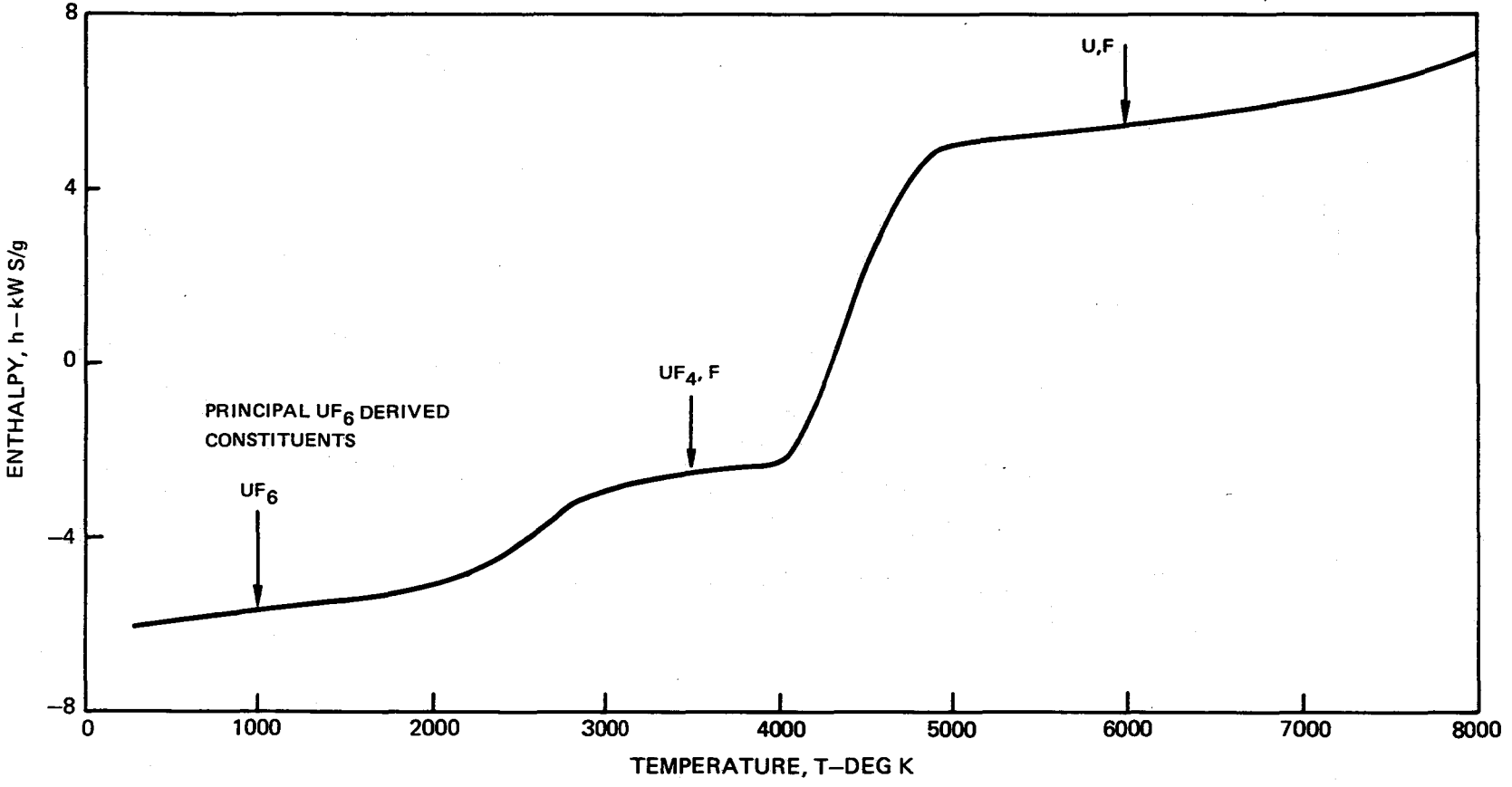

FIG. 33